Scaffolds for Liver Tissue Engineering:

In vitro Co-culture & *In Vivo* Release

John Stotesbury Hammond

BMedSci BM BS MRCS

Thesis submitted to the University of Nottingham

for a Doctor of Philosophy

November 2008

To my father

Contents

Table of Figures		vi
List of Tables		vii
Abbreviations		viii
Acknowledgements		ix
Statement of Originality		x
Abstract		xi
Chapter 1 Introduction		1
1.1	Liver Surgery	1
1.1.1	Surgery for Liver Cancer	1
1.1.2	Liver Surgery for Liver Failure	2
1.1.3	The Future of Liver Surgery	3
1.2	Regenerative Medicine	5
1.2.1	Cell Sourcing	5
1.2.2	Signal Delivery	6
1.2.3	Cytokine and Growth Factor Delivery	7
1.2.4	Extracellular Matrix Signal Delivery	7
1.2.5	Intercellular Signalling	8
1.2.6	Microenvironment & Physical Signalling	9
1.2.7	Resolution of Underlying Disease	10
1.3	The Ultrastructure and Cell Biology of the Liver	11
1.3.1	The Hepatocyte	12
1.3.2	Sinusoidal Endothelial Cells	12
1.3.3	Kupffer Cells	13
1.3.4	Pit Cells	13
1.3.5	Hepatic Stellate Cells	13
1.3.6	The Extracellular Matrix	15
1.4	Liver Regeneration	16
1.4.1	Animal Models	16
1.4.2	Partial Hepatectomy	17
1.4.3	Regenerative Cycle	18
1.4.4	Hepatocyte Priming & the Stimulus for Regeneration	18
1.4.5	Changes in Hepatic Blood Flow	19
1.4.6	The Innate Immune Response	20
1.4.7	Cytokines	21
1.4.8	Growth Factor Release and Action	22
1.4.9	Hepatocyte Growth Factor	22
1.4.10	Epidermal Growth Factor Receptor Ligands	23
1.4.11	Fibroblast Growth Factor 1 / Acidic & Fibroblast Growth Factor 2 / Basic	24
1.4.12	Other Factors	26
1.4.13	Termination of Regeneration	26
1.4.14	Transforming Growth Factor $_{\beta}$	27
1.4.15	Other Inhibitors of Regeneration	27
1.4.16	The Role of the Extracellular Matrix	27
1.5	Liver Tissue Engineering	29
1.5.1	Cell Sourcing in Liver Tissue Engineering	29
1.5.2	*In Vitro* Liver Tissue Engineering	30
1.5.3	*In Vitro* Signal Delivery	30
1.5.4	Scaffolds *In Vitro*	31
1.5.5	Spatial Signalling and Scaffold Structure	34
1.5.6	Applications for *In vitro* Liver Tissue Engineering	35

1.5.7	*In Vivo* Liver Tissue Engineering	36
1.5.8	Cell Delivery *In Vivo*	36
1.5.9	The Scaffold as a Delivery Device	38
1.5.10	Intrahepatic Scaffold Implantation	38
1.5.11	Applications for *In Vivo* Liver Tissue Engineering	39
1.5.12	Overview	40
1.6	Study Background, Design & Hypotheses	41
Chapter 2 Hepatocyte-HSC Co-Culture on Three-Dimensional Microporous $P_{DL}LA$ Scaffolds		43
2.1	Introduction	43
2.2	Materials & Methods	46
2.2.1	Hepatocyte Isolation	46
2.2.2	Hepatic Stellate Cell Isolation	46
2.2.3	Scaffold Manufacture	47
2.2.4	Allylamine Plasma Deposition	47
2.2.5	Sodium Hydroxide Treatment	48
2.2.6	Cell Seeding & Maintenance	48
2.2.7	Scanning Electron Microscopy	48
2.2.8	Albumin Production	49
2.2.9	Testosterone Metabolism Assay	50
2.2.10	Statistical Analysis	51
2.3.1	Results Morphology	52
2.3.2	Results Function	55
2.4	Discussion	60
2.5	Conclusion	64
Chapter 3 Polymer-Based Intra-Hepatic Growth Factor Delivery		65
3.1	Part 1: Implant Development & Pilot Study	68
3.1.1	Introduction	68
3.2	Materials & Methods	70
3.2.1	Implant Manufacture	70
3.2.2	Implant Characterisation: Micro CT	71
3.2.3	Animals	71
3.2.4	Anaesthetic Protocol	71
3.2.5	Operative Technique	72
3.2.6	Necropsy Protocol	73
3.2.7	Liver Weight Analysis	73
3.2.8	Liver Function	74
3.2.9	Processing & Histology	74
3.2.10	MIB-5 / Ki-67 Immunohistochemistry	74
3.2.11	Imaging and Analysis	75
3.2.12	Statistical Analysis	75
3.3	Results	76
3.4	Discussion	82
3.5	Conclusion	85
3.6	Part 2: A Comparative Study	86
3.6.1	Implant Manufacture	88
3.6.2	L-ECM Manufacture	89
3.7	Materials & Methods	91
3.7.1	Animals	91
3.7.2	L-ECM Isolation	92

3.7.3	Polymer Implants	93
3.7.4	Liver ECM Implants	93
3.7.5	Implant Characterisation: Liver-ECM Distribution	94
3.7.6	Implant Characterisation: Release Profiling	94
3.7.7	Anaesthetic Protocol & Operative Technique	95
3.7.8	Necropsy Protocol	96
3.7.9	Liver Weight Analysis	96
3.7.10	Processing & Histology	96
3.7.11	ED-1 Immunohistochemistry	97
3.7.12	Desmin Immunohistochemistry	97
3.7.13	BrdU Immunohistochemistry	98
3.7.14	Imaging and Analysis	98
3.7.15	BrdU Count	99
3.7.16	Statistical Analysis	100
3.8	Results	102
3.8.1	BrdU Immunohistochemistry: Implant *versus* Sham	116
3.8.2	BrdU Immunohistochemistry: Implant *versus* Control	116
3.9	Discussion	121
3.9.1	Implant Characterisation	121
3.9.2	Liver Weights	123
3.9.3	Histological Characterisation	124
3.9.4	ECM Deposition & Cell Migration	124
3.9.5	The Peri-implant Parenchyma	127
3.9.6	Vascular Proliferation	127
3.9.7	The L-ECM Only Implant	128
3.9.8	Proliferation	129
3.9.9	MIB-5 Immunohistochemistry	131
3.9.10	Summary	132
3.1	Conclusions	134
Chapter 4 Intrahepatic Growth Factor Delivery Following Partial Hepatectomy		135
4.1	Introduction	135
4.2	Materials & Methods	139
4.2.1	Animals	139
4.2.2	Study Implant Manufacture	139
4.2.3	Anaesthetic Protocol	140
4.2.4	Operative Technique	140
4.2.5	Necropsy Protocol	141
4.2.6	Liver Weight Analysis	142
4.2.7	Histology, H & E and BrdU Immunohistochemistry	142
4.2.8	BrdU Count	142
4.2.9	Liver Function	144
4.2.10	Statistical Analysis	144
4.3	Results	145
4.4	Discussion	158
4.4.1	Study Design & Pilot	158
4.4.2	Liver Weight Analysis	159
4.4.3	Liver Function	161
4.4.4	Basic Histology	161
4.4.5	Proliferation	162
4.4.6	Summary	163
4.5	Conclusion	165

Chapter 5 166

5.1 *In vitro* study 166
5.2 *In vivo* study 168
5.3 The Future of Liver Tissue Engineering for Liver Surgery 169

Bibliography 171

Appendices

A1 Appendix 1 180
A2 Appendix 2 181
A3 Appendix 3 182
A4 Appendix 4 183
A5 Appendix 5 184
A6 Appendix 6 185
A7 Appendix 7 186
A8 Appendix 8 187

Table of Figures

Figure

1.1 The burden of liver disease in the U.K. 4
1.2 Schematic of liver lobule 11
1.3 Mouse livers before and after PH 17
1.4 The multi-step model of liver regeneration 19
1.5 Liver regeneration 28
2.1 Hepatocyte-HSC co-culture 44
2.2 SEM of hepatocytes mono-culture 52
2.3 SEM of HSC mono-culture 53
2.4 SEM of hepatocyte-HSC co-culture 54
2.5 Synthetic Function 1 55
2.6 Synthetic function 2 56
2.7 Synthetic function 3 57
2.8 Metabolic function 1 58
2.9 Metabolic function 2 59
3.1 Implant development and pilot study design 69
3.2 Pilot implant 76
3.3 Pilot LBWs 77
3.4 Pilot ASTs 78
3.5 Pilot H&E mapping 79
3.6 Pilot H&E overview 80
3.7 Pilot MIB-5 immunohistochemistry 81
3.8 Impact of PEG on the Tg of PLGA 89
3.9 Comparative study design 91
3.10 Image J analysis methodology 99
3.11 BrdU image mapping 100
3.12 Comparative study implants 102
3.13 Quantitative release data 102
3.14 Bioactivity release data 103
3.15 Comparative LBWs 104
3.16 Comparative MTRs 105

3.17	Comparative H&E overview	106
3.18	H&E at T_0 & day 2	107
3.19	Plain-polymer at days 7 and 56	108
3.20	Day 7 comparison	108
3.21	Neovascular and inflammatory changes	109
3.22	Liver tissue in growth comparison	110
3.23	Peri-implant inflammatory band thickness comparison	111
3.24	Masson's trichrome staining	112
3.25	ED-1 immunohistochemistry	113
3.26	Desmin immunohistochemistry	114
3.27	L-ECM only implant	115
3.28	BrdU comparison	117
3.29	Day 4 BrdU IHC	118
3.30	BrdU immunohistochemistry demonstrating banding	119
3.31	BrdU band comparison	119
3.32	Non-parenchymal cell proliferation	120
4.1	Partial hepatectomy study design	138
4.2	Image map for BrdU scoring following partial hepatectomy	143
4.3	Cumulative mean of BrdU scoring	143
4.4	Necropsy following PH	145
4.5	PH LBWs	146
4.6	PH ITWs	147
4.7	Serum ASTs	148
4.8	PH H&E overview	149
4.9	Mitosis, neovascularisation & inflammation after PH	150
4.10	BrdU immunohistochemistry overview	151
4.11	BrdU immunohistochemistry 2 days after PH in a non-implanted liver	152
4.12	BrdU immunohistochemistry banding comparison	153
4.13	BrdU immunohistochemistry at day 1 & 2 after PH	154
4.14	BrdU comparison	155
4.15	PH + implant BrdU banding comparison day 1	156
4.16	PH + implant BrdU banding comparison day 2	156
4.17	Implant + PH BrdU banding comparison day 1	157
4.18	Implant + PH BrdU banding comparison day 2	157
4.19	ITW curves	161
A1	Schematic for $P_{DL}LA$ cut down	180
A2	Schematic of Teflon mould design	181
A3	Photograph of vacuum press circuit	181

List of Tables

3.1	Growth factor dosage for the pilot study	71
3.2	Summary of growth factor infusion in normal liver	87
3.3	Growth factor dosage for the comparative study	93
3.4	Percentage BrdU positive hepatocytes in the comparative study	117
3.5	Proliferative markers in rat liver	131
4.1	Summary of growth factor infusion following partial hepatectomy	136
4.2	Growth factor dosage for the partial hepatectomy study	140
4.3	Resected lobe weight analysis	145
4.4	Percentage BrdU positive hepatocytes in the partial hepatectomy study	155
A1	Processing schedule	182

Abbreviations

ABC	Avidin-biotin complex
ALF	Acute liver failure
ANOVA	Analysis of Variance
ASGPR	asialoglycoprotein receptor
AST	Aspartate aminotransferase
BrdU	5-bromo-2-deoxyuridine
C	Complement
c-GMP	Cyclic guanosine monophosphate
CT	Computed tomography
CYP	Cytochrome P450
d	Deionised
DAB	3.3'-diaminobenzidine
DMEM	Dulbecco's Modified Eagle Medium
DPX	Di-n-butyl phthalate in xylene
EBSS	Earle's balanced salt solution
ECM	Extracellular matrix
EDTA	Ethylenediaminetetraacetic acid
EGF (R)	Epidermal growth factor (Receptor)
EGTA	Ethylene glycol tetra acetic acid
ELISA	Enzyme-Linked ImmunoSorbent Assay
EtO	Ethylene oxide
FCS	Fetal calf serum
FGF (R)	Fibroblast growth factor (receptor)
GAG	Glycosaminoglycans
H&E	Hematoxylin & eosin
HB	Heparin-binding
HCC	Hepatocellular carcinoma
HPLC	High performance liquid chromatography
HRP	Horseradish peroxidase
HSC	Hepatic stellate cells
IACUC	Institutional Animal Care & Use Committee
ICAM	Intercellular adhesion molecule
IHC	Immunohistochemistry
IL (R)	Interleukin (Receptor)
IP	Interferon gamma induced protein
LBW	Liver: body weight ratio
L-ECM	Liver derived ECM
LPS	Lipopolysaccharide (endotoxin)
MAP	Mitogen-activated protein
MET	Mesenchymal-epithelial transition factor
MHC	Major histocompatibility complex
MIG	Monokine induced by gamma interferon
MIP	Macrophage Inflammatory Protein
MMP	Matrix metalloproteases
MTR	Middle: total liver weight ratio
NA	Noradrenaline
NFκB	Nuclear factor κ B
NO (S)	Nitric oxide (synthase)
PBS (T)	Phosphate buffered saline (Tween)
PCS	Porto-caval shunting
$P_{DL}LA$	Poly (D,L-lactic acid)
PEG	Poly (ethylene glycol)
PET	Polyethylene terephthalate
PH	Partial hepatectomy
PLA	Poly (lactic acid)
PLGA	Poly (lactic-co-glycolic acid)
PLLA	Poly (L-lactic acid)
PDMS	Polydimethylsiloxane
PTFE	Poly (tetrafluoroethene)
PVA	Polyvinyl acetate
PVLA	polyvinylbenzyl-galactopyranosyl-gluconamide
rh	Recombinant human
RLV	Residual liver volume
SEM	Scanning electron microscopy
SPSS	Statistical Package for the Social Sciences
STAT	Signal Transducers and Activator of Transcription
TBS	Tris-Buffered Saline
TCP	Tissue culture plastic
TEM	Transmission electron microscopy
T_g	Glass transition temperature
TGF	Transforming growth factor
TMB	3,3',5,5'-Tetramethylbenzidine
TNF	Tumor necrosis factor
Tris	Tris (hydroxymethyl) aminomethane
Tween	Polysorbate 20
UDP	Uridine diphosphate
VEGF	Vascular endothelial growth factor
μ-CT	Micro computed tomography

Acknowledgements

To Mr Ian Beckingham, Professor Kevin Shakesheff & Professor Brian Rowlands for their support and guidance throughout my research fellowship, for giving me the freedom to develop new ideas and the direction to keep the work on track.

Dr Steve Badylak for the opportunity to spend six months in his excellent laboratory at the McGowan Institute for Regenerative Medicine in Pittsburgh, for welcoming me into his research group and making my time there so productive.

Dr Abed Zaitoun and Professor George Michalopoulos for their knowledge of liver regeneration, interpretation of liver histology and blinded validation of the proliferative data.

The Royal College of Surgeons of England & the Wellcome Trust for their Clinical Research Training Fellowship Awards.

I would also like to acknowledge:

John Barry, Jennifer De Barr, Neil Hand, Daniel Howard, Buffie Kerstigier, Scott Johnson, Teresa Marshall, Kate Shepherd, Ann Stewart-Akers, Iain Walker, Lisa White, Anne Wilson & Tollevin S. Williams.

Statement of Originality

The work contained in this thesis has been conceived and designed by me with guidance from Mr Ian Beckingham, Professor Kevin Shakesheff, Dr Steve Badylak and Professor George Michalopoulos. The cell culture, scaffold design and production were performed in the Nottingham Tissue Engineering Group laboratories at the University of Nottingham. The animal work was piloted in the Biomedical Sciences Unit at University of Nottingham Medical School and undertaken at the M^{c}Gowan Institute for Regenerative Medicine at the University of Pittsburgh. Histology and immunohistochemistry were performed in the Departments of Pathology at University Hospital Nottingham and the University of Pittsburgh Medical Centre.

The pilot animal study was conducted in accordance with protocols set out in the Home Office Project Licence PPL 40/2880 using personal licence PIL 40 / 8256. The comparative and partial hepatectomy studies were conducted in accordance with protocols set out in the University of Pittsburgh's Institutional Animal Care and Use Committee Protocols 0609564-2 and 0612048-2 respectively.

All the work presented in this thesis has been performed by me with the exception of: supercritical polymer processing and micro x-ray analysis, performed by Daniel Howard, John Barry and Lisa White; histological processing and staining, performed by Anne Wilson in Nottingham and Jennifer De Barr in Pittsburgh; immunohistochemistry, performed by Neil Hand in Nottingham and by Ann Orr in Pittsburgh; and serum biochemistry, performed by staff in the clinical chemistry departments of Nottingham University Hospital & UPMC Children's Hospital.

Abstract

This thesis presents the development and evaluation of two applications for scaffolds in the field of liver tissue engineering. In the first study a poly (D,L lactic acid) ($P_{DL}LA$) scaffold is used as a three-dimensional template for hepatocyte–hepatic stellate cell (HSC) co-culture. To enhance $P_{DL}LA$ ligand binding capacity scaffolds are surface modified using allylamine plasma deposition and treatment with NaOH. Primary adult rat hepatocytes and HSC are then seeded onto these scaffolds and cultured in static conditions. Scanning electron microscopy (SEM) is used to assess mono-culture and co-culture morphology whilst synthetic and cytochrome P_{450} function are measured using albumin and testosterone assays.

The second study explores the potential for intrahepatic growth factor and extracellular matrix (ECM) delivery from a biodegradable polymer scaffold to promote liver growth and to enhance regeneration. The study is undertaken in rats. The scaffold design and implantation technique are first piloted in a short survival study. Hepatocyte growth factor (HGF), epidermal growth factor (EGF), fibroblast growth factor $(FGF)_1$, FGF_2 and liver derived ECM (L-ECM) are then loaded into poly(lactic-*co*-glycolic acid) (PLGA) + 5% poly(ethylene glycol) (PEG) scaffolds and implanted into normal and partially hepatectomised liver. Implant morphology is assessed by micro-CT reconstruction. Growth factor bioactivity and release are confirmed by *in vitro* profiling. Liver growth and volume redistribution are assessed by liver weight analysis. Parenchymal injury and function are quantified by measuring serum aspartate aminotransferase (AST) & bilirubin. 5-bromodeoxyuridine (BrdU) inclusion & MIB-5 immunohistochemistry (IHC) are used to identify hepatocyte and non-parenchymal cell proliferation. Liver-scaffold interaction is characterised by H&E and Masson's trichrome staining. Non-parenchymal cell migration is assessed by ED-1 and desmin IHC. All histology is then subjected to image analysis.

Chapter 1 Introduction

1.1 Liver Surgery

Liver surgery has evolved within one surgical lifetime into a repertoire of operations that can remove or replace nearly any amount of liver tissue [1]. Liver resection and transplantation are first line treatments for a range of liver diseases, and in the case of malignant disease and liver failure, offer the only chance of a cure [2-4].

1.1.1 Surgery for Liver Cancer

Primary and secondary liver cancers are common and their incidence and mortality rates in the UK are rising [5, 6] (*figure 1.1, top left*). Hepatocellular carcinoma (HCC) is responsible for approximately 1,500 deaths per year in the U.K. [7]. Without treatment 20% of patients will survive for 3 years [7], with liver transplantation survival is improved to 65% at 5 years [3, 8]. Liver resection for HCC offers similar short term survival to transplantation, but local recurrence rates at five years are much higher (50-60%) [3]. Currently therefore liver transplantation offers the best chance of cure for HCC, but a chronic shortage of donor tissue means that this is not available for every patient [7](*figure 1.1, bottom left*).

The liver is also a common repository for tumour cells, second only to lymph nodes as a site for metastatic disease [9]. Frequently liver metastases are associated with systemic malignancy, however as the liver is the first major organ reached by venous blood

draining from the intestinal tract; the liver may be the only site of metastatic disease from the large intestine [2]. Without treatment the 5 year survival for patients with colorectal liver metastases is less than 5% [10]. This improves to 37% with resection [2, 11]. It is estimated that 5-10 % of all patients with colorectal liver metastases are eligible for resection [9], which equates to over one thousand patients per year in the UK [12]. The extent of resection remains limited by the need to retain an adequate post-resection residual liver volume, a failure to do so resulting in higher rates of liver dysfunction and other complications [13, 14] (*figure 1.1, top right*). Developing strategies to boost functional liver capacity or enhance regeneration may improve outcome in patients undergoing radical resection.

1.1.2 Surgery for Liver Failure

Cirrhosis and liver failure are the leading causes of death from non-malignant digestive diseases in the U.K. [12] and their incidence is rising [15]. The only established treatment for liver failure is transplantation [16]. Without it liver failure has a mortality rate of 60-80% [17], but with transplantation the one year survival is over 90% and the predicted ten year survival is over 70% [4]. Unfortunately with increasing demand for donor tissue one third of patients die while waiting for a liver transplant [16] (*figure 1.1, bottom right*). If it were possible to provide extracorporeal liver support to these patients as their livers regenerated or as a bridge to transplantation it may be possible to further improve survival in this challenging group.

1.1.3 The Future of Liver Surgery

With the incidence and mortality rates of liver disease in the UK rising, a new set of challenges exist for clinicians and scientists. Further developments in surgical technology and local and systemic treatments for malignant and non-malignant disease will continue to improve patient outcome, but to address the major challenges of donor shortfall and functional liver support new therapeutic pathways must be explored. The following sections will explore how regenerative medicine may offer the solution.

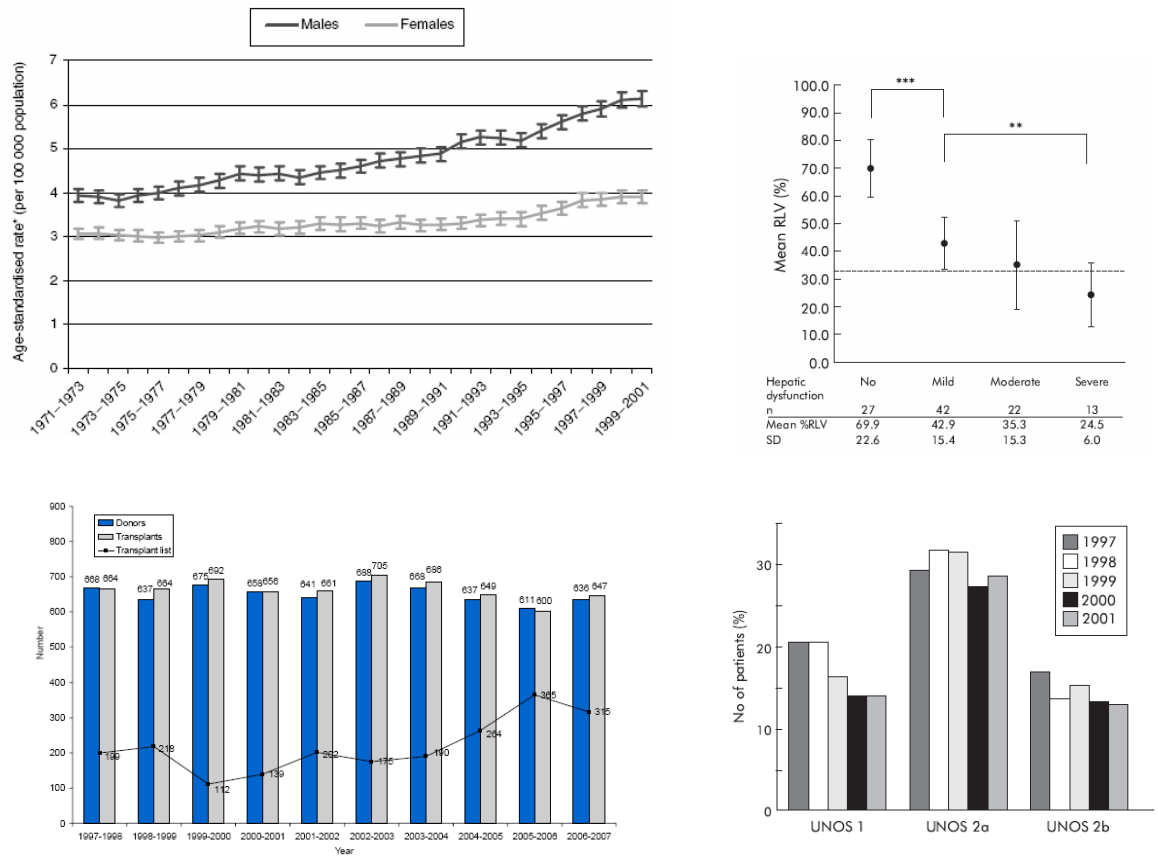

Figure 1.1 A snapshot of the burden of liver disease in the U.K. Trends in age-standardised incidence rates from 1971 to 2001 in England and Wales of all malignant cancers of the liver, gallbladder and biliary tract, by sex (3 year rolling averages). Bars are standard errors (*top left*) [6]. Mean (SD) relative residual liver volume (RLV %) in patients with no, mild, moderate, and severe hepatic dysfunction following liver resection (one way between group ANOVA; **p = 0.005,***p,0.0001). Reference line indicates 33% residual liver volume (*top right*) [13]. Deceased donor liver programme in the UK, 1 April 1997 - 31 March 2007 Number of donors, transplants and patients on the active transplant list at 31 March 2007 (*bottom left*) [18]. Annual death rates on the waiting list for liver transplantation between 1997 and 2001 in UNOS categories 1 (acute/fulminant liver failure), 2a (decompensated chronic liver disease urgently requiring transplant), and 2b (decompensated chronic liver disease requiring transplant less urgently) (*bottom right)* [16].

1.2 Regenerative Medicine

Regenerative medicine is a modern scientific discipline that seeks to capture the intrinsic power of biology to replace, regenerate or repair diseased or damaged tissue [19]. Tissue growth and regeneration are complex processes that vary between tissues, with age and in the presence of disease. Designing tailor-made regenerative medicine solutions requires a clear understanding of the target tissue's ultrastructure and cell biology as well as the pathophysiology of any underlying disease process.

As a result of inter-tissue and inter-disease variation, it is not possible to present a single solution to tissue design and assembly. Instead this chapter focuses on the core challenges of therapeutic regenerative medicine (cell sourcing, signal delivery and disease resolution) and presents a range of successful strategies.

1.2.1 Cell Sourcing

The ability to source cells and modulate tissue growth is a central concept in regenerative medicine. In order to increase the functional capacity of a target tissue, the cell population must be restored. This can be achieved either by stimulating growth or regeneration in the native cell population or by delivery of regeneration-competent cells from an exogenous source (autologous, allogeneic or xenogeneic, differentiated or undifferentiated stem or progenitor cells) [20].

Stimulating a tissue to grow or regenerate may be achievable if appropriate signals are delivered to the native cell population. However this approach is limited by the native tissue's capacity for self-renewal. Exogenous cell delivery also has a range of advantages and disadvantages. Autologous cell implantation is non-immunogenic but provides relatively low yields and is usually associated with some donor site morbidity. Allogeneic and xenogeneic cells are readily available but unpopular due to concerns over immunogenicity and risk of infection. Stem and progenitor cell delivery therefore offers the greatest potential as a tissue-specific, renewable cell source for tissue engineering but remains in the early stages of development [20].

1.2.2 Signal Delivery

In order to stimulate a tissue to regenerate or to assemble *de novo* appropriate cell signals must also be delivered. In general four classes of signal should be considered when designing a tissue engineering application: growth factor and cytokine signals, extracellular matrix (ECM) signals, intercellular interactions and physical signals (spatial, mechanical, electrical and microenvironment) [21, 22]. A detailed understanding of the target tissue's ultrastructure and cell biology is therefore a prerequisite for effective design.

A range of natural or synthetic constructs, known as "scaffolds", can be used for signal delivery [23]. The role of these scaffolds varies between applications. They may be used simply as a supportive framework for *in vitro* or *in vivo* tissue assembly or as a more complex signal delivery system.

1.2.3 Cytokine and Growth Factor Delivery

Cytokines and growth factors play a key role in regulating tissue growth and regeneration. These molecules, which are released locally and systemically, bind to cell-surface receptors that trigger intracellular signalling cascades [21]. Their actions vary between tissues, at different stages of development, at different concentrations and can also be influenced by the presence of other growth factors.

A range of controlled release systems have been utilised for growth factor delivery. These systems are capable of delivering molecules at different rates, for different durations in different tissues. For example, hydrogel based systems provide a rapid but short release profile [21, 24], whilst protein encapsulation into solid polymers by double emulsion techniques or supercritical processing may provide a more sustained release profile [24, 25]. Alternatively growth factors and other bioactive molecules may be bound to the surface of polymers and are only released upon cell mediated degradation of the scaffold [24]. The challenge in developing a tissue specific strategy is to determine the regenerative cycle of that tissue and match the growth factor (s) and release technology accordingly.

1.2.4 Extracellular Matrix Signal Delivery

The ECM is an insoluble network of proteins and carbohydrates that provides architectural and structural integrity to a tissue and enables phenotypic expression, migration and regeneration of its cell population [21, 26, 27]. The basic structure of the ECM is defined by a collagen scaffold. Adhesive glycoproteins (laminin, tenascin) and proteoglycans adhere to

this scaffold and interact with the cells in or adjacent to it via matrix receptors (integrins) [26]. This integrin-mediated cell-matrix binding, stimulates intracellular signalling cascades that can result in functional changes within the cell as well as aiding cell spreading and migration [21]. Deposited throughout the ECM are also cytokines and growth factors, matrix metalloproteases (MMPs), which promote ECM remodelling [27], and collagen breakdown products that exert their own chemoattractant forces [28].

ECM signals may be delivered to the target tissue in a number of ways. *In vitro*, ECM molecules or ECM-like molecules may be delivered by coating culture surfaces with ECM products or incorporating ECM proteins into gels and scaffolds [24, 29, 30]. *In vivo* whole sheets of decellularised animal derived ECM may be implanted to aid wound repair and tissue regeneration. This approach has been used very effectively to induce regeneration without immunogenic or inflammatory reaction [31]. ECM may also be delivered directly by ECM producing cells incorporated into a cell-based tissue engineering system. For example hepatic stellate cells (HSC) release ECM and improve hepatocyte viability and function *in vitro* [32-34].

1.2.5 Intercellular Signalling

Homotypic and heterotypic intercellular interactions are important in many cell types for normal expression of phenotype and retention of regenerative capacity. Intercellular interactions occur either through direct contact (tight junctions, gap junctions, cadherins and desmosomes) or via secreted molecules (ECM components, cytokines and growth factors) [21]. In order to assemble a tissue *de novo* or stimulate regeneration the tissue

engineer must re-establish these signalling pathways. Soluble factors and ECM components may be delivered as described previously, but to restore normal intercellular interactions, appropriate cells must be sourced and delivered into a micro-environment optimised for that cell population.

1.2.6 Microenvironment & Physical Signalling

Restoration of normal microenvironment and delivery of appropriate physical signals are essential for functional tissue assembly. *In vitro*, cells exposed to the correct oxygen partial pressure retain phenotype and have enhanced migration, proliferation and function [35-37]. Optimisation of cell culture microenvironment may be achieved within a closed system bioreactor, where different physical parameters can be regulated. Once conditions have been standardised for specific cell and tissue types, the potential to scale-up the system becomes more realistic. *In vivo* microenvironment is also important. Implantation sites must have adequate blood supply and be free from underlying disease. Vascular access, implantation site and method of delivery must therefore be considered in the development process.

Spatial signals influence phenotype and function. Growing cells in three-dimensions increases cell-cell contact, mimics *in vivo* architecture and encourages the formation of differentiated ultrastructure [21, 33, 38]. If a scaffold is to support a cell population it should deliver the appropriate spatial cues either by providing a temporary three-dimensional support (as with many biodegradable porous constructs) or by directly mimicking the

complex architecture of the target tissue ECM, through a range of novel manufacturing techniques[38-40].

Electrical and mechanical signals have also been implicated in tissue morphogenesis and regeneration. Electrical signalling enhances nerve and muscle regeneration [22, 41, 42] and mechanical forces have been shown to influence cell orientation, migration and ECM deposition in dermal tissue [40, 43].

1.2.7 Resolution of Underlying Disease

The aim of regenerative medicine is to replace, regenerate or repair diseased or damaged tissue [19]. The resolution of underlying disease is therefore central to the success of any regenerative medicine strategy. The microenvironment of diseased tissue may not be supportive of an implanted cell population and the underlying disease process may also affect the implanted tissue. It is desirable to ensure adequate treatment or excision of the diseased tissue before implantation or to consider implantation at an alternative site.

The tissue engineering system may also be used to treat underlying disease. Implantation of a cell based or controlled release system may positively influence disease resolution through the modulation of inflammation and the restoration of functional tissue rather than non-functional fibrous material. This has been achieved in a range of tissues through the delivery of ECM signals that encourage regeneration without scarring [44].

1.3 The Ultrastructure & Cell Biology of the Liver

The liver has a unique architecture. In figure 1.2 it is viewed at a microscopic level, demonstrating the relationship between its ultrastructural building blocks: the portal tracts (comprising branches of the hepatic artery, portal vein & bile ducts); the lobules (the structural unit of the liver, comprising a prism of parenchymal plates which surround the sinusoidal channels that run from the peripheral portal tracts to a central vein), and its individual functional components (cells and the ECM).

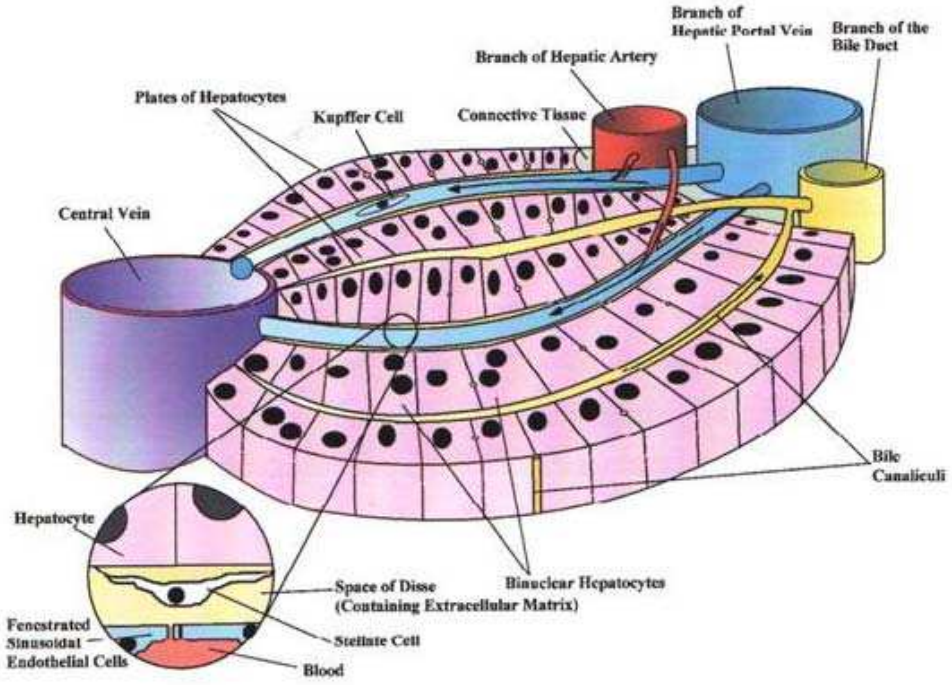

Figure 1.2 Schematic of liver lobule [45]

1.3.1 The Hepatocyte

Hepatocytes make up 87% of the total liver volume and are its key functional component. *In vivo*, hepatocytes are attached in parallel plates that run from a portal tract to a central vein, with a sinusoid on one side and a bile canaliculus on the other (Figure 1.2). Along the length of the sinusoid hepatocytes are exposed to different oxygen partial pressures and metabolic conditions. This gradient directly influences hepatocyte phenotype and results in hepatocyte sub-populations with different functional profiles [46]. *In vivo* normal hepatocyte function requires a stable microenvironment and normal ultrastructure. Disruption of these by toxic injury or fibrogenesis causes hepatocyte dysfunction [47]. Likewise, *in vitro* the hepatocyte is also sensitive to changes in its microenvironment. Hepatocytes cultured in non-enhanced culture conditions rapidly loose function (de-differentiation) and die. When signals and microenvironment mimicking *in vivo* conditions are restored, so too are hepatocyte viability and function [48].

1.3.2 Sinusoidal Endothelial Cells

Sinusoidal endothelial cells make up 2.5% of the total liver volume. *In vivo* they act as a filtration system for fluid passing from the sinusoidal lumen into the space of Disse and regulate uptake of lipid, cholesterol and vitamin A [49]. *In vitro* isolated endothelial cells differentiate in response to ECM exposure and when co-cultured with hepatocytes form heterotypic aggregates with differentiated hepatic ultrastructure and enhanced hepatocyte functionality [50, 51].

1.3.3 Kupffer Cells

Kupffer cells make up 2% of the total liver volume, and are found anchored to or inserted into the endothelial lining. They are the primary immune cell of the liver and are responsible for clearing damaged and foreign material from the blood (old cells, cellular debris, parasites, bacteria, viruses and tumour cells). When activated they secrete a range of cytokines (TNFα, IL-1, IL-6) and other pro-inflammatory mediators (prostaglandins, peroxidases, NO), regulated by autocrine and negative feedback loops. Their activation occurs in response to a range of stimuli (resection, ischaemia, toxins), and is central to the liver's response to injury [49]. Of particular interest is how Kupffer cells as part of the innate immune response prime hepatocytes for regeneration.

1.3.4 Pit Cells

Pit cells make up <1% of total liver volume and are located in or on the endothelial lining. They are morphologically similar to large granular lymphocytes and possess a MHC class II unrestricted killer cell activity against tumour cells and virus infected cells [49].

1.3.5 Hepatic Stellate Cells

HSC (also known as Ito cells, vitamin A storage cells, lipocytes or fat-storage cells) make up 1.4% of the total liver volume [49]. In the normal liver they have a myofibroblast-like morphology with an additional fat storage component, and are found in the space of Disse,

separated from the sinusoidal lumen by the endothelial filter. HSCs communicate with the sinusoidal endothelium, ECM and parenchyma via long cytoplasmic processes [52, 53].

The HSC exhibits two phenotypes: a quiescent vitamin A storage type and an activated type. The quiescent HSC is characterised by the presence of cytoplasmic lipid droplets. Upon activation the cell looses these lipid droplets and transforms into a pure myofibroblast-like cell, expressing α-smooth muscle actin and desmin [47].

The HSC has a number of important functions. The quiescent HSC stores and regulates vitamin A levels and can induce contraction and dilation of the sinusoidal lumen in response to a range of stimuli (prostaglandins, endothelin, thromboxane). The activated HSC plays an important role in liver regeneration and ECM remodelling in health and disease by the production of ECM components (collagen types I, III, IV & VI, fibronectin, laminin, proteoglycans and MMPs), growth factors (HGF, TGFα, TGF_{β}) and cytokines. The role of the HSC in ECM remodelling and fibrogenesis has made it a potential target for modulation of fibrogenesis in specific disease states [47].

In vitro the phenotype of the HSC is influenced by the culture micro-environment. When isolated HSC are cultured on tissue culture plastic they become activated, proliferate and secrete ECM and growth factors, similar to the HSC seen *in vivo* following liver injury. When HSC are cultured in an ECM rich environment, they revert to their quiescent phenotype, again demonstrating the importance of the ECM in regulating liver cell function [47, 49]. How the HSC impacts on hepatocyte viability and function in culture will be discussed in detail in chapter 2.

1.3.6 The Extracellular Matrix

The liver ECM makes up 3% of the total liver volume. The main sites of ECM within the liver are the external capsule (Glisson's capsule), the portal tracts, the sinusoidal walls and the central veins. Its major constituents are collagens (types I, III, IV, V and other isoforms), glycoproteins (laminin, fibronectin, tenascin, nidogen amongst others) and proteoglycans (dermatan, chondroitin sulphate, hyaluronic acid, byglycan and decorin). In addition stored within this network are a cocktail of growth factors (HGF, EGF TGF_{β}), hormones (insulin), cytokines and enzymes (matrix metalloproteases (MMPs)), which can be liberated as the ECM is broken down [54].

The liver ECM has a dual function; it provides mechanical coherence and resistance, and regulates cell proliferation, migration, differentiation and gene expression by providing a network that allows the continuous exchange of signals between cells. In the early phase of regeneration ECM remodelling provides the first burst of growth factor release [54]. Abnormal ECM deposition (fibrosis) is a major cause of chronic hepatic dysfunction, leading to reduced endothelial porosity (leading to impaired sinusoidal exchange), changes in HSC phenotype (quiescence to activation) and impaired hepatocyte function [54].

1.4 Liver Regeneration

Liver regeneration is an orchestrated response induced by specific external stimuli and involving sequential changes in gene expression, growth factor production and morphologic structure [55]. The capacity of the liver to heal is unique. Because of the organ's susceptibility to major cellular damage and the impact this would have on the organism's survival, numerous pathways have evolved to ensure that restoration of hepatic functional mass is achieved, even if components of these pathways are lost [56]. Throughout regeneration the liver tissue retains its functional capacity, in contrast to other organ systems where function is lost or impaired whilst regeneration takes place.

1.4.1 Animal Models

The use of animal models has been central to our understanding the pathways that regulate liver regeneration. To provoke a regenerative response, two strategies can be employed: surgical resection or toxic injury. Surgical resection by partial hepatectomy (PH) enables the study of regeneration in normal liver [57]. Toxic injury models are more complex, because by causing generalised hepatic injury, the resultant regenerative response requires both inflammation and proliferation. This review will focus on the pathways elucidated from the PH model.

1.4.2 Partial Hepatectomy

The model of PH devised by Higgins and Anderson in 1931 enables the study of regeneration in normal liver [57]. As the liver lobes in the rat are separate and have long vascular hila it is possible to resect lobes without compromising vascular inflow to the residual liver tissue.

Following resection of the left and middle lobes (70% hepatectomy) the residual liver will undergo compensatory hyperplasia and hypertrophy until the original liver mass has been restored at which point regeneration halts. The end result being a restoration of liver mass, but not regrowth of the resected lobes.

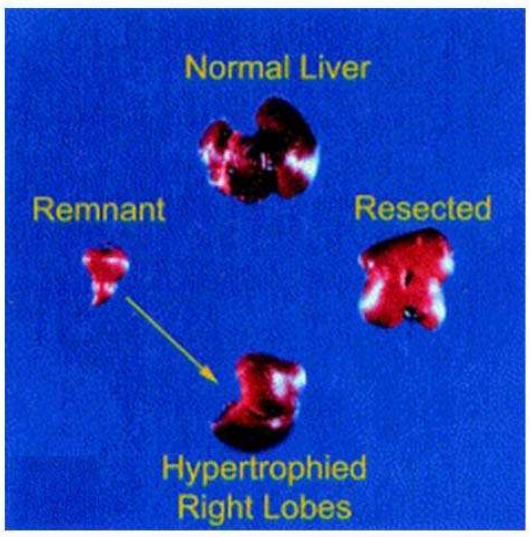

Figure 1.3 Normal mouse livers before and after 70% partial hepatectomy and the regenerated remnant 6 days later [58]

1.4.3 The Regenerative Cycle

After 70% PH in the rat, most liver mass is restored by day 3 and regeneration is complete by day 7 [57]. This repopulation is achieved by proliferation of the hepatocyte population [59]. This occurs as a wave of proliferation beginning in the peri-portal zones spreading towards each central vein [60]. Hepatocyte DNA synthesis begins to increase 12 hours after PH and peaks at 24 hours. The non-parenchymal cell response is slower, with DNA synthesis peaking at 48 hours. Regeneration will be complete within 1.6 cycles of replication [61, 62]. Whilst this process is associated with modifications in cell-cell and cell-matrix interactions, full restoration of normal architecture will not occur until liver mass has been restored, thereby optimising the return to normal function [56, 62].

In other liver injury models, different cell populations (the oval cell, haematopoietic stem cells) differentiate and proliferate to repopulate the liver; however their contribution is not significant following PH [63].

1.4.4 Hepatocyte Priming & the Stimulus for Regeneration

The normal hepatocyte resides in its quiescent G_0 state, and does not enter G_1 of the cell cycle until it has been has been "primed" (the process that sensitizes a cell to growth factors, leading to DNA replication and proliferation) (figure 1.4) [64]. As a result in healthy liver less than 1% of all hepatocytes are in mitosis at any one time [65].

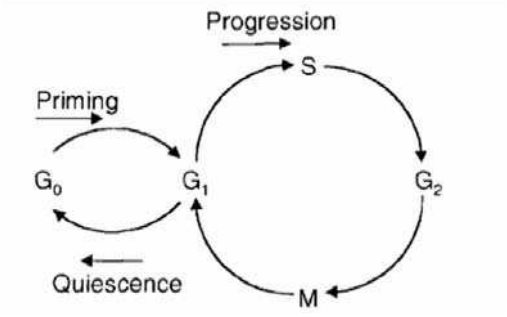

Figure 1.4 The multi-step model of liver regeneration proposed by Fausto, in which liver regeneration is divided into 2 phases, priming and cell cycle progression [64]

Hepatocyte priming occurs in response to a range signals initiated simultaneously within the liver. Following PH hepatic blood flow is altered [66, 67]and the innate immune system is triggered [59, 68]. The non-parenchymal cell population becomes activated, releasing cytokines and growth factors that causing the hepatocyte population to move from quiescence into the S-phase of the cell cycle.

1.4.5 Changes in Hepatic Blood Flow

Nitric Oxide (NO) is a free radical that influences a wide range of physiological processes throughout the body. It is synthesised from L-arginine by nitric oxide synthase (NOS) and mediates many but not all of its physiological functions via the activation of soluble guanylate cyclase and the resultant increase in cGMP levels [69]. In the normal liver, NO is present at only low levels where it is thought to regulate hepatic blood flow [70]. Following PH levels of NO increase [71, 72] This increase in NO production has been shown to exert a protective affect on the liver, by inhibiting apoptosis and other cytokine mediated responses[70].

The mechanism of NO release following PH relates to changes in hepatic blood flow. After PH, all the blood from the portal circulation passes through the much smaller residual liver tissue. It has been shown that this increase in sinusoidal blood flow causes an increase in endothelial shear stress, and that this shear stress is associated with NO release [73]. This relative increase in portal vein blood flow through the residual liver reduces oxygen partial pressure in the sinusoidal blood and may cause hypoxic changes within the liver parenchyma. In addition it increases the availability of hepatotrophic stimuli passing though the liver (EGF, insulin, lipopolysaccharide (LPS) and nutrients) [74]. Together these changes act as the trigger for regeneration after PH [74, 75].

1.4.6 The Innate Immune Response

Part of the liver's unique regenerative capacity stems from its ability to modify the host immune response by releasing immunomodulatory molecules that are active in restoring the structural and functional integrity of the liver [68]. The innate immune system, which exists to provide a rapid response to a wide spectrum of pathogenic signals, becomes activated after PH. It does so in a number of ways.

Levels of LPS, a key activator of the innate immune system, are increased following PH. In its absence the regenerative cycle is impaired [76, 77]. Complement activation has also been shown to influence liver regeneration after PH. C5a enhances the LPS dependent release of (interleukin) IL-6 from Kupffer cells and inhibition of C3a and C5a significantly impairs liver regeneration after PH [78, 79]. Other components of the innate immune system are also

upregulated during liver regeneration after PH. These include acute phase proteins [79] and intracellular adhesion molecules (ICAMs) [80].

1.4.7 Cytokines

TNFα and IL-6 are responsible for "priming" hepatocytes for proliferation [64], and it appears that it is the interplay between these cytokines and growth factors that regulates liver regeneration [59].

Following PH Kupffer cells release TNFα [81]. This release occurs in part due to activation of the innate immune response [64]. TNFα binds to TNF receptors on both Kupffer cells and hepatocytes [82]. In both cell types this leads to activation of nuclear factor κ B (NFκB). In the Kupffer cell causing an upregulation of IL-6 [55, 83], and in the hepatocyte, "priming" the cell to make it more receptive to the effects of growth factors [84]. TNFα is itself not directly mitogenic to hepatocytes; however its inhibition does slow the regenerative response [85].

IL-6 released by Kupffer cells binds to its receptor (IL-6R), which activates MAP kinase and STAT3 signalling cascades [86]. These signalling pathways activate the acute phase response, inhibit cell death and prime for regeneration [59]. At normal physiological concentrations IL-6 is not directly mitogenic to hepatocytes, however its over-expression is associated with hepatic hyperplasia [87, 88].

1.4.8 Growth Factor Release & Action

Once the hepatocyte has been primed, it becomes more sensitive to the effects of growth factors. A number of growth factors have been implicated in liver regeneration; of these hepatocyte growth factor (HGF) is the most potent hepatic mitogen.

1.4.9 Hepatocyte Growth Factor

HGF, also known as scatter factor, is a heterodimeric molecule made up of a 69 kDa α-chain and a 34 kDa β-chain. It is synthesised and secreted as biologically inactive single-chained precursor (pro-HGF), which is activated by serine proteases (urokinase-type plasminogen activator, HGF activator (HGFA) and plasminogen) [89]. HGF exerts its effect by binding to its receptor c-Met. The c-Met receptor is composed of a 50 kDa α-chain and a 145 kDa β-chain. The α-chain is extracellular whilst the β-chain is a trans-membrane subunit with an intra-cellular tyrosine kinase domain [90]. Binding of HGF to c-Met results in phosphorylation of the tyrosine residue, which in turn recruits a range of intra-cellular signalling pathways (Gab-1, phospholipase c-γ, STAT-3) [89]. In addition to its mitogenic effect, HGF / c-Met coupling results in a range of responses in a variety of cells, including, motogenic, morphogenic, neurite extension and anti-apoptotic effects [89].

In the normal liver, HGF is synthesised by non-parenchymal cells (HSCs and endothelial cells) [91] and deposited in the ECM [92, 93]. Following PH, HGF levels increase rapidly and remain elevated until the functional liver cell population has been restored. The initial increase in HGF levels occurs as a result of ECM remodelling, which liberates the pro-

HGF stored within it. More sustained release of HGF then occurs from *de novo* synthesis by activated HSCs [91]. When antibodies against HGF are delivered after a toxic injury liver the regenerative response is significantly impaired [94]. Infusion of HGF into the portal circulation results in an increase in the liver mass [95-99].

In addition to its hepatic activity, HGF has a range of actions in a variety of tissues; both in development and in specific disease states (pregnancy, cardiac and peripheral vascular disease, tumour metastases). Serum levels of HGF vary throughout life, under normal conditions, between sexes, in pregnancy and with age [89]. When exogenous HGF is injected intravenously it is taken up by a wide range of tissues (liver, adrenal gland, spleen, kidney, lung, stomach and intestine) and is rapidly cleared. Clearance is achieved predominantly through the liver (70%) and to a lesser extent by the kidneys (10%) [89].

In animal models of parenchymal liver disease administration of exogenous HGF suppresses the onset of liver fibrosis, prevents progression to cirrhosis, and prevents death from hepatic dysfunction [100, 101]. This demonstrates a potential therapeutic application for HGF delivery.

1.4.10 Epidermal Growth Factor Receptor Ligands

Epidermal growth factor (EGF) & transforming growth factor (TGF)α are members of a group of growth factors that bind to the EGF receptor (EGFR). The EGFR (present on most cell types), is a large (170 kDa) trans-membrane glycoprotein, with tyrosine kinase activity. Binding to the receptor initiates a number of signalling cascades (including phospholipase

c-γ, MAP kinases and STAT-3) and a range of responses in different tissues (mitogenesis, motogenesis, differentiation, de-differentiation and repair as well as tumour progression, invasion and metastasis) [102].

EGF is synthesised as a large (130 kDa) precursor which is then cleaved to a mature (6 kDa) molecule. It is secreted primarily by exocrine glands and is found in nearly all bodily secretions (Brunner's gland, seminal, mammary and saliva) [103]. EGF has a direct mitogenic effect on hepatocytes *in vitro* and *in vivo* [97]. When it is infused into the portal circulation it is deposited in the ECM and is cleared in one pass [56]. There is no increase in the level of EGF in the serum following PH despite EGFR upregulation.

TGF-α, which is produced by hepatocytes along with most replicating epithelial cells, is also synthesised as a precursor that is then cleaved to a smaller (6 kDa) active molecule. It is directly mitogenic to hepatocytes, but its effects are more potent than EGF [97, 104]. TGF-α levels increase following PH. This commences 3-5 hours after PH and peaks at 24 hours [105]. The absence of TGF-α does not significantly impair liver regeneration, but the expression of EGFR by most hepatic cell types (parenchymal and non-parenchymal) suggests that the role of TGF-α may be to stimulate mitogenesis in different liver cell populations during regeneration [84].

1.4.11 Fibroblast Growth Factor 1 / Acidic & Fibroblast Growth Factor 2 / Basic

FGF_1 and FGF_2 are members of the FGF superfamily of growth factors. FGF_1 is a 16 kDa polypeptide found predominantly in neural tissue and FGF_2 is a 17 kDa protein found in a

wider range of tissues (including plasma, brain, kidney and adrenal). Both FGF_1 and FGF_2 have a strong affinity for glycosaminoglycans (GAGs), and binding to which potentiates their activity. It has been suggested that this affinity for GAGs relates to their role in ECM remodelling and the angiogenesis of repair [106].

The FGF group of growth factors act by binding to the FGF receptor (FGFR), of which there are 4 isoforms. These isoforms display ligand variability, resulting in different FGF subtypes having different affinities for the different FGFR isoforms. The FGFR is a transmembrane tyrosine kinase receptor, which activates a range of signalling pathways (including phospholipase CY and MAP kinase cascades). *In vitro* both FGF_1 and FGF_2 stimulate DNA synthesis and cell division and *in vivo* they are strongly angiogenic, enhance wound healing and have been implicated in tumour-genesis [107, 108].

In the liver increased expression of both FGF_1 and FGF_2 has been observed during regeneration [109], although their absence does not inhibit the rate of regeneration [56]. *In vitro* both FGF_1 and FGF_2 are mitogenic to hepatocytes, although to a lesser extent than HGF, TGF-α or EGF [110]. Whilst the FGFR ligands are less influential on liver regeneration than HGF, TGF-α or EGF, their ability to promote angiogenesis in growing tissue makes them an attractive target for regenerative medicine [111].

1.4.12 Other Factors

A number of other factors have a role in liver regeneration: Insulin and glucagon promote liver regeneration after PH [112, 113]. Although neither factor can induce DNA synthesis *in vivo*, the absence of insulin slows the rate of regeneration [114]. The Wnt family of growth factors have diverse roles in regulating cell fate, proliferation, migration and death in developing and adult cells, and recent studies indicate that they may have an important role in regulating hepatocyte proliferation following PH [58, 115].

A number of chemokines (interferon-inducible protein 10 (IP-10), monokine induced by gamma interferon (MIG) and macrophage inflammatory protein 1 (MIP-1)-α) are expressed following liver injury and may play a role in regulating hepatocyte proliferation [116]. Prostaglandins have also been implicated in the initial triggering of the liver regeneration cascade [75].

Thyroid hormone (T_3) is a powerful inducer of hepatocyte proliferation *in vitro* and *in vivo*, although liver regeneration is normal in the absence of T_3 [117]. Sex hormones (oestradiol) are also known to increase after PH [118]. Noradrenaline (NA) augments the effects of HGF and EGF and inhibits the action of TGF_β an inhibitor of regeneration [56].

1.4.13 Termination of Regeneration

Once the liver mass has been restored, regeneration is terminated. The signals that lead to this cessation are not well understood. A number of factors have been implicated.

1.4.14 Transforming Growth Factor β (TGF_β)

TGF_β is produced in the liver by the parenchymal and non-parenchymal cells of the liver, particularly the HSCs [119]. It is secreted in its inactive form bound to an inhibitory protein complex. This inhibitory protein complex binds TGF_β to the ECM [120]. It is then activated by cleavage from its binding protein by proteases (MMPs, plasmin) [121]. Levels of active TGF_β increase within 4 hours of PH and peak at 72 hours [122]. The upregulation of TGF_β leads to liver fibrosis and hepatocyte apoptosis [123, 124], and its administration after PH inhibits regeneration [125]. Conversely inhibition of TGF_β stimulates hepatocyte proliferation [126].

1.4.15 Other Inhibitors of Regeneration

Several checkpoints exist in the STAT-3 pathway that provide mechanisms whereby feedback inhibition of specific growth factor / cytokine mediated pathways can regulate organ size [59].

1.4.16 The Role of the Extracellular Matrix

Extracellular proteases mobilise the cytokines and growth factors that are anchored within the ECM providing the crucial start and stop signals for intracellular signalling during liver regeneration [121].

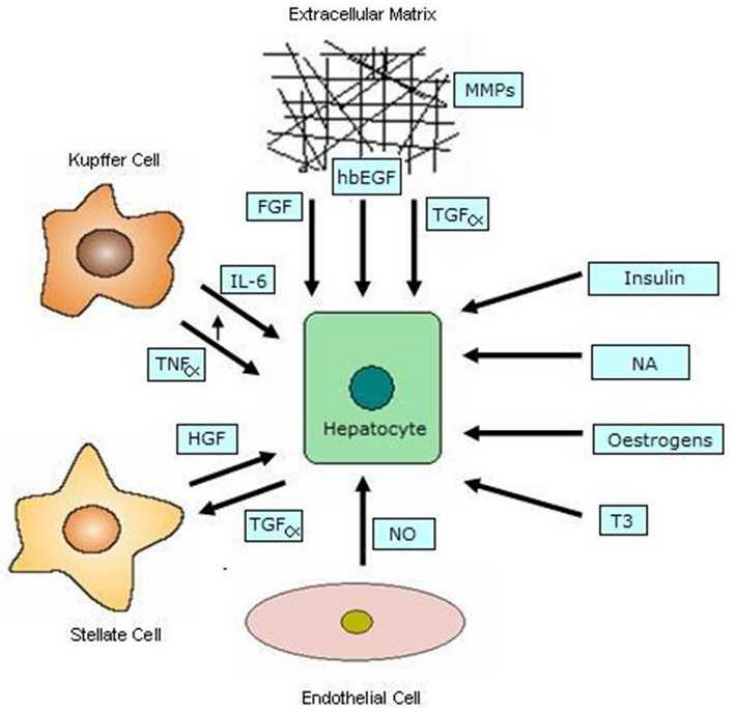

Figure 1.5 Schematic illustrating the complex interplay between parenchymal cells, non-parenchymal cells, the ECM and other co-mitogens during liver regeneration after PH

1.5 Liver Tissue Engineering

Early attempts to engineer liver aimed to provide a better understanding of the pathophysiology of liver disease or to develop *in vitro* models for toxicological and pharmacological testing. With the establishment of regenerative medicine as a modern scientific discipline the focus of liver tissue engineering has shifted to defined clinical endpoints.

Liver tissue engineering can be separated into two approaches; *in vitro* systems that use cell and scaffold technologies to manufacture functional liver tissue *de novo*, and *in vivo* systems that aim to boost functional liver capacity by implantation of exogenous cell populations or by promoting growth or regeneration in the existing liver cell population. This section reviews *in vitro* and *in vivo* liver tissue engineering strategies with a particular emphasis on the core principles of regenerative medicine and discusses their therapeutic potential.

1.5.1 Cell Sourcing for Liver Tissue Engineering

For both *in vitro* and *in vivo* liver tissue engineering, the issue of cell sourcing is a major limitation. An exogenous source of regeneration-competent parenchymal and non-parenchymal liver stem cells has yet to be identified. As a result *in vitro* systems and *in vivo* cell delivery systems must rely on isolated primary cells or cell lines. For basic science research these cell types are useful and are used widely, but for therapeutic applications they are undesirable due to concerns over immunogenicity, the risks of infection and

malignant transformation. Those *in vivo* strategies that seek to harness the liver's innate regenerative capacity to boost functional liver mass are therefore currently at an adavantage.

1.5.2 *In Vitro* Liver Tissue Engineering

The long term aim of *in vitro* liver tissue engineering is to assemble and maintain functional liver tissue *de novo*. However manufacturing liver tissue is not straightforward. The liver has a complex architecture; its main functional component (the hepatocyte), rapidly de-differentiates in the absence of appropriate signal delivery; and normal hepatic function requires not only a hepatocyte population but also non-parenchymal cells and an ECM. In the short term the objective of liver tissue engineers is to improve hepatocyte viability and function.

1.5.3 *In Vitro* Signal Delivery

An isolated hepatocyte grown in a monolayer de-differentiates and dies within 10 days [48]. This occurs due to loss of its ECM and intercellular interactions and disruption of its normal micro-environment [127]. Hepatocytes attach to the ECM via transmembrane integrin receptors, which allow adhesion and influence cell migration and phenotypic expression. In doing so the ECM provides structural support and facilitates continuous exchange of signals between cells. In studies where hepatocyte-ECM signals are restored, by culturing hepatocytes with collagen and other ECM components (e.g. monolayer, sandwich), significant but not complete improvement in viability and function are seen [29, 128-130].

The benefits of restoring intercellular signalling have been demonstrated in a series of three–dimensional aggregate studies [131-133]. Homotypic hepatocyte aggregates have better viability and function than an equivalent hepatocyte population on a collagen monolayer. Further improvement in viability and function are seen when non-parenchymal cells (fibroblasts, endothelial cells and HSCs) are introduced into the culture [32, 134, 135].

The mechanisms of hepatocyte aggregation and surface attachment have been studied in detail by Griffith *et al*. They demonstrated that hepatocytes will form aggregates when the forces of intercellular attraction exceed the cell-surface adhesion strength. By observing hepatocyte aggregate morphology in different matrigel concentrations they found that at low matrigel concentrations (low adhesion strength) aggregates formed, whilst at high matrigel concentrations (high adhesive strength) hepatocytes attached in a monolayer [136]. In a second study looking at how the cell surface interaction influences hepatocyte behaviour, it was found that the ability of a hepatocyte to attach to a surface is influenced not just by the concentration of the surface ligand but also its microdistribution [137].

1.5.4 Scaffolds *In Vitro*

Scaffolds are natural or synthetic constructs that are used to direct, supplement or replace the function of living tissues [23]. The concept of using a scaffold as a three-dimensional supporting template for tissue regeneration has been successfully demonstrated in numerous applications including the repair of bone [138], cartilage [139]and vascularised skeletal muscle [140]. In the context of *in vitro* liver tissue engineering the scaffold should

provide support for the growing tissue, channels for cell migration and mass-transfer and surface features for cell attachment.

The choice of scaffold material depends on its intended application. Animal-derived ECM scaffolds provide binding sites for integrin-mediated cell adhesion, but have poor mechanical strength, may suffer interbatch variability and are not immediately scaleable [141, 142]. Alternatively biodegradable polymers can be manufactured into complex micro-scaffolds, may behave more predictably *in vitro*, biodegrade to natural metabolites and can be modified to improve cell-surface attachment [143].

Lin and Sellaro have used a naturally derived, decellularised liver ECM (L-ECM), produced by mechanical and chemical treatment of porcine small intestinal submucosa for liver cell culture. This natural biomaterial contains a number of ECM components including collagen I, collagen IV, laminin and fibronectin, as well as growth factors, and when hepatocytes are cultured on it, they maintain synthetic and metabolic for over 30 days [30, 144].

The potential of inorganic biomaterials has also been explored. Petronis used microporous titania ceramic scaffolds manufactured by injection moulding. The titania ceramic which has good biocompatibility and has been shown to be non-cytotoxic to hepatocytes encouraged hepatocyte aggregate formation without the need for ECM coating [145]. The non-biodegradability of this biomaterial would limit its use to *in vitro* applications.

The poly (α hydroxy acid) group of polymers have excellent biocompatibility and are widely used in tissue engineering [146, 147]. Unmodified poly (L-lactic acid) (PLLA) scaffolds can support functional hepatocyte populations [148], and a range of surface modification techniques have been developed to increase their surface ligand availability. Nam *et al* used alkali hydrolysis to enhance hepatocyte attachment on PLLA [149] and plasma alyllamine surface deposition could also be used for this purpose [150].

It is possible to improve the adhesion strength of polymers by incorporating bioactive compounds at the time of manufacture. Gutsche demonstrated that by incorporating lactose and heparin into the matrix of porous polystyrene scaffolds, hepatocyte adhesion was increased and hepatocyte function improved compared with an unmodified polymer scaffold [151].

Polyethylene terephthalate (PET) has been used by Risbud to support hepatic endothelial cell populations. Here a woven PET fabric with macropores was coated in a collagen-chitosan gel matrix. This fabric-gel complex supported an endothelial cell population and encouraged adhesion and retained function [152, 153]. Mayer *et al* found that by EGF coating their woven PET fabric scaffold they could improve rates of hepatocyte aggregation and organisation [154]. Likewise Takei *et al* improved hepatocyte attachment, aggregation and function by coating PVLA with α-ASGPR, a monoclonal antibody with ECM protein-like properties [155]. These are all good examples of surface modification of low surface adhesion strength polymers to improve surface signalling for a liver cell population. Having chosen the biomaterial and surface modification technique the next step in the design process is to determine its optimum structure.

1.5.5 Spatial Signalling and Scaffold Structure

A range of scaffold designs have been trialled for liver cell culture. Porous scaffolds provide a large surface area to volume ratio, have little limitation on mass transfer and have good biocompatibility [156]. Several studies have explored the effect of porosity on liver cell culture morphology and function. Ranucci demonstrated that by increasing the pore size of a PLLA scaffold, hepatocytes were more likely to form aggregates than attach in a monolayer, and that this change in morphology was associated with an improvement in their functional profile. The study suggested that a pore size of 100 μm was optimum for hepatocyte culture on PLLA scaffolds [157, 158]. Work by Glicklis also demonstrated that a pore size diameter of 100 μm in an alginate scaffold provided optimum viability and function, and that increasing pore size above that level led to mass transfer limitations and central necrosis within the aggregate [159].

The density of cell seeding is also important, and must be compatible with the biomaterials chemistry and internal morphology, whether or not it is adhesive to cells. Preferably this method must be rapid and allow high yields of cell entrapment with uniform distribution. Dvir-Ginsberg *et al* found that in order to optimise cell aggregation and function on a micro-porous alginate scaffold, cell densities of up to 5.7 x 10^6 cells/cm^3 were required. These denser cultures produced larger aggregates that interconnected with one another and retained hepatocyte specific function for over 7 days [160].

In addition to the microporous and mesh-type scaffolds, new polymer processing techniques have led to the development of more sophisticated scaffold designs. Using a cell

assembly apparatus that incorporates prototyping, computer-aided design and image processing to generate three-dimensional cell-biomaterial constructs, Yan *et al* produced a hepatocyte-gelatin-alginate hydrogel composite. This composite remained viable and performed function for over 12 days, the hepatocytes organising into aggregates within the gel [161].

Vozzi and Bhatia have produced micro-fabricated PLGA scaffolds using micro-syringe deposition operated on a three-axis micropositioner. By varying the pressure, speed and solution viscosity a wide range of complex scaffolds can be produced. Whilst the impact of these scaffolds on hepatocyte culture has yet to be established the concept has potential [39].

An approach that breaks away from the aggregate based strategies discussed above is Ostrovidov's use of a collagen coated PDMS microporous micro-membrane in a perfused bed bioreactor. The micro-porous PDMS membrane was produced in a mould and designed to simulate the plate-like arrangement of hepatocytes in the parenchyma [162]. This produced promising functional data, and highlighted the benefits of developing a liver cell culture system within a bioreactor both for regulating microenvironment and offering real scale-up potential.

1.5.6 Applications for *In vitro* Liver Tissue Engineering

There are a range of clinical and basic science applications for *in vitro* liver tissue engineering systems. Bioartificial liver support devices have been developed to treat patients with acute liver failure (ALF) and to act as a bridge to transplantation [163]. A

controlled trial has shown some improvement in short-term survival for a subgroup of patients with ALF treated using a porcine-hepatocyte based bioartificial liver, but a larger trial is required before its use becomes routine in a clinical setting [164]. Similar *in vitro* systems may also prove useful in basic science for toxicological and metabolic studies and for studies of disease processes for example hepatitis C.

1.5.7 *In Vivo* Liver Tissue Engineering

The aim of *in vivo* liver tissue engineering is to increase the liver's functional capacity, either by delivery of an exogenous liver cell population or by expansion of the native liver cell population. In the context of *in vivo* liver tissue engineering, scaffolds may be used to support a liver cell population or to act as a signal delivery system for growth factors, cytokines and other bioactive materials.

1.5.8 Cell Delivery *In Vivo*

When isolated hepatocytes are transplanted intrahepatically or intra-splenically they exhibit long-term survival but cannot be delivered in large enough quantities to boost functional liver capacity [165]. Similarly when hepatocytes bound to microcarriers are injected into rats that had and undergone uniformly lethal liver resection or UDP-glucuronyltransferase deficient Gunn rats (rats incapable of conjugating bilirubin), metabolic improvements were demonstrated but no long-term survival benefits were seen [166, 167].

Cell delivery via intra or extra-hepatically implanted scaffolds may allow delivery of a greater hepatocyte load. In early studies where cell-scaffold composites were implanted extra-hepatically (subcutaneous, mesenteric, omental, retroperitoneal), cells near the implanted surface survived but those deep within the scaffold died due to inadequate mass-transfer [168]. Strategies to pre-vascularise scaffolds prior to cell delivery have been used to improve mass-transfer. If a scaffold (+/- angiogenic factors) is implanted into the target site before cell seeding there is an opportunity for vascular in growth to occur. At a later point cells can then be seeded via an open procedure or through a catheter into the scaffold. Stein used this approach to improve hepatocyte engraftment in PVA discs implanted into the mesentery [143] and Kedem used it to enhance engraftment in alginate scaffolds implanted onto the liver edge [169]. Whether these pre-vascularised cell-scaffold composites can allow delivery of liver cell populations that are large enough to increase total functional capacity is not yet known.

Different implantation sites will be appropriate for different clinical scenarios. For example, in the presence of malignancy or cirrhosis it may be preferable to implant the liver cell population away from the diseased liver so that the donor tissue remains unaffected by the underlying pathology. If liver cells are to be delivered extrahepatically, they must be provided with hepatotrophic stimulation. Hepatotrophic stimuli are important for hepatocyte differentiation and engraftment *in vivo* and their absence has been implicated in the failure of extra-hepatic scaffold implantation studies [170]. Porto-caval shunting (PCS) provides hepatotrophic stimulation at extrahepatic sites by preventing first pass metabolism of liver mitogenic factors. Mooney *et al* used PCS to improve hepatocyte engraftment on porous PLGA scaffolds implanted into the mesentery of Lewis rats [171].

Kneser also used PCS to enhance hepatocyte engraftment, demonstrating long term hepatocyte engraftment on porous PVA scaffolds in rats up to one year [172]. In addition to the loss of hepatotrophic stimuli, by choosing to implant a scaffold extra-hepatically bile excretion will also be lost. This may not be appropriate for all clinical applications.

1.5.9 The Scaffold as a Delivery Device

When growth factors are infused into the liver it is possible to induce a range of effects. Direct infusion of HGF and EGF receptor ligands into the liver has been shown to enhance liver growth [95-97]. Only a limited number of studies, have investigated the impact of intrahepatic growth factor delivery via scaffolds. Mooney used a polymer-based scaffold delivery system to improve engraftment of hepatocytes in an extra-hepatic, hepatotropically enhanced implantation site. By incorporating EGF microspheres into the hepatocyte-PLGA composite further improvements in rates of hepatocyte engraftment were seen [171]. Oe *et al* investigated the controlled release of HGF in a rat cirrhosis model. Using intraperitoneally injected biodegradable gelatin microspheres into loaded with HGF; they showed that delivery of HGF enhanced recovery from cirrhosis [173].

1.5.10 Intrahepatic Scaffold Implantation

An alternative to transplanting a hepatocyte population is to encourage synthesis of new liver tissue *in vivo*. Takimoto *et al* implanted collagen-polypropylene composite scaffolds into rat livers. Two weeks after implantation the scaffold was filled with oval cells, by three weeks it was invaded by activated HSCs and by one month mature hepatocytes were

identified. After six months mature liver tissue, juxtaposed with bile ducts and blood vessels, was seen throughout the collagen-polypropylene scaffolds. This is the first example of liver tissue formed *de novo*, although it was not associated with an increase in the total liver cell mass [174].

1.5.11 Applications for *In Vivo* Liver Tissue Engineering

In vivo liver tissue engineering is in the early stages of development. The limited successes of isolated hepatocyte transplantation have now been superseded by cell delivery via prevascularised scaffold systems and the use of signal delivery via biodegradable scaffolds. Having the ability to increase the liver's functional capacity is an exciting prospect. It could be used to treat metabolic diseases of the liver [165]; to act as a bridge to (or in place of) liver transplantation in patients with acute or chronic liver failure or to boost the functional liver mass after liver resection for cancer, allowing larger resections and faster patient recovery.

1.5.12 Overview

In the past 20 years we have seen major advances in the regeneration of structural tissues, like cartilage and bone, but because the liver is architecturally and functionally more complex, progress with liver regeneration has been less dramatic. There are a number of areas for improvement.

By developing a better understanding of the factors that regulate hepatocyte regeneration and phenotypic expression and then delivering these factors via controlled release strategies it may become possible to offset hepatocyte de-differentiation *in vitro*. Improved cell densities will be possible with new scaffold fabrication techniques providing more authentic ultrastructure and better cell surface attachment. Cell survival and vascularisation in implanted hepatocyte populations will increase as we improve our ability to prevascularise and incorporate hepatotrophic factors into the scaffolds via controlled release systems. Stem cell science may also provide a new cell source to populate all these applications.

Recent studies have shown a short-term survival benefit for a porcine-hepatocyte liver support system [164]. As our *in vitro* culture technologies improve the use of biological liver support devices for the treatment of liver failure may become a reality, but realistically this will take another 10-15 years. In the short term, small scale *in vitro* systems will become available for metabolic studies and studies of disease and drug metabolism.

1.6 Study Background, Design & Hypotheses

This thesis presents two approaches to liver tissue engineering. The first is an *in vitro* model that combines the benefits of hepatocyte-HSC co-culture and three-dimensional tissue assembly in one culture system. The second approach is an *in vivo* system that harnesses the regenerative capacity of the liver to boost functional liver mass using a biodegradable polymer-based growth factor and ECM delivery system.

Study 1: Hepatocyte-Hepatic stellate cell co-culture on three-dimensional microporous $P_{DL}LA$ scaffolds

Hypothesis

Co-culture of hepatocytes with HSC on a three-dimensional $P_{DL}LA$ scaffold enhances hepatocyte viability and function.

The objectives of this study are to evaluate hepatocyte-HSC co-culture on $P_{DL}LA$ scaffolds, determine the impact of $P_{DL}LA$ surface modification on culture morphology and function and to compare this approach with existing hepatocyte culture strategies.

Study 2: Intrahepatic growth factor and ECM delivery via biodegradable polymer scaffolds

Hypothesis

Intrahepatic delivery of growth factors and liver derived ECM proteins can stimulate functional liver tissue growth in normal and regenerating liver.

The objectives of this study are to develop an intrahepatic growth factor and ECM protein delivery device and evaluate its impact on liver growth in normal liver and in an animal model for PH.

Chapter 2 Hepatocyte-HSC Co-Culture on Three-Dimensional Microporous $P_{DL}LA$ Scaffolds

2.1 Introduction

The rapid de-differentiation of primary hepatocytes in culture can be offset by the restoration of normal intrahepatic *in vivo* signalling. In Guillouzo's detailed review of *in vitro* models for toxicology, a wide range of liver cell culture strategies are described [48]. These strategies achieve modest improvements in cultured hepatocyte viability and function by restoring single intrahepatic signalling pathways. To produce a culture system that sustains a hepatocyte population with levels of differentiation and a proliferative capacity that matches that of a healthy *in vivo* hepatocyte population more sophisticated culture systems must be developed.

By designing a liver cell culture strategy in which multiple pro-differentiation signals are delivered simultaneously, *in vitro* hepatocyte viability and function may be sustained at higher levels than is achievable in traditional culture systems. A number of pro-differentiation signals have been identified. These include homotypic and heterotypic intercellular interactions, ECM ligand binding, delivery of soluble factors and restoration of three-dimensional architecture [48]. This study will set out to trial a culture system that delivers multiple signals simultaneously, by co-culturing hepatocytes with HSC on a three-dimensional scaffold.

The HSC is an attractive target for *in vitro* liver tissue assembly. *In vivo* it is an important regulator of liver regeneration [47, 52], and *in vitro* has been shown to enhance hepatocyte viability and function by restoring heterotypic intercellular interactions and ECM ligand binding [33, 34]. When hepatocytes are co-cultured with HSCs in a non-adherent tissue culture environment, the HSC population becomes activated, attaches to the hepatocyte population via long dendritic processes and draws them into a mixed cell aggregate (figure 2.1) [33]. When imaged after 48 hours using transmission electron microscopy (TEM) these aggregates have differentiated hepatic ultrastructure[33]. Comparative studies demonstrate that the metabolic and synthetic functional profile of these aggregates is significantly greater than in conventional liver cell culture systems[34]. The next step is to determine how this co-culture model performs within a three-dimensional scaffold.

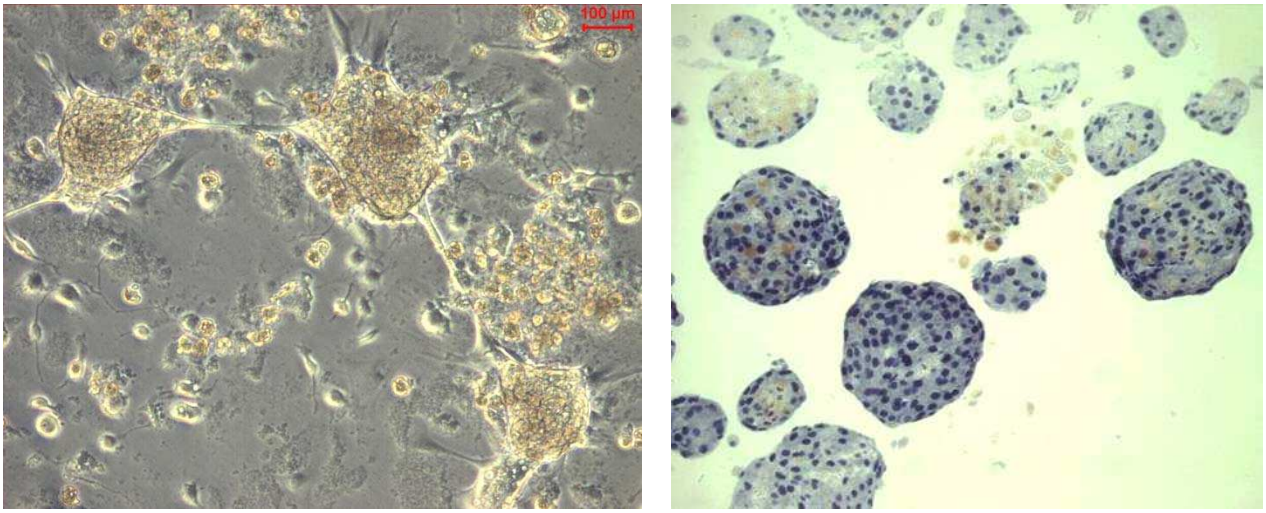

Figure 2.1 Time lapse microscopy of a hepatocyte-HSC co-culture at 24 hours post seeding (*left*) and light microscopy of haemotoxylin stained hepatocyte-HSC aggregates 5 days after seeding (*right*). When hepatocytes are co-cultured with HSCs in a low adherent tissue culture environment the HSCs become activated and hepatocytes aggregate around them. Within 4 days they have formed viable circular aggregates with differentiated hepatic ultrastructure and function [34]

A range of biomimetic scaffolds have been developed for three-dimensional cell culture[175]. For this study a scaffold that could be optimised for liver cell culture was required. Microporous poly (α hydroxy acid) scaffolds have previously been shown to support hepatocyte culture [148], and work by Ranucci *et al* has defined the optimal pore diameter for this application (100 μm) [157]. $P_{DL}LA$ is a member of this group of polymers and can be foamed to a mean pore diameter of 100 μm using supercritical CO_2 processing [176]. It is also possible to surface modify $P_{DL}LA$ using allylamine plasma deposition or NaOH treatment to increase the ligand availability on the surface of the scaffold without altering its bulk properties. These surface modification techniques have been used to improve hepatocyte attachment on glass and PLA respectively [149, 150].

The aim of this study was to evaluate hepatocyte-HSC co-culture on three-dimensional microporous $P_{DL}LA$ scaffolds, to determine if surface modification of the $P_{DL}LA$ could impact on the morphology and function of the cell population and to compare the functional profile of hepatocyte-HSC co-culture on a $P_{DL}LA$ scaffold with traditional culture models. The objectives of the study were to develop a seeding and culture protocol for hepatocyte-HSC co-culture on microporous $P_{DL}LA$ scaffolds and to evaluate the morphology and function of the scaffold cultures. Cells were cultured on plain $P_{DL}LA$ and $P_{DL}LA$ that had been surface modified using allylamine plasma deposition and $P_{DL}LA$ modified by NaOH treatment. Hepatocytes and HSCs isolated from rat livers were seeded onto the scaffolds. The morphology of the scaffold cultures were imaged using scanning electron microscopy (SEM). To assess the synthetic function albumin production was measured and to assess metabolic function testosterone metabolism assays were performed. The function of these cell scaffold co-cultures was then compared with conventional

hepatocyte culture systems (tissue culture plastic (TCP) & type I collagen) and with culture on an alginate scaffold.

2.2 Materials and Methods

2.2.1 Hepatocyte Isolation

Hepatocytes were isolated from adult male Wistar rats weighing 150-250 g using a modified 2-step collagenase perfusion technique [177]. In brief, rats were killed by cervical dislocation and the liver perfused with 0.5 mM EGTA in Hanks-Hepes buffer at 15 ml/min for 15 min at 37º C, followed by Hanks-Hepes buffer containing 5 mM $CaCl_2$ and 100 U/ml Type IV Collagenase (Sigma) for a up to 30 min until digested. The liver was then disaggregated, filtered and washed in Williams E media (Gibco) containing 10% foetal calf serum (FCS) (Sigma), and the hepatocytes purified by density gradient centrifugation (45% Percoll (Sigma, density 1.125-1.135 g/ml), 5% 10x Hanks-Hepes solution, 45% Williams E media, 5% FCS). Cell density and viability were counted on a haemocytometer following trypan blue exclusion (Sigma). Viability typically exceeded 90%.

2.2.2 Hepatic Stellate Cell Isolation

HSC were isolated from the hepatocyte washes and density gradient supernatant from the hepatocyte isolation as previously described by Riccalton-Banks [178]. In brief, the hepatocyte washes and density gradient supernatant from the hepatocyte isolation were combined, centrifuged three times at 50 g for 5 min and the pellets discarded. The final

supernatant was centrifuged at 250 g for 5 min, the pellet resuspended in stellate cell media (Dulbecco's modified Eagle's medium (DMEM) (Gibco) supplemented with 10% FCS Gold (PAA Laboratories), 5 mM L-glutamine (Gibco), 100 μg streptomycin and 250 ng amphotericin B (Gibco)) and grown to confluence in T75 tissue culture flasks (Sigma).

2.2.3 Scaffold Manufacture

Microporous $P_{DL}LA$ scaffolds were manufactured by foaming using supercritical CO_2 as previously described by Barry [179]. In brief, 130 mg of $P_{DL}LA$ (mw 52 Polyscience Inc) was placed in each well of a 10 well poly (TetraFluoroEthylene) (PTFE) mould. The polymer was melted in a custom made 60 ml pressure vessel using 230 bar pressure of CO_2 at 35º C for 60 min followed by a 60 min controlled decompression. Once the system had depressurised, the scaffolds were removed and left for 60 min to allow residual CO_2 to leave the scaffolds. To prepare the scaffolds for use the $P_{DL}LA$ cylinders had there non-porous skin removed and were then sliced into 1 mm thick wafers and stored at 4º C.

2.2.4 Allylamine Plasma Deposition

Allylamine plasma deposition was performed as described by Barry [176]. In brief, the 1 mm $P_{DL}LA$ scaffold wafers were placed into a plasma chamber. The vacuum chamber was evacuated and stabilized at 39.9 Pa of O_2 and a glow-discharged plasma formed (3 W for 180 sec). The scaffolds were exposed to allylamine vapour for a further 10 min. Deposition proceeded until an equivalent thickness of polymer was formed on the quartz microbalance positioned opposite the substrates. The samples were stored at 4º C for a maximum of 2

weeks before use. Prior to cell seeding the scaffolds were pre-wet in PBS in a vacuum and washed once in seeding medium.

2.2.5 Sodium Hydroxide Treatment

The 1 mm $P_{DL}LA$ scaffold wafers were pre-wet with PBS in a vacuum and immersed in 0.5 M NaOH solution for 20 min at 37º C. The scaffolds were removed from the NaOH solution and washed 3 times in PBS. Before cell seeding the scaffolds were washed in seeding medium.

2.2.6 Cell Seeding & Maintenance

$0.6x10^6$ freshly isolated primary rat hepatocytes and $0.3x10^6$ pre-isolated rat HSC suspended in 200 μl of hepatocyte medium (William's E media supplemented with 5 mM L-glutamine, 50 μg/ml gentamicin, 5 mM nicotinamide, and 10 mU/ml insulin, 10 μM dexamethasone) were seeded directly onto scaffolds pre-wet in a vacuum with Williams E media containing 10% foetal calf serum and incubated for 1 hour. 1 ml of hepatocyte medium was then added to each of the wells and the cultures incubated at 37° C in a humidified atmosphere of 5% CO_2 and 95% air. Media was changed daily.

2.2.7 Scanning Electron Microscopy

Cells were fixed in a 3% glutaraldehyde solution (TAAB Laboratories) followed by staining with 1% osmium tetroxide solution (TAAB Laboratories). The samples then

underwent stepwise dehydration in ethanol (25%-100%) before drying in hexamethyldisilazane (Sigma). The scaffolds were sputter-coated with gold and imaged with a JSM-6060LV (Jeol Ltd) variable pressure scanning electron microscope (SEM). Hepatocyte, HSC and co-culture morphology was examined on all scaffolds at 48 hours after seeding and on NaOH treated $P_{DL}LA$ at 5, 7 and 14 days. 3 samples were examined for each cell-scaffold configuration at each time point. Cells selected for imaging by starting at a representative area and rotating clockwise, taking up to 10 images per sample. Representative images are shown.

2.2.8 Albumin Production

Albumin levels in supernatants of cultures were measured using a rat albumin enzyme-linked immuosorbent assay (ELISA) according to the manufacturer's instructions (Bethyl Laboratories E110-125). In brief, culture media was aspirated from the wells, centrifuged and stored at -20º C. A 96-well high-affinity ELISA plate (Costar) was coated with a 1 in 100 dilution of anti-rat albumin for 1 hour at 37º C and washed (0.05% Tween 20 / Tris buffered saline solution (Sigma)). The plate was blocked (0.05% bovine serum albumin) for 30 min, washed and incubated with appropriate dilutions of standards and samples. After 60 min the plate was washed and incubated for a further 60 min with a 1 in 40,000 dilution of the HRP conjugated antibody, rewashed and developed with 3,3',5,5'-Tetramethylbenzidine (TMB) (Sigma) for 15 min before the reaction was terminated with 2M H_2SO_4 and the optical density measured at 450 nm using a MRX plate reader (Dynex Technologies). All standards and samples were analysed in triplicate.

2.2.9 Testosterone Metabolism Assay

The testosterone metabolism assay was performed as previously described [34]. At different time points media was aspirated from the wells and the cultures incubated for 1 hour in 1 ml of EBSS containing 1mM Ca^{2+},1 mM Mg^{2+} and 100 μM testosterone at 37º C. The solution was aspirated, centrifuged and the supernatant stored at -20º C for later analysis. Samples were analysed using a Beckman High pressure liquid chromatography (HPLC) 1090 fitted with a Zorbax 300 SB-C18 4.6 mm x 15 cm column maintained at 50º C (Beckman Coulter Inc). Mobile phase A consisted of 450 ml H_20:50 ml Acetonitrile:250 μl Formic acid, and mobile phase B consisted of 50 ml H_20:450 ml Acetonitrile:75 μl Formic acid. The mobile phase was run at 1 ml/minute, starting at 15% B and increasing over 10 minutes to 50% B, with a sample injection volume of 40 μl. UV absorbance was detected at 245 nm with an integral diode array detector. Each run was controlled by intermittent injection of an external standard containing 6β-hydroxytestosterone (Sigma) and 4-androstene-3,17-dione (Sigma).

In rat hepatocytes 6β-hydroxylation of testosterone is mediated predominantly by cytochrome P_{450} (CYP) 3A1 [180, 181] and oxidation of testosterone to 4-androstene-3,17-dione is mediated predominantly by CYP 2B1 [181]. The testosterone metabolism assay measures the activity of CYP 3A1 and CYP 2B1 in our hepatocyte population by detecting levels of their metabolites (6β-hydroxytestosterone and 4-androstene-3,17-dione) after a 1 hour incubation with testosterone. Enzyme activity at each time point is presented as a percentage of the activity found in a freshly isolated population of hepatocytes in a

matched culture environment. CYP3A1 activity was only detected in hepatocyte mono-culture on collagen at day 3 and not on any of the scaffold cultures (not shown).

2.2.10 Statistical analysis

Data was analysed using the Statistical Package for Social Sciences (SPSS) (Version 14 for Windows; GmbH, Germany). Data are expressed as the mean +/- standard deviation. The statistical significance of differences among groups was assessed by the independent Student t test or the one way analysis of variance (ANOVA) with Tukey post test as appropriate. P values less than 0.05 were regarded as statistically significant.

2.3 Results

2.31 Morphology

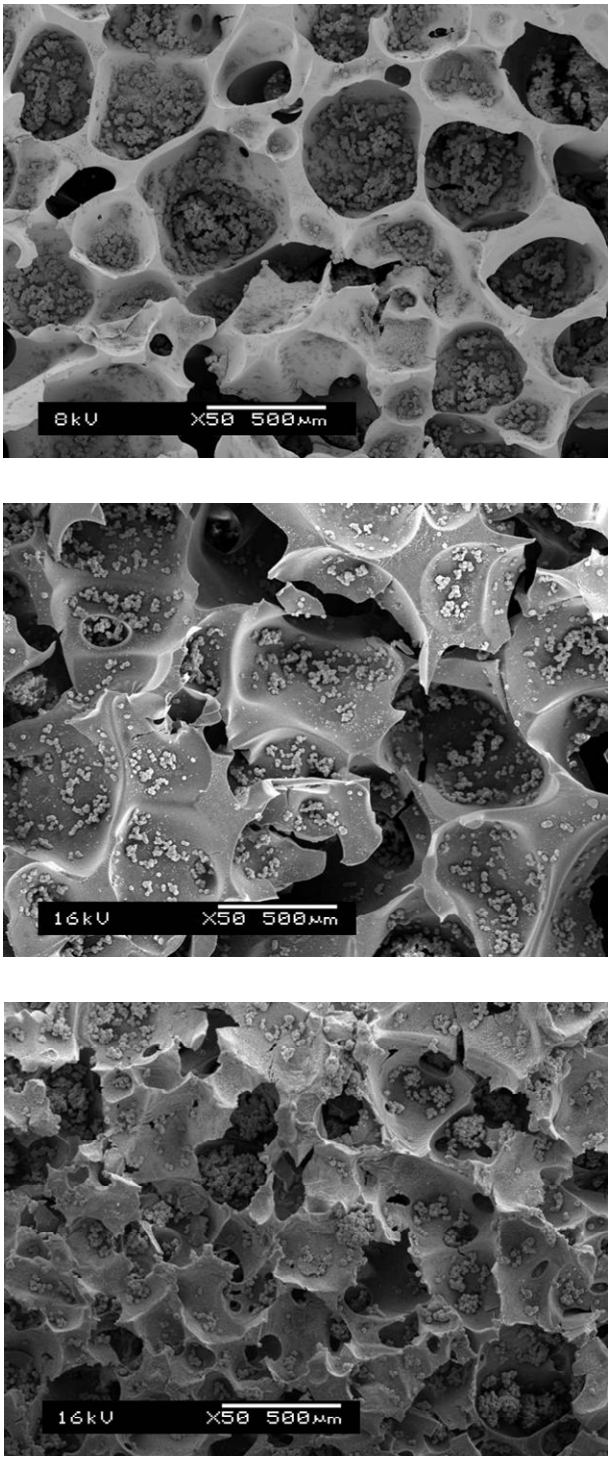

Figure 2.2 SEM of hepatocytes seeded in monoculture on unmodified (*top*) plasma coated (*middle*) and NaOH treated (*bottom*). Hepatocytes on the unmodified $P_{DL}LA$ aggregated at the base of the pores with limited attachment to the scaffold surface. Those seeded onto plasma coated and NaOH treated $P_{DL}LA$ attached to the scaffold surface and fewer, smaller cellular aggregates were present.

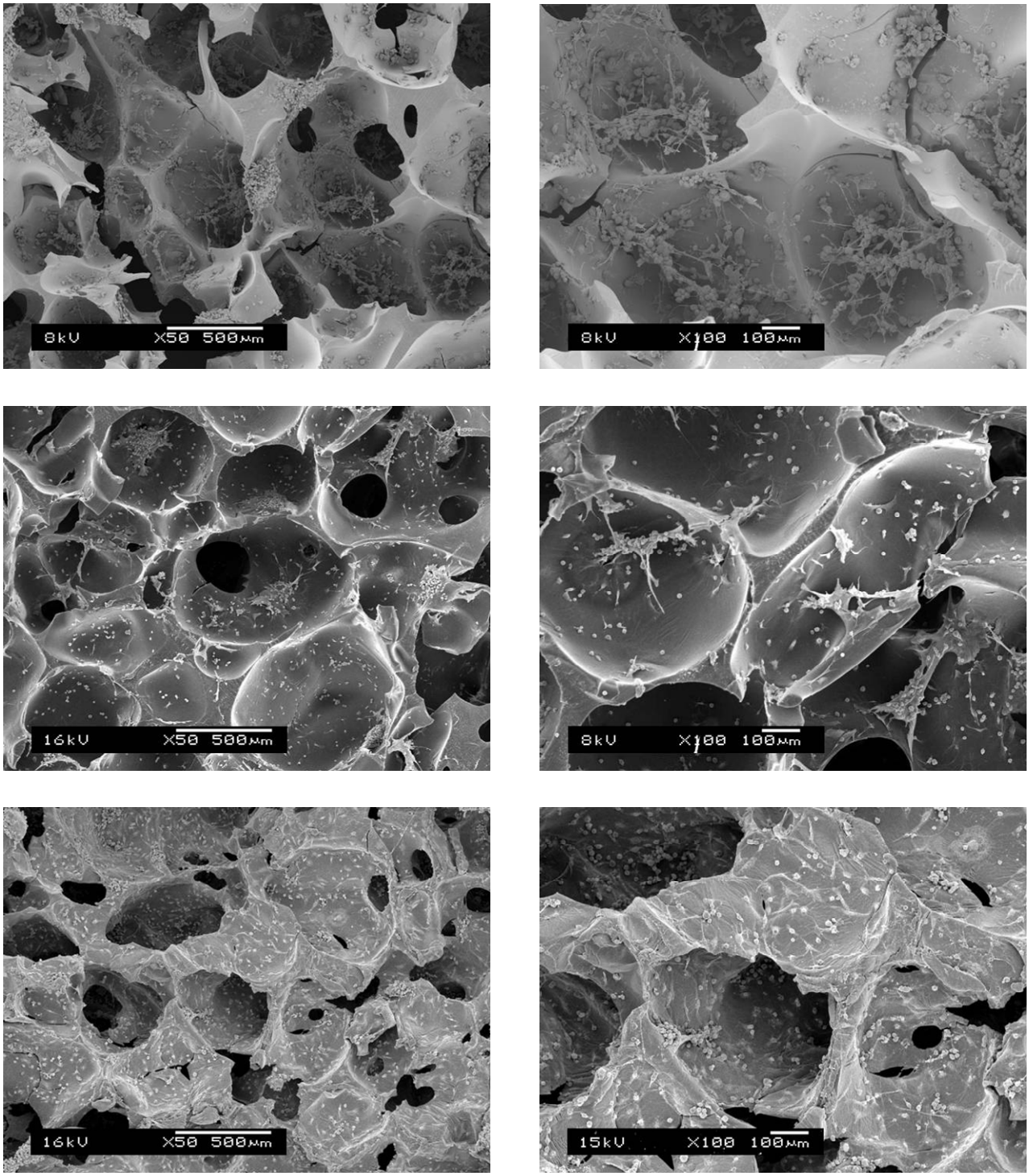

Figure 2.3 SEM of HSC seeded in mono-culture onto unmodified (*top*) plasma coated (*middle*) and NaOH treated (*bottom*) $P_{DL}LA$. When HSC were seeded onto the unmodified scaffolds they developed an activated morphology and formed aggregates. When HSC were seeded onto plasma and NaOH treated scaffolds they developed a predominantly quiescent morphology with flattened cells attaching directly to surface of the scaffold and fewer activated HSC or cell aggregates visible.

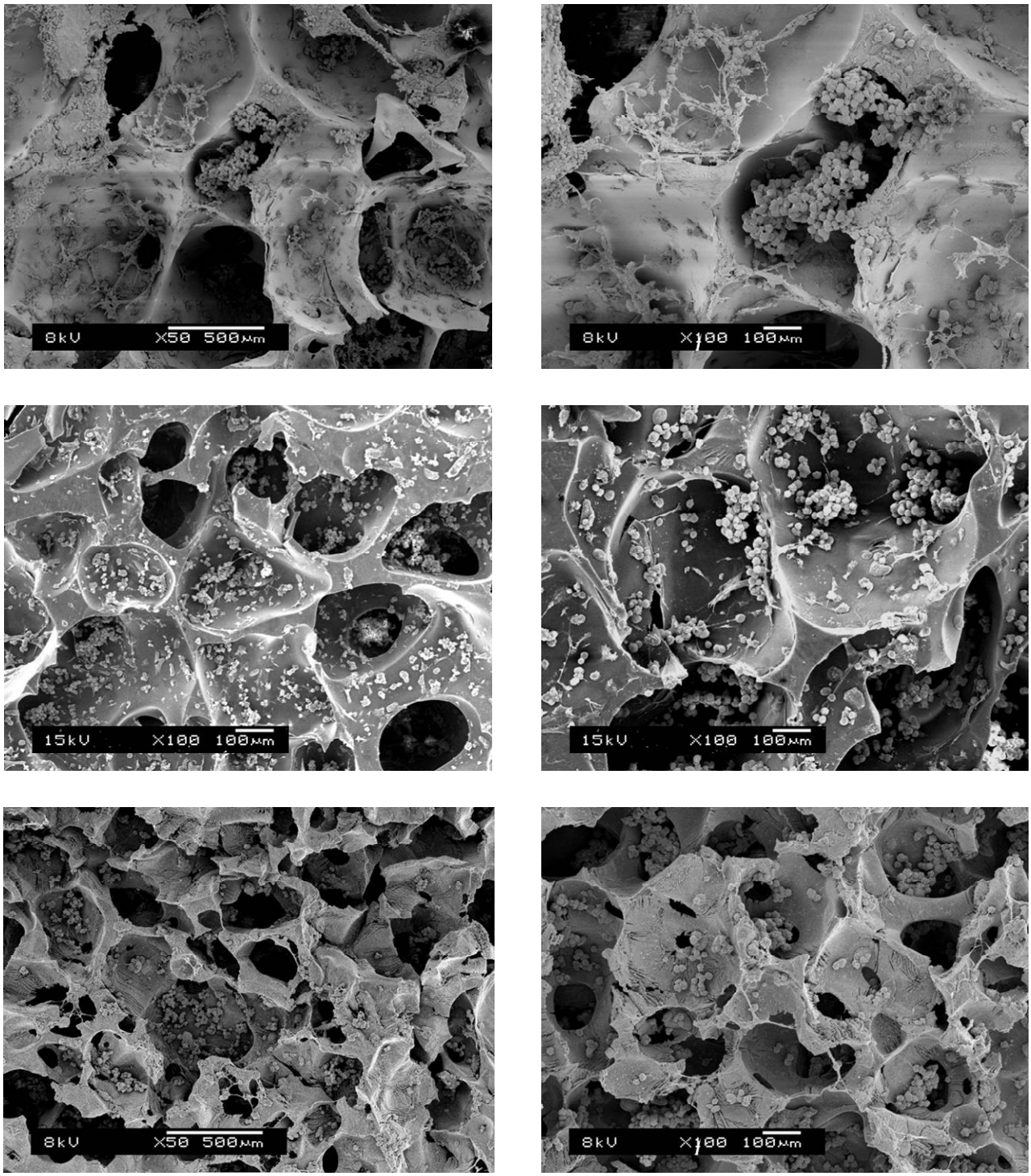

Figure 2.4 SEM of hepatocyte-HSC co-culture on unmodified (*top*) plasma coated (*middle*) and NaOH treated (*bottom*) $P_{DL}LA$. On unmodified $P_{DL}LA$ the HSC developed an activated morphology attaching to hepatocytes in mixed cell aggregates. On the plasma coated and NaOH treated $P_{DL}LA$ hepatocytes and the predominantly quiescent HSCs attached directly to the scaffold surface, with few aggregates present.

2.3.2 Function

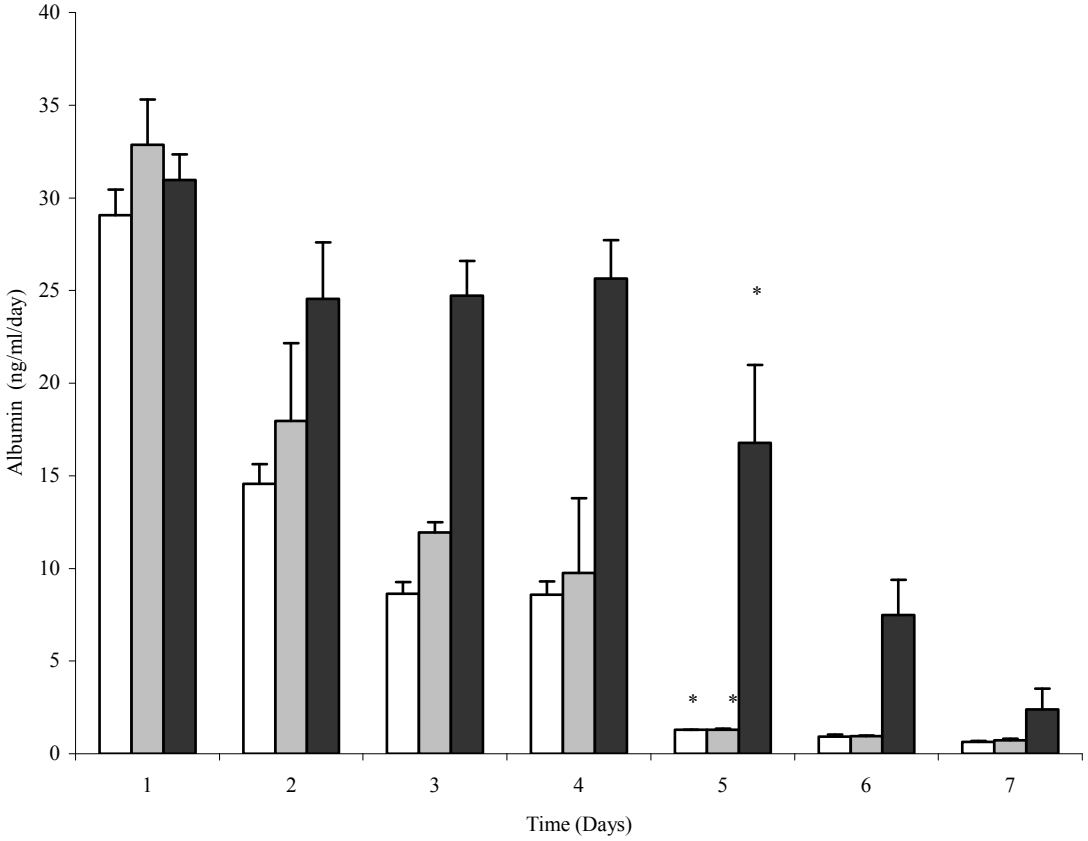

Figure 2.5 Albumin concentration in the media of hepatocyte-HSC co-cultures on unmodified (*white*), plasma coated (*light grey*) and NaOH treated (*dark grey*) $P_{DL}LA$ up to 7 days after seeding +/- SD mean (n=3). There was no significant difference in the level of albumin production between the 3 scaffold types for the duration of the experiment. On all scaffolds albumin production dropped significantly between day 4 and 5. *$P < 0.05$ compared with equivalent scaffold culture on day 4.

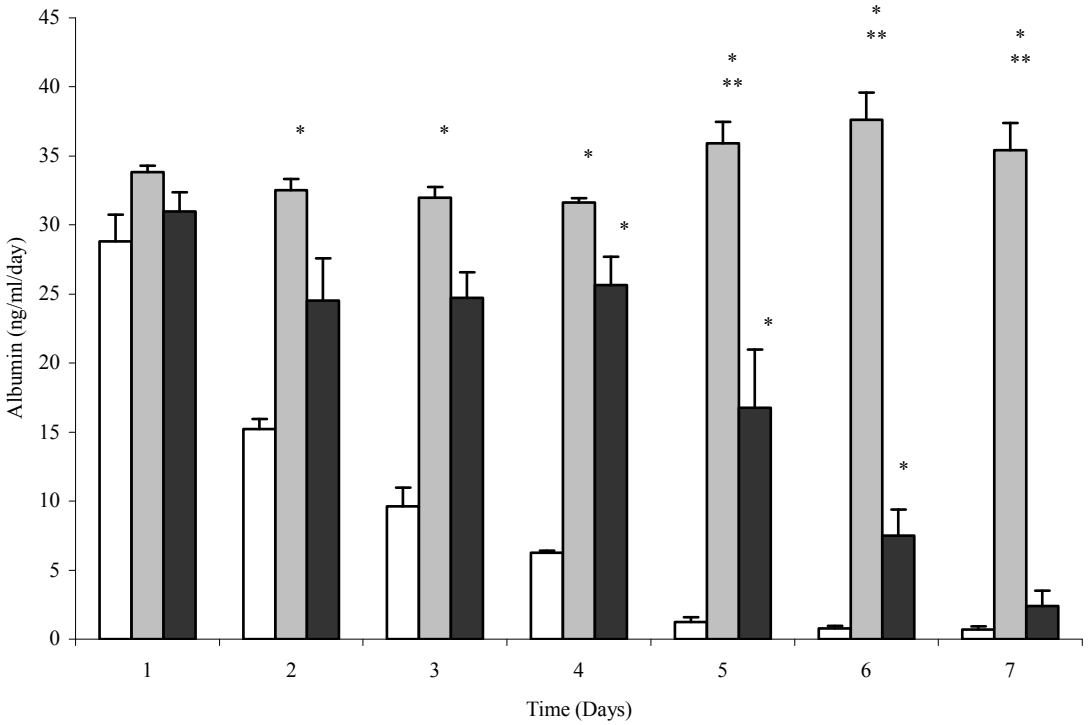

Figure 2.6 Albumin concentration in the media of hepatocytes cultured on TCP (*white*), type 1 collagen (*light grey*) and hepatocytes co-cultured with HSC on NaOH treated $P_{DL}LA$ (*dark grey*) up to 7 days after seeding +/- SD mean (n=3). Albumin concentrations were maintained in the collagen cultured hepatocyte population for the duration of the study significantly exceeding levels in both the mono-culture on TCP and co-culture on NaOH treated $P_{DL}LA$. The concentration of albumin in the co-cultures dropped significantly between days 4 and 5, but remained significantly higher than mono-culture on TCP up to day 6. *$P < 0.05$ compared with mono-culture on TCP and **$P < 0.05$ compared with co-culture on NaOH treated $P_{DL}LA$.

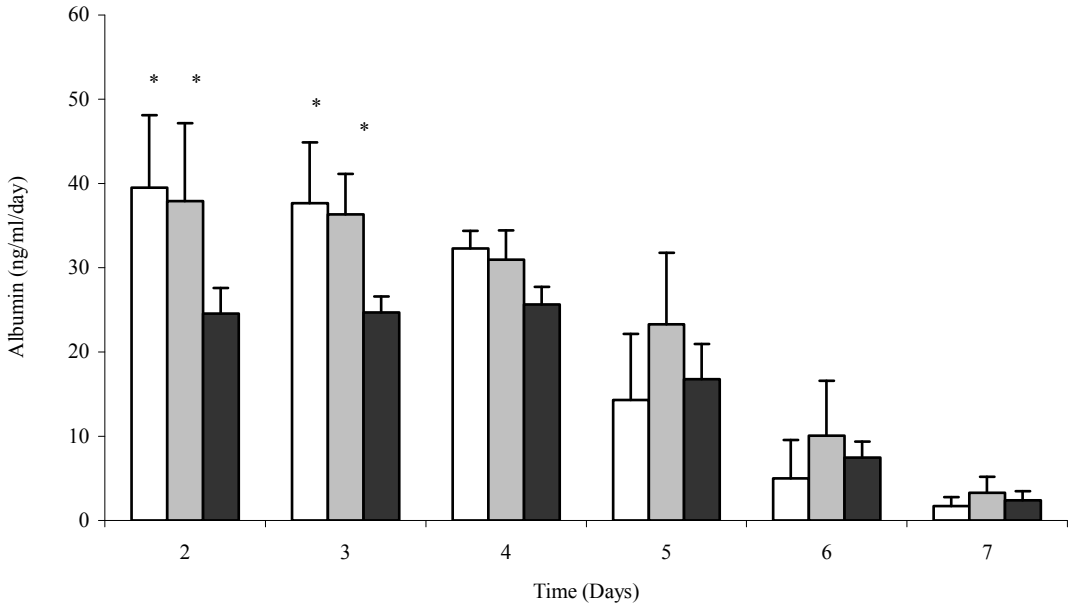

Figure 2.7 Albumin concentration in the media of hepatocyte mono-culture (white) and co-culture (light grey) on an alginate scaffold with co-culture on NaOH treated $P_{DL}LA$ (dark grey) up to 7 days after seeding +/- SD mean (n=3). Mono-culture and co-culture on the alginate scaffolds had significantly higher levels of albumin than co-culture on the NaOH treated scaffold up to day 3. Albumin levels on the alginate scaffolds fell significantly between day 4 and 6. There was no significant difference between albumin production by mono-culture and co-culture on the alginate scaffolds. *$P < 0.05$ compared with co-culture on NaOH treated $P_{DL}LA$.

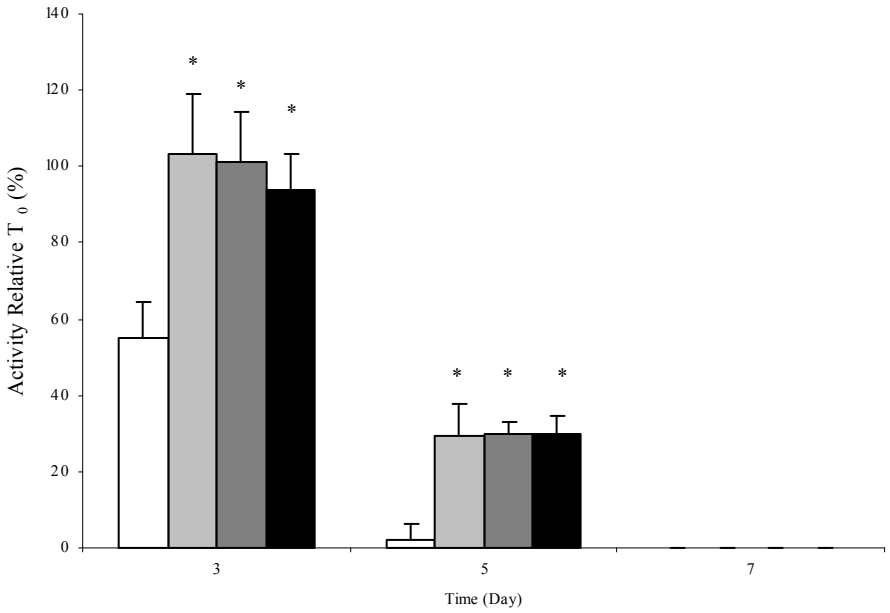

Figure 2.8 Average CYP2B1 activity relative to activity at T_0 in hepatocytes mono-cultured on unmodified $P_{DL}LA$ (white) and co-cultured on unmodified (light grey), plasma coated (darker grey) and NaOH treated (black) $P_{DL}LA$ at days 3, 5 and 7 after seeding +/- SD of mean (n=3). CYP2B1 activity in the hepatocytes co-cultured with HSC on $P_{DL}LA$ was significantly greater than in the mono-cultured hepatocytes at day 3 and 5 after seeding. On all scaffolds CYP2B1 activity fell significantly between day 3 and day 5. The metabolite was not detectable in any of the cultures at day 7. *$P < 0.05$ compared with mono-culture on unmodified $P_{DL}LA$.

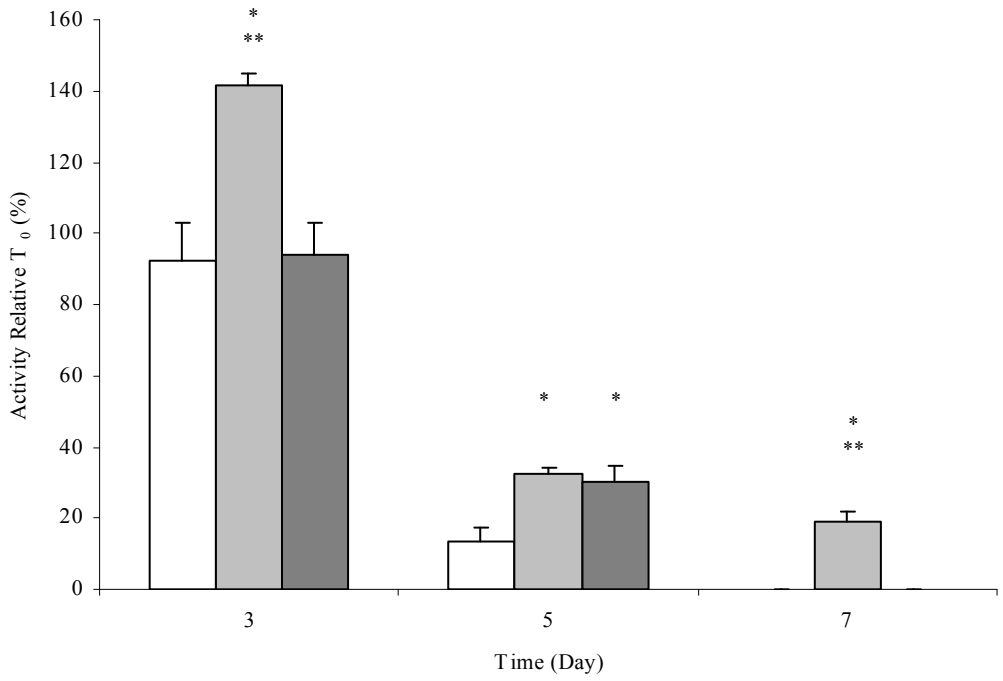

Figure 2.9 Average CYP2B1 activity relative to activity at T_0 in hepatocytes mono-cultured on TCP (white) and type I collagen (light grey) and co-cultured with HSC on NaOH treated $P_{DL}LA$ (dark grey) at days 3, 5 and 7 after seeding +/- SD of mean (n=3). At day 5 CYP2B1 activity was significantly greater in the collagen and on NaOH treated $P_{DL}LA$ cultures than on TCP. Only hepatocytes on collagen had CYP2B1 activity at day 7. * $P< 0.05$ compared with mono-culture on TCP and ** $P < 0.05$ compared with co-culture on NaOH treated $P_{DL}LA$.

2.4 Discussion

The aim of this study was to evaluate hepatocyte-HSC co-culture on three-dimensional $P_{DL}LA$ scaffolds, to determine the impact of surface modification on scaffold morphology and function and to compare their functional profile with traditional culture models. Using microporous $P_{DL}LA$ scaffolds manufactured using supercritical CO_2 foaming and surface modified using allylamine plasma deposition and NaOH treatment the morphology and function of these co-cultures was assessed.

A series of preliminary studies were undertaken to optimise the seeding technique and culture protocol. To improve the level of cell attachment, cells were seeded in low volumes (200 μl) onto scaffolds that had been pre-wet in a vacuum with media containing FCS and were incubated for one hour before hepatocyte media was added. This approach minimised the "wash-off" of cells from the scaffolds and did not significantly impact on hepatocyte function.

The characteristics and extent of ligand availability on the surface of a biomaterial influences cell culture morphology, cell phenotype and function [48, 136, 137]. Surfaces with limited ligand availability exert a low cell-substratum adhesion force. When cells are seeded onto these surfaces the forces of intercellular attraction exceed the cell-substratum adhesion forces and the cells preferentially aggregate. When cell-substratum adhesion forces increase, more cells attach to the surface and less aggregation occurs [136, 137].

Previous work has shown that unmodified $P_{DL}LA$ has limited ligand availability [176], as a result when hepatocytes are seeded onto it they preferentially aggregate and do not attach [33 32]. Allylamine plasma deposition and NaOH treatment increase the ligand availability on the scaffold surface without altering its bulk properties and have been used to aid hepatocyte attachment [149, 150]. Allylamine plasma deposition coats $P_{DL}LA$ with a layer of amine groups that encourage secondary ECM deposition and cellular attachment [150, 176] whilst NaOH treatment generates functional hydroxyl groups on the polymer surface to which cells can attach [149].

In this study when the $P_{DL}LA$ surface was modified, more hepatocytes attached directly to the polymer surface and the aggregate sizes were smaller. This was demonstrated with hepatocytes in mono-culture on both the plasma deposited and NaOH treated scaffolds. Surface characteristics also influenced cell phenotype. When HSCs were seeded onto unmodified $P_{DL}LA$ they developed an activated morphology with multiple cytoplasmic processes attaching to the scaffold surface. When ligand availability was increased, HSCs reverted to a predominantly quiescent phenotype as seen on the plasma and NaOH treated scaffolds. In co-cultures on unmodified $P_{DL}LA$ again there was much less hepatocyte attachment to the scaffold and more HSCs had an activated morphology than on the plasma treated and NaOH treated $P_{DL}LA$. On the surface modified scaffolds hepatocytes and HSCs attached directly to the scaffold surface with a few activated HSC and small cell aggregates visible.

The differences in attachment profile and culture morphology did not impact on the functionality of the co-cultures. When albumin production and CYP activities on the different cell-scaffold configurations were compared no difference was identified. Overall the functionality of mono-cultures and co-cultures on $P_{DL}LA$ in static conditions was disappointing, with both metabolic and synthetic function dropping significantly after 3-4 days in culture. Co-culture on $P_{DL}LA$ did significantly outperform hepatocyte mono-culture on TCP. However both synthetic and metabolic functions in the co-cultured scaffolds were significantly lower than that seen with hepatocyte mono-culture on collagen, a conventional hepatocyte culture system that hepatocyte-HSC co-culture in low adherent tissue culture conditions had previously been shown to significantly outperform [32, 34].

The significant drop in the synthetic and metabolic function of the hepatocyte populations that occurred after 3-4 days correlated with the non-viable appearance of the cell populations at day 5. This rapid decline in function was also seen when hepatocytes and HSCs were cultured on alginate scaffolds. It is unclear from this data, why this drop in function occurred. Previous work by Ranucci has shown that microporous PLA scaffolds can support functional hepatocyte monocultures for up to one week [157]. There have been no previous studies exploring how co-cultures behave on $P_{DL}LA$ in static conditions.

The scaffold culture system may have failed because: there was inadequate mass transfer of O_2 and nutrients into the scaffold pores; the seeding density of hepatocytes and HSCs was inadequate (preventing the formation of homotypic and heterotypic intercellular

interactions) or the release of lactic acid from the $P_{DL}LA$ was hepatotoxic. A range of modifications could be made. The scaffolds could be maintained within a bioreactor. Previous studies have shown that liver cell culture in microfluidic environments enhances hepatocyte synthetic function [182], allows differentiation of phenotype within a hepatocyte sub-population [37] and optimises mass transfer [159]. In addition micro-channels could be drilled through the scaffolds to further improve mass transfer. Alternative seeding densities may be trialled. Studies by Dvir-Ginzberg have shown that alteration in seeding densities can significantly impact on liver cell culture viability and function [160]. Microporous poly (α hydroxy acid) scaffolds have been shown to support liver cell culture but they may not be the "ideal" biomaterial for liver tissue engineering and alternative biomaterials or scaffold structures may be better suited for hepatocyte-HSC co-culture and warrant investigation.

Limitations in this study relate to the functional assays. In the testosterone metabolism assay, metabolites were detected by HPLC. After 3 days the levels of testosterone metabolites were very low even under optimal culture conditions [34]. In future an additional more robust metabolic assay (urea or CYP1A) could be used. It would also be beneficial to express functional data relative to total cell number. This could be achieved by performing a DNA assay in conjunction with the functional data.

2.5 Conclusion

The surface characteristics of $P_{DL}LA$ influence HSC phenotype and hepatocyte-HSC co-culture morphology. Under static conditions the long-term viability and function of these co-cultures is limited. This study supports further development of a HSC-based *in vitro* liver tissue engineering system but significant modifications to the culture system design are required.

Chapter 3 Polymer-Based Intra-Hepatic Growth Factor Delivery

Partial hepatectomy (PH) induces a proliferative response in liver that differs to the regenerative pathways seen in other tissues. Rather than proliferation of a sub-population of stem or progenitor cells or the recruitment of cells from the peripheral circulation, liver regeneration following PH is mediated by proliferation of the adult hepatocyte and non-parenchymal cell populations throughout the liver, not just in isolated lobes or at the resection surface. Remarkably whilst this expansion of liver mass occurs, the liver retains its functional capacity [59, 74].

The sequence of events that leads to this proliferative response is complex, involving interplay between the hepatocyte and non-parenchymal cell populations (endothelial cell, Kupffer cell and HSC) and the ECM. The trigger for regeneration is the change that occurs in hepatic blood flow (hepatic dysoxia, endothelial shear stress, increased hepatotrophic stimuli availability) [75] [74]. This is followed by an increase in urokinase activity [183, 184], remodelling of the ECM and mobilisation of HGF [185] [91]. At the same time, Kupffer cells begin to release TNFα and IL-6 [64, 122], which sensitise the hepatocyte population to the effects of HGF and EGF receptor ligand (TGF_{β}, EGF, HB-EGF) binding [96, 97]. The activation of the HGF and EGF receptors induces a number of intracellular signalling pathways resulting in rapid induction of more than 100 genes [59]. After the initial burst release of growth factors from the ECM, the HSC population becomes activated and begins to release HGF, TGF_{β} and ECM [47, 91] [93] [74] and the

hepatocyte population upregulates FGF_1 and FGF_2 expression [56, 109, 186]. In the rat liver this leads to restoration of liver mass within 7 days [57].

HGF is the liver's key mitogen. When its action is blocked, liver regeneration is impaired [187, 188] and when it is delivered into normal liver it can stimulate a proliferative response and even hepatic enlargement [95, 96 98, 99]. When it is delivered into partially hepatectomised liver or liver pre-treated with collagenase, this response is increased [96 97]. EGF receptor ligands are also mitogenic to hepatocytes, when injected into normal liver they stimulate only a modest proliferative response, but when they are injected into partially hepatectomised liver or liver pre-treated with collagenase the proliferative response is significant [97 74]. FGF_1 and FGF_2 are also mitogenic to hepatocytes [110], but their effects on liver mass have not been studied in detail.

ECM remodelling is another important element in the liver's regenerative cycle. In the early phase of regeneration the ECM acts as a reservoir for growth factors [121]and its breakdown products exert a direct chemotactic effect [28]. Whilst in the later stages of regeneration reorganisation of the ECM may act as a stop signal to the regenerative response [74, 189].

The aim of this study was to investigate the effects of intrahepatic delivery of the liver's key mitogens (HGF, EGF, FGF_1 and FGF_2) along with liver-derived ECM proteins via biodegradable polymer scaffolds, with the aim of inducing proliferation in normal hepatic parenchyma. This study was undertaken in rats and is presented in 2 parts. Part 1 focuses

on implant development and a pilot study, using only growth factor delivery, to assess the implantation technique and make a preliminary assessment of the proliferative response. Part 2 compares different polymer-based growth factor and ECM delivery systems.

3.1 Part 1: Implant Development & Pilot Study

3.1.1 Part 1 Introduction

A range of polymer-based growth factor delivery systems have been described [24, 146, 190]. For this study a delivery system and manufacturing technique that provided sustained release and allowed a high level of protein loading without loss of bioactivity was desirable. Supercritical processing of poly (α hydroxy acid) polymers using high pressure CO_2 reduces the glass transition temperature (T_g) of the polymer allowing melting and protein incorporation at physiological temperatures [25, 191, 192]. This method has been used to manufacture growth factor delivery systems that provide sustained release and have superior retention of bioactivity compared with alternative processing techniques and release technologies [192, 193].

Takimoto *et al* described implantation of a non-biodegradable polypropylene cone into rat liver [174]. In that study a 1 cm x 2 cm cone was pushed through the middle lobe of the liver and locked in place with extra-hepatic upper and lower stabilising discs. For this study a smaller implant that could be implanted into any lobe and did not require external stabilisation was required.

Part 1 of this study was undertaken in 2 steps: step 1 implant development and step 2, a pilot study. The objective of the implant development process was to design a polymer-based growth factor delivery system based on choice of biomaterial, size of implant,

processing technique and implantation method and then develop and optimise a surgical protocol for polymer scaffold implantation, using cadaveric and terminal anaesthetic studies, before embarking on survival surgery. The objectives of the pilot study were to assess the implantation technique using survival rates, liver weights and serum liver function, and to perform a preliminary characterisation of the liver- implant interaction over 14 days, using H&E staining and MIB-5 immunohistochemistry (IHC) as a proliferative marker. Control animals underwent a sham procedure or received a plain polymer implant. An overview of the study design is shown in figure 3.1.

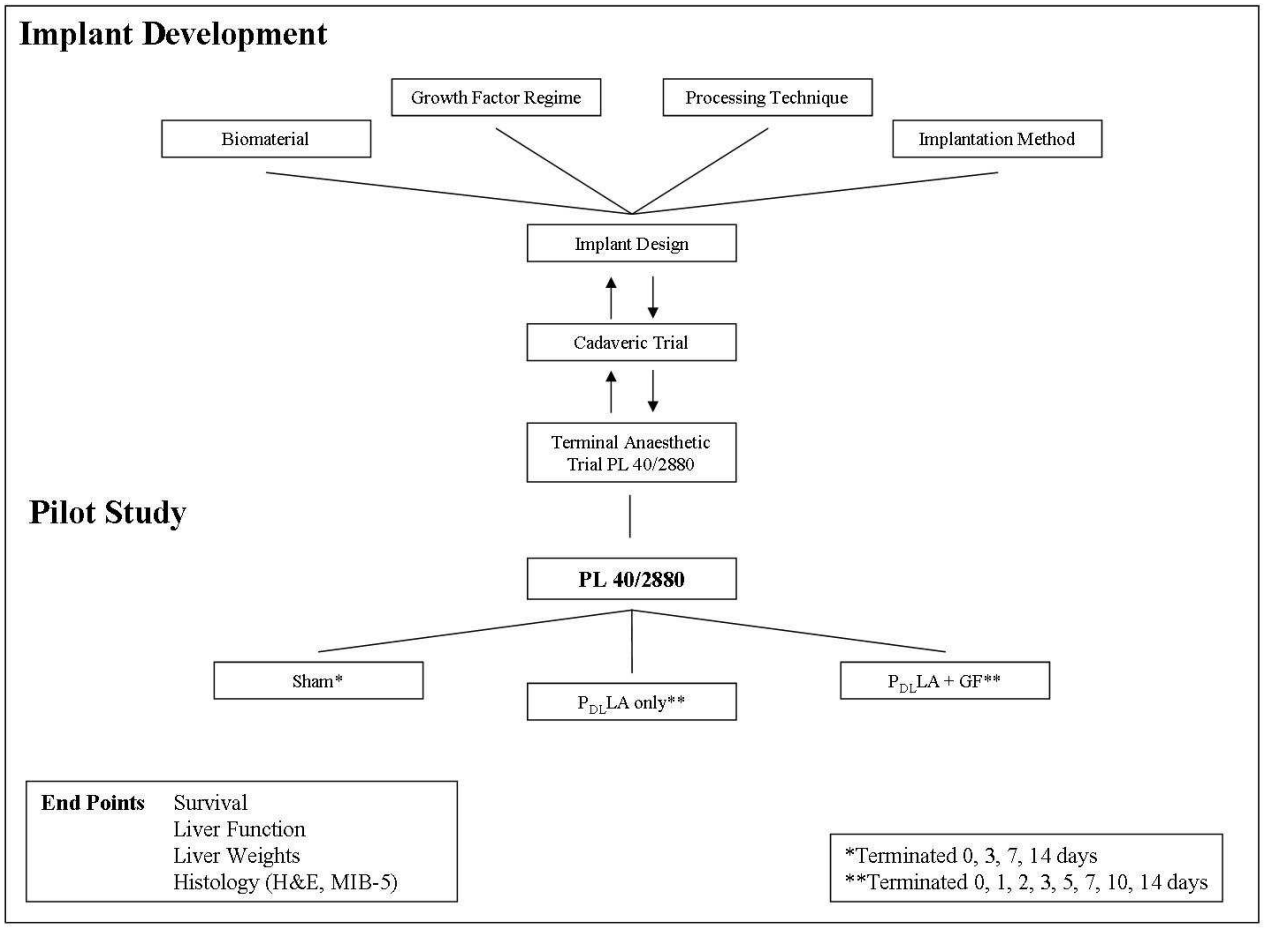

Figure 3.1 Implant development and pilot study design

3.2 Materials & Methods

3.2.1 $P_{DL}LA$ Implant Manufacture

Porous $P_{DL}LA$ cylinders were manufactured as previously described [150]. In brief, to manufacture a plain $P_{DL}LA$ implant, 130 mg of $P_{DL}LA$ (mw 52 Polyscience Inc) was placed in a 1cm x 1 cm poly (tetrafluoroethylene) (PTFE) mould, melted using a 230 bar pressure of CO_2 at 35º C for 60 min followed by a 60 min decompression. The 1 cm x 1 cm porous $P_{DL}LA$ cylinder was then machine cut on a Boley lathe at 3000 rpm (Boley) down to a 3 mm x 4 mm porous cone and stored at 4º C until implantation (Appendix 1).

To manufacture a growth factor loaded $P_{DL}LA$ implant,130 mg of $P_{DL}LA$ was blended with a growth factor solution (0.4 μg/ml of recombinant human (rh) HGF, 20 μg/ml rh EGF, 2 μg/ml rh FGF_1 and 2 μg/ml rh FGF_2 (Autogen Bioclear Ltd)). The polymer-growth factor blend was freeze dried, placed in the PTFE mould and supercritically processed in CO_2. The growth factor loaded $P_{DL}LA$ cylinder was machine cut as above. Before implantation each cone was centrifuged at 100 g with a 8 μl solution containing 0.4 μg of HGF, 0.4 μg of EGF, 0.4 μg of FGF_1 and 0.4μg of FGF_2 for 5 min, freeze dried at -20º C and stored at 4º C until implantation (Table 3.1).

Table 3.1 Growth factor dosage for the pilot study

Growth Factor	Supercritically Incorporated	Surface Adsorbed	Total
HGF	30 ng	400 ng	430 ng
EGF	550 ng	400 ng	950 ng
FGF_1	170 ng	400 ng	570 ng
FGF_2	170 ng	400 ng	570 ng

3.2.2 Implant Characterisation: Micro CT

μCT images of implants were obtained using a high resolution μCT system (μCT 40, Scanco Medical). Scaffolds were mounted on a stage within the imaging system and scanned at 55 kV with a current of 143 mA. Samples were scanned at 12 μm resolution with an integration time of 300 msec to produce three dimensionally reconstructed images. Raw tomographic images were thresholded to remove background data, and porosity and pore diameter were calculated using Scanco image analysis software.

3.2.3 Animals

The pilot study was approved by the U.K. Home Office and conducted in accordance with protocols laid out in Project Licence PL 40/2880. 70 adult male Wistar rats (Charles River) (200-300 g) were housed in the Biomedical Sciences Unit of the University of Nottingham, given access to standard laboratory rat chow and water *ad libitum* and maintained in a standard 12-hour light-dark cycle.

3.2.4 Anaesthetic Protocol

Animals were anaesthetised in a closed box using 1.5% isoflurane and oxygen. The unconscious rat was weighed and a given a subcutaneous injection of buprenorphine (2.5 mg/kg). The animal was then transferred on to a warming mat where anaesthesia was delivered via a face mask. Depth of anaesthesia was assessed by confirming a negative response to a painful stimulus (squeezing web space between toes of the hind feet) and monitored throughout surgery by assessing respiratory rate and response to painful stimuli.

3.2.5 Operative Technique

The abdomen was shaved, cleaned with 10% aqueous betadine and draped. A 2 cm upper midline abdominal incision was made and using bilateral subcostal compression the middle lobe delivered. Holding the middle lobe between the thumb and index finger a 1 mm capsular incision was made on the anterior surface of the lobe to a depth of 0.5 mm using a number 11 scalpel blade. The cone was then implanted into the liver so that its edges sat below the capsule. Haemostasis was achieved where necessary by gentle compression with a cotton bud. The lobe was then returned to the abdomen, the abdominal cavity inspected and the abdominal wall closed in layers with 3/0 vicryl on a cutting needle. The animal was recovered on a warming mat, weighed and housed under standard conditions with buprenorphine given for 2 days post-operatively. In those

animals undergoing a sham procedure an upper midline incision, middle lobe delivery and liver capsule incision was performed.

3.2.6 Necropsy Protocol

At allocated time points the animals were anaesthetised (section 3.2.4) and weighed. Blood samples were collected by cardiac puncture and the animals sacrificed with an intra-cardiac bolus of phenobarbital. After death was confirmed (loss of light reflex and heart beat), a full length midline abdominal incision was made, the liver was dissected from surrounding tissue and removed. The total liver weight was recorded and the livers prepared for histology.

3.2.7 Liver Weight Analysis

The growth of liver tissue was assessed using the following equation:

Equation 1

$$\text{Liver body weight ratio (LBW)} = \frac{\text{Total liver weight}}{\text{Body weight at termination}}$$

3.2.8 Liver Function

Serum aspartate aminotransferase (AST) and total bilirubin were measured using a Vitros chemistry plate analyser (Ortho-Clinical Diagnostics, Johnson & Johnson) as described in Vitros Chemistry Publications 815 9931, 843 3815.

3.2.9 Processing & Histology

At sacrifice the livers were removed and fixed in 10% phosphate buffered formalin (Sigma), stored for up to 1 month and processed on a vacuum tissue processor (Leica Microsystems) (Appendix 3). Paraffin sections were stained with haemotoxylin & eosin (H&E) for routine histology.

3.2.10 MIB-5 / Ki-67 Immunohistochemistry

MIB-5 index was detected as previously described [194, 195] (Appendix 7). 4 μm sections were dewaxed in histoclear and immersed in 10 mM sodium citrate (pH 6.0), washed, incubated in H_2O_2 blocking solution, washed in dH_2O, rinsed in 0.005 M TRIS/HCl Buffered Saline (TBS) pH 7.6 and incubated in a 1:100 Ki-67 antibody solution for 30 mins (M7248, Dako Systems). Slides were then agitated TBS, incubated in dextran antibody solution (Dako Systems), washed, incubated in DAB chromogen solution, washed, counterstained in Gill's haematoxylin, washed and differentiated in 1% acid

alcohol. Finally the slides were washed, dehydrated in alcohol and transferred to alcohol and histoclear before mounting in DPX.

3.2.11 Imaging and Analysis

Histological evaluation was undertaken by a blinded independent pathologist (A. Zaitoun). H&E and IHC slides were imaged using a digital NanoZoomer (Hamamatsu, Photonics Ltd). Representative images were selected for presentation.

3.2.12 Statistical Analysis

Data was analysed using the SPSS. Data are expressed as the mean +/- standard deviation. The statistical significance of differences among groups was assessed by the independent Student t test or the one way ANOVA with Tukey post test as appropriate. P values less than 0.05 were regarded as statistically significant.

3.3 Results

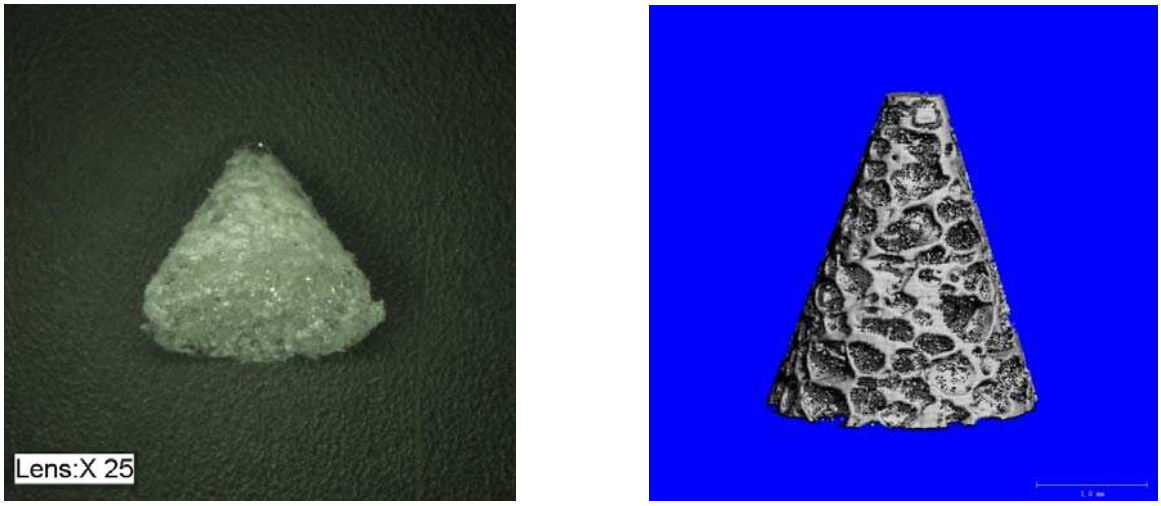

Figure 3.2 Photograph (*left*) and μCT reconstruction (*right*) of a machine cut $P_{DL}LA$ implant. Conical implants (base 3 mm x height 4 mm) were machine cut from $P_{DL}LA$ cylinders foamed by supercritical CO_2 processing, yielding implants with a mean porosity of 30.8% and a mean pore diameter of 103.8 μm as determined by μCT reconstruction (*right*).

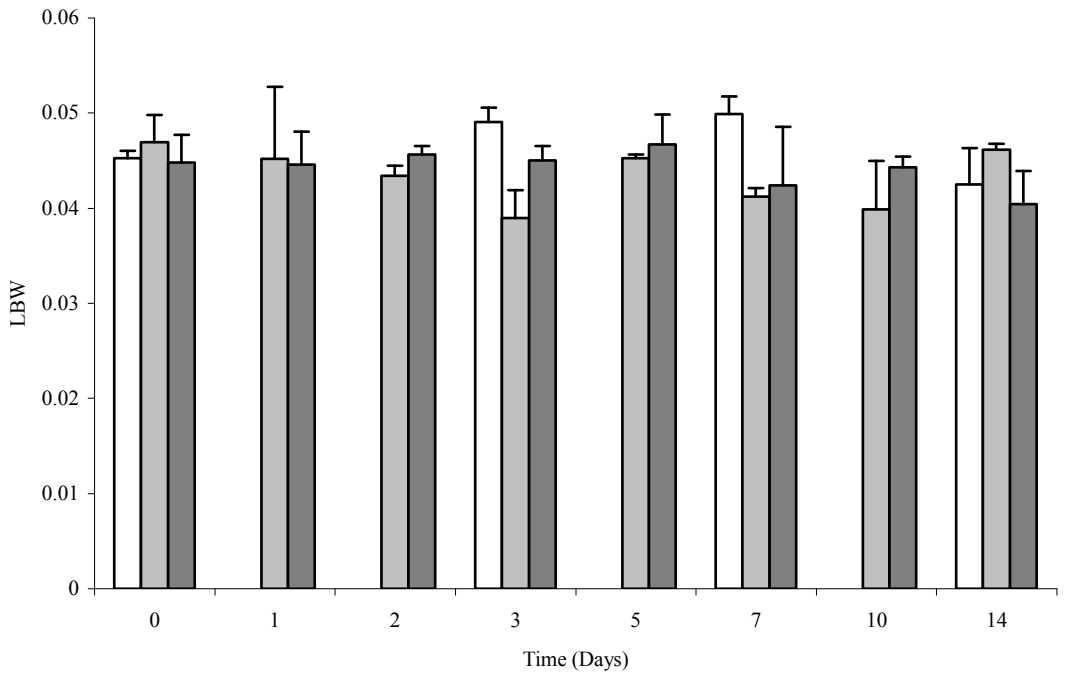

Figure 3.3 LBWs (calculated using equation 1) following sham procedure (*white*), plain polymer (*light grey*) and growth factor loaded cone (*dark grey*) implantation (+/- SD of mean) (n=3). There was no significant difference LBWs between the sham, plain polymer and growth factor loaded polymer groups.

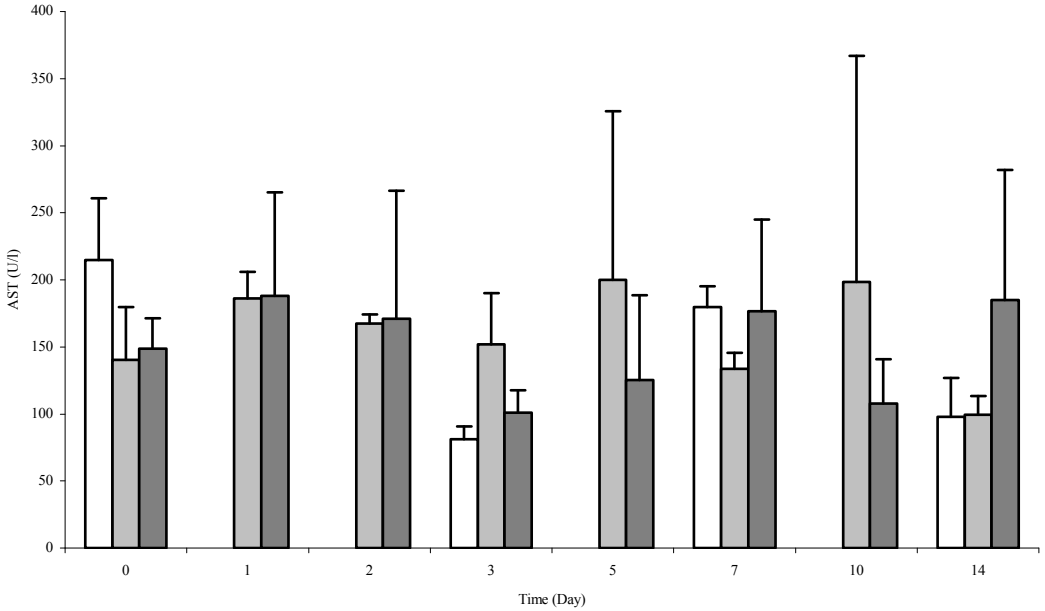

Figure 3.4 Serum AST for the pilot study up to 14 days after implantation. Following sham procedure (*white*), plain polymer (*light grey*) and growth factor loaded cone (*dark grey*) implantation (+/- SD of mean) (n=3). There was no significant difference in serum AST levels between groups. Serum bilirubin was undetectable for the duration of the study.

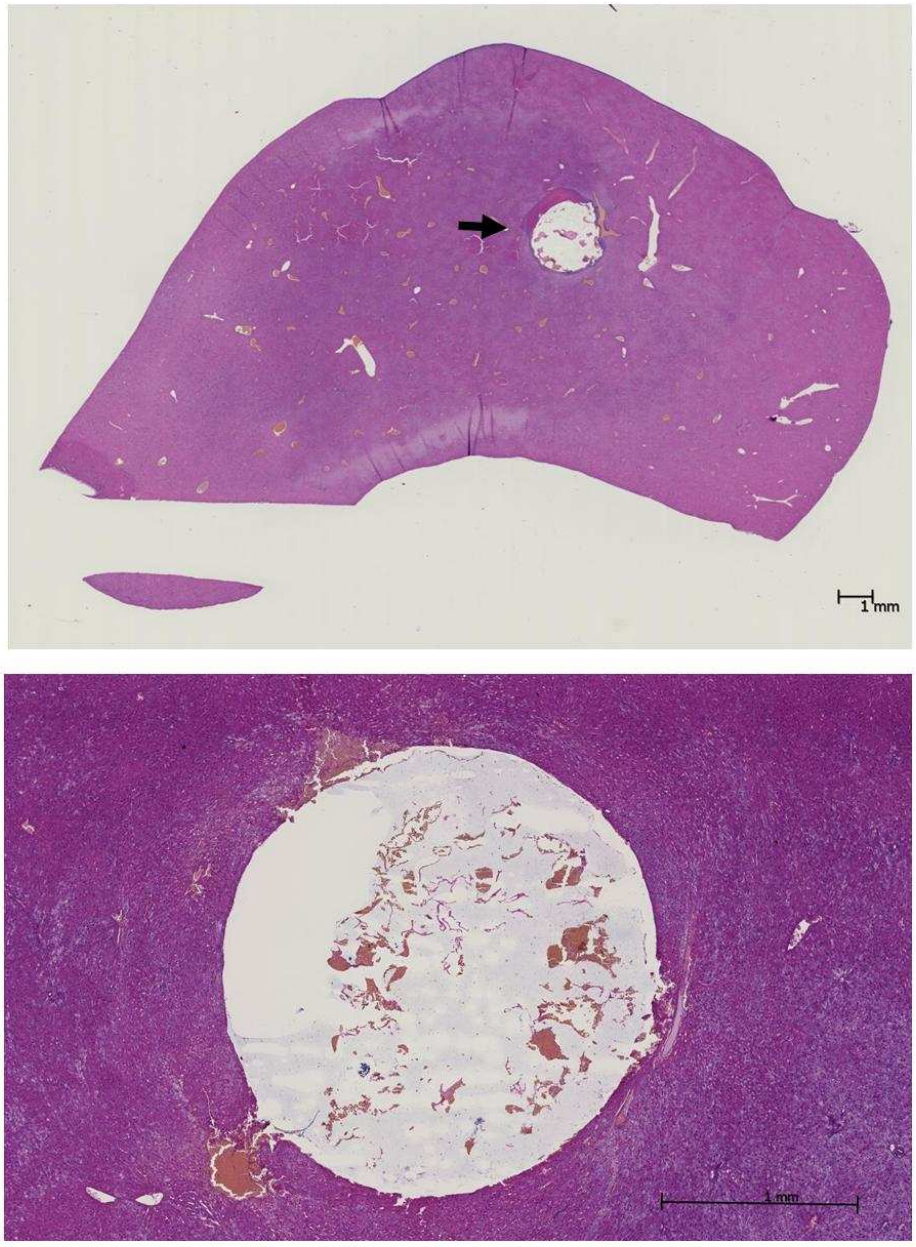

Figure 3.5 H&E staining of $P_{DL}LA$ scaffolds implanted into rat liver for the pilot study. Low power demonstrating a scaffold implanted into the medial lobe (*top*) and higher power demonstrating the porous scaffold and surrounding parenchyma at T_0 (*bottom*). Following implantation, the porous cones compressed the surrounding liver tissue and erythrocytes filled the pores. Original magnification top 1.25X and bottom 2.5X.

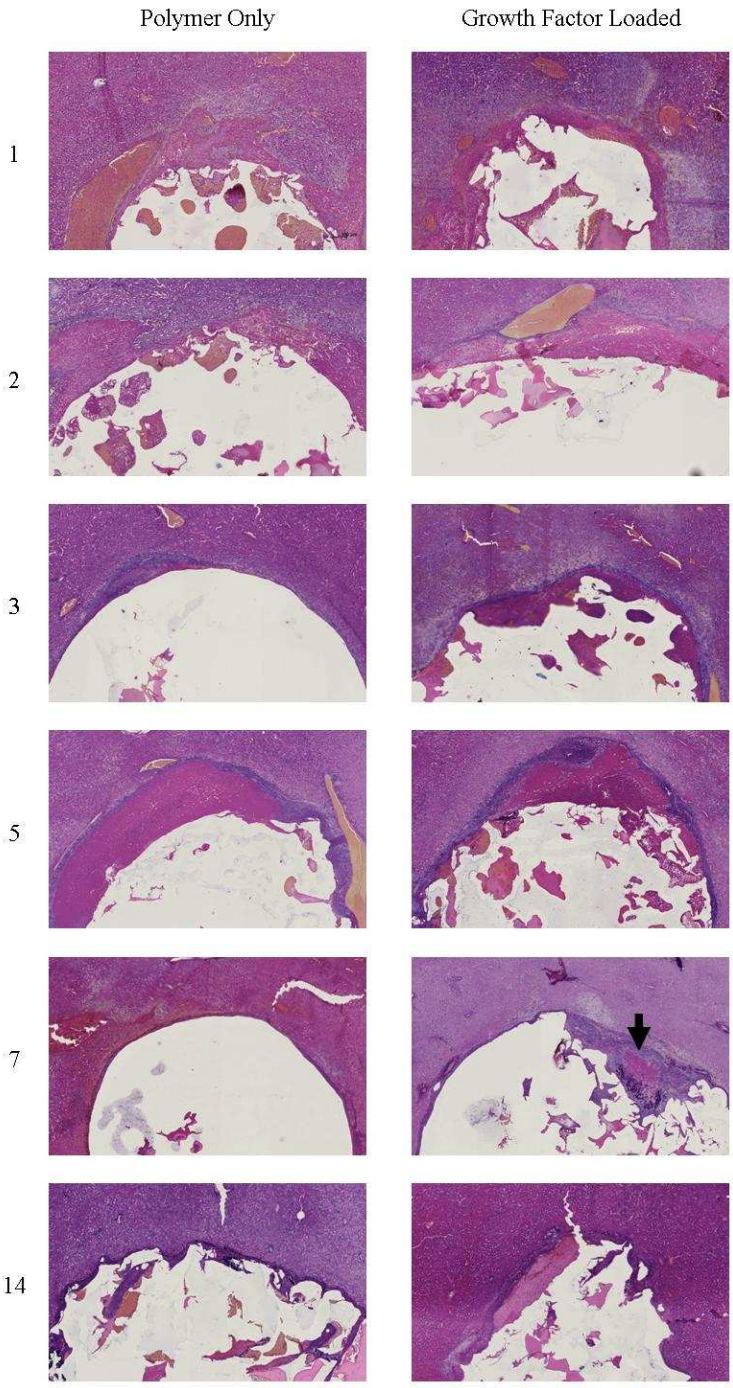

Figure 3.6 H&E of plain polymer (*left*) and growth factor loaded (*right*) scaffold implanted livers at up to 14 days after implantation. By day 2 a band of inflammation surrounded each implant; by day 5 the band of inflammation had decreased in size and had become well demarcated and by day 7 there was evidence of cell migration / ECM deposition in the pores of the growth factor loaded scaffolds (*arrowed*). Cell migration / ECM deposition was present in all scaffolds at day 14. Original magnification 2.5X.

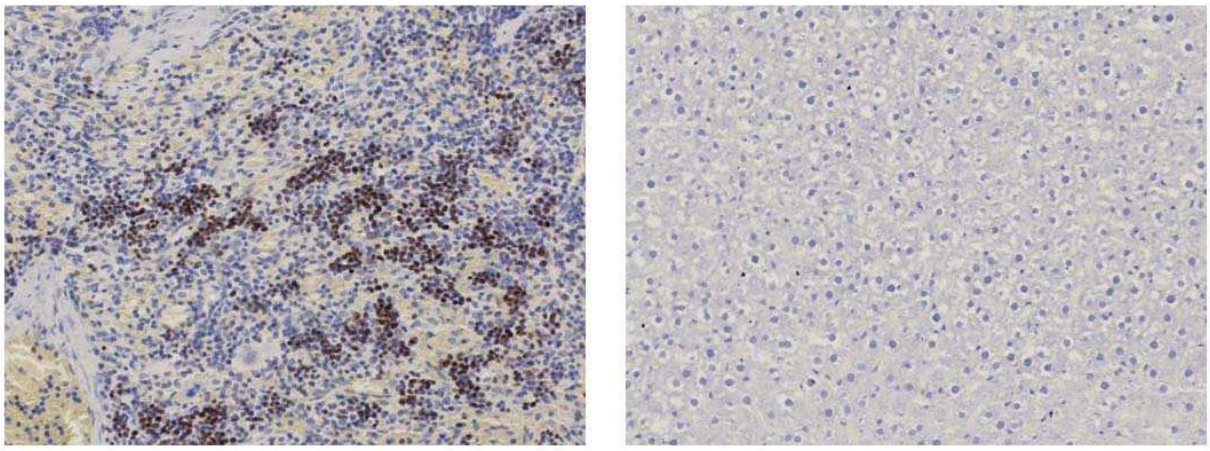

Figure 3.7 MIB-5 IHC of rat spleen (*left*) and peri-implant parenchyma 4 days after implantation of a growth factor loaded scaffold into normal liver (*right*). MIB-5 positive nuclei are stained brown & peroxidase activity is stained blue. MIB-5 positive nuclei were present in the control tissue but despite changes on H&E staining of the implanted liver tissue that were consistent with active mitosis no MIB-5 stained cells present on any of the samples for the duration of the study. Original magnification 20X.

3.4 Discussion

Supercritical processing of $P_{DL}LA$ exhibits high protein loading and sustained release kinetics [25, 191, 193, 196]. Growth factor containing $P_{DL}LA$ scaffolds were used for direct implantation into the middle lobe of anaesthetised rats. Pre-process loading and direct surface adsorption allowed the production of implants that contained a total of 430 ng of HGF, 950 ng of EGF, 570 ng of FGF_1 and 570 ng of FGF_2.

Following a series of cadaveric studies a 3 mm x 4 mm cone was selected because it could be implanted easily without parenchymal fracture. The surgical protocol was then developed and optimised. A further series of terminal anaesthetic studies were undertaken to ensure that the cones could be implanted safely and to identify and resolve any peri-operative complications (haemorrhage, parenchymal fracture and implant migration).

The study describes a method of intrahepatic scaffold implantation that is feasible and well tolerated. In the pilot study there were no surgical or anaesthetic complications and all animals recovered and survived until the allocated time points.

Liver and body weight analysis did not detect any difference in LBW between the sham, polymer only or growth factor loaded groups. In future studies the implanted lobe weight will be measured to improve the sensitivity of the liver weight analysis.

Isolated increases in serum AST occurred in both implantation groups. The increase in AST after implantation resulted from mobilisation of the liver and parenchymal trauma during capsule incision. Later elevation of serum AST may have related to peri-implant inflammation.

Histology confirmed successful implantation of the cones into the middle lobe of the liver. There were no episodes of implant migration. Implantation of plain polymer and growth factor loaded cones resulted in an initial inflammatory reaction that resolved with time and was followed by cell migration and ECM deposition into the pores of the scaffolds. There was no evidence of inflammation in the sham group, although the capsule incision site was difficult to localise by day 3. The pattern of inflammation was similar in the plain polymer and growth factor loaded implants. Cell migration / ECM deposition was present in the pores of the growth factor loaded scaffolds by day 7 and was present in both scaffold types by day 14.

At this stage the significance of peri-implant inflammation was unclear. Liver regeneration is a multi-step process requiring "priming" of the hepatocyte population, and so some peri-implant inflammation may enhance the activity of growth factors being released from the scaffolds. The inflammatory response therefore needs to be characterised further. Similarly cell migration and ECM deposition within the pores of the scaffolds is potentially beneficial as it increases liver-scaffold interaction and may encourage mobilisation of growth factors from the polymer matrix. The nature of this interaction also requires more detailed characterisation.

MIB-5 IHC failed to identify proliferating parenchymal or non-parenchymal liver cells in the sham, plain polymer or growth factor loaded implant groups despite changes in the parenchyma and scaffolds suggestive of proliferation. MIB-5 antibody binds to the Ki-67 related nuclear protein present throughout the cell cycle and has previously been shown to correlate well with existing proliferative markers in rodent tissue [194, 195]. Expression and localisation of the nuclear protein does vary between tissues and with fixation and processing protocols [195, 197]. The size of the liver samples may have led to inadequate fixation of cells and a failure to detect the cell related nuclear antigen. In future studies modifications to the histology protocols will be made to ensure adequate fixation (see below) and BrdU incorporation will be undertaken in conjunction with the MIB-5 IHC to ensure that any proliferating cells are identified.

The limitations in this study relate to release profiling and histological processing. Release profiling of the growth factors incorporated in this study was not performed. Whilst interpretation of *in vitro* release data has limited applicability to the *in vivo* setting, having an indicator that growth factors are present within the implant and that they have retained their bioactivity after processing would be desirable. An *in vitro* release study should therefore be performed prior to embarking on the next phase of the study. Limitations in the fixation and processing protocols were demonstrated in the pilot study. In future studies, liver will be cut up into 1 cm x 1 cm blocks before fixation and will be fixed in a vacuum for a minimum of 48 hours before processing, rather than fixing whole lobes of liver with the capsule still intact. These modifications along with the use of BrdU

IHC to quantify proliferation and IHC to characterise cell migration and ECM deposition and inflammation will be carried forward to the comparative study.

3.5 Conclusion

This study presents a new method of intrahepatic polymer scaffold implantation that is safe and well tolerated. Intrahepatic implantation of porous $P_{DL}LA$ stimulates a peri-implant inflammatory reaction that resolves with time and is followed by cell migration and ECM deposition in the pores of the scaffold. No proliferative response was identified in the livers implanted with the polymer based delivery system.

3.6 Part 2: A Comparative Study

The doses of HGF, EGF, FGF_1 and FGF_2 (alone or in combination) required to induce a proliferative response in normal rat liver is not known. Several studies have explored the dose response for HGF and EGF delivery in rodent liver. These studies (summarised in table 3.2) have used different rodent species and strains, different infusion techniques, and different HGF and EGF preparations measured to different end points. The route, method and duration of delivery all impacted on the proliferative response. Growth factors have short half lives *in vivo* and are rapidly cleared [99]. Delivering the growth factors directly into the liver parenchyma will therefore have a different effect to delivery into the portal or systemic circulation. These studies demonstrate that large doses of individual growth factors are required to induce pan-hepatic enlargement in normal liver, but that smaller doses can stimulate increases in proliferation when delivered into liver "primed" for regeneration [97 96]. There are no reports of the effects of delivering multiple growth factors directly into the hepatic parenchyma.

Table 3.2 summarises the results of 6 studies exploring the impact of intra-hepatic growth factor delivery in rodent liver. Where response to growth factor delivery is not known the section is blank

Study	Species & Strain	Growth Factor	Route	Dose	Outcome				
					Proliferation			Liver weight	
					Measure	Response			
Patijns *et al* *1998*[95]	Mouse ♀ C57BL/6 & NIH3	rh HGF	Portal vein	5 mg/kg/day for 5 days	BrdU	↑	-	↑	x2.5
Roos *et al*[198] *1995*	Mouse ♂ C3H/HeJ	rh HGF + dextran sulphate	Intraperitoneal	2.4 mg/kg/day for 3 days	Mitotic bodies	↑	-	↑	x1.3
Ishii *et al*[99] 1995	Rat ♂ Wistar	HGF	Jugular Vein	100 µg/kg/day up to 5 days	BrdU	↑	x6	→	-
Liu *et al*[96] 1994	Rat ♂ Fisher 344	rh HGF	Portal Vein	100 µg/kg	BrdU	↑	x4	-	-
Webber *et al*[97] 1994	Rat ♂ Sprague-Dawley	rh HGF	Portal Vein	80 µg	3H-thymidine	↑	x2	-	-
Fujiwara *et al*[98] 1993	Rat ♂ Sprague-Dawley	h and rh HGF	Femoral Vein	600 µg/kg	BrdU	↑	-	-	-
Webber *et al*[97] 1994	Rat ♂ Sprague-Dawley	rh EGF	Portal Vein	80 µg	3H-thymidine	↑	x2	-	-

3.6.1 Implant Manufacture

Supercritical processing using high pressure CO_2 incorporates growth factors and other bioactive molecules into poly (α hydroxy acid) scaffolds without major loss of bioactivity [191, 193, 196]. In the pilot study growth factors were loaded prior to processing in high pressure CO_2. As a result, polymer containing growth factor was lost during cut down to the conical implants. To improve the efficiency of this process an alternative method that retained the benefits of supercritical processing but eliminated the cut down step was developed.

Work by Hamilton *et al* has shown that blending 50:50 PLGA with PEG_{400} reduced its T_g (figure 3.9) [199]. At 5% PEG inclusion the T_g of PLGA is reduced to 35-40º C. A PLGA + 5% PEG blend can then be mixed in high pressure CO_2 and melted at temperatures that will not denature the growth factors or ECM proteins incorporated into it. For the comparative study, growth factors and L-ECM were incorporated into PLGA + 5% PEG in high pressure CO_2. This was milled into microparticles and sintered at 40º C in a conical teflon mould. This modification to the implant manufacturing step increased the efficiency of growth factor loading and enabled larger doses of individual growth factors to be incorporated.

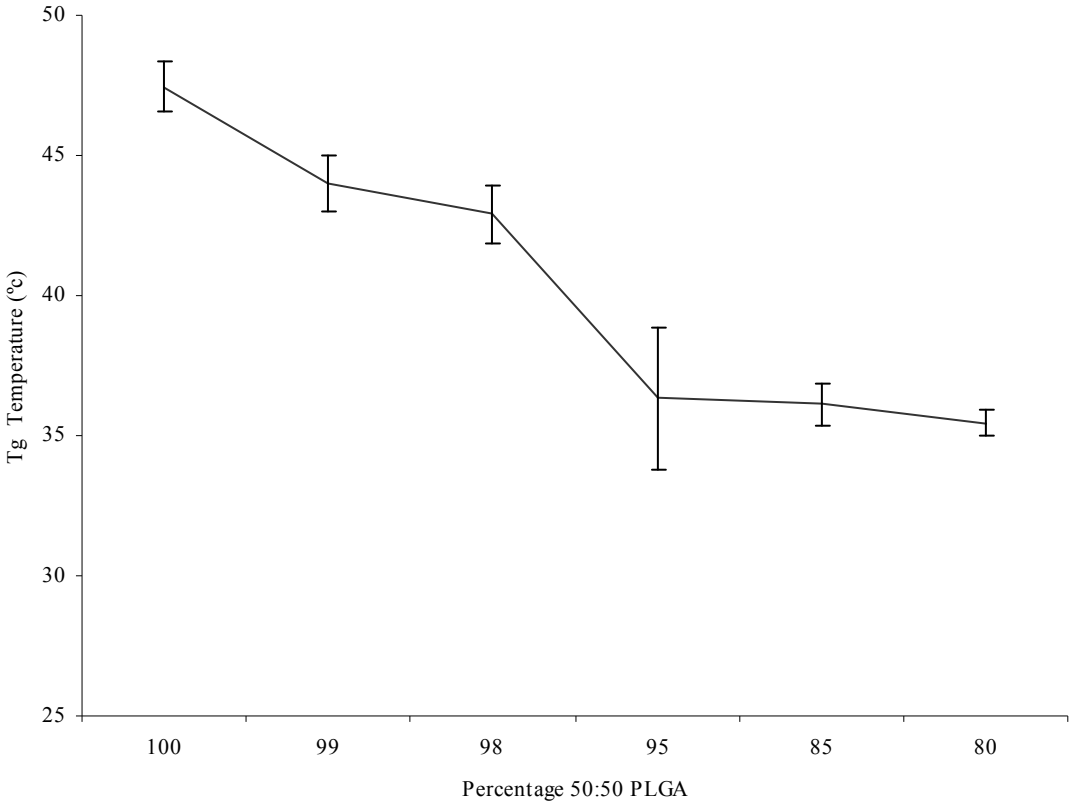

Figure 3.8 Impact of PEG_{400} incorporation on the Tg of 50:50 PLGA. As the amount of PEG blended with PLGA increases the Tg of the polymer blend decreases. At 5% loading of PEG the Tg has fallen into a physiological range (35-40º C)[199]

3.6.2 L-ECM Manufacture

L-ECM is manufactured by decellularising slices of porcine liver. This produces a sheet made up of structural (collagens, glycoproteins and proteoglycans) and functional proteins, including growth factors [43]. *In vitro* L-ECM has been shown to maintain hepatocyte viability and function [144] and promote sinusoidal endothelial cell differentiation [30]. *In vivo* similar naturally derived ECM products have been used to stimulate regeneration without scarring in a range of tissues [31].

L-ECM was incorporated into the polymer cones by milling sheets of lyophilised L-ECM into sub 220 μm microparticles and mixing them with the polymer in high pressure CO_2. The maximum amount of L-ECM that could be incorporated into the cone implants was 20% by weight. Loading the L-ECM at levels above 20% resulted in softening of the implants at body temperature, which made implantation difficult. .

The pilot study demonstrated that intrahepatic biodegradable polymer scaffold implantation was feasible and identified modifications to the implant design and study protocol necessary to optimise the data set. These modifications were implemented into the study design. The objectives of the comparative study were to characterise the interaction between the liver and the growth factor and or L-ECM loaded polymer implants and to compare the proliferative response induced in the surrounding parenchyma. Again the study was undertaken in rats. Animals were maintained for up to 56 days post-implantation. Control animals underwent a sham procedure (laparotomy & capsule incision) or had a plain polymer or plain L-ECM cone implanted. An overview of the study design is shown in figure 3.9.

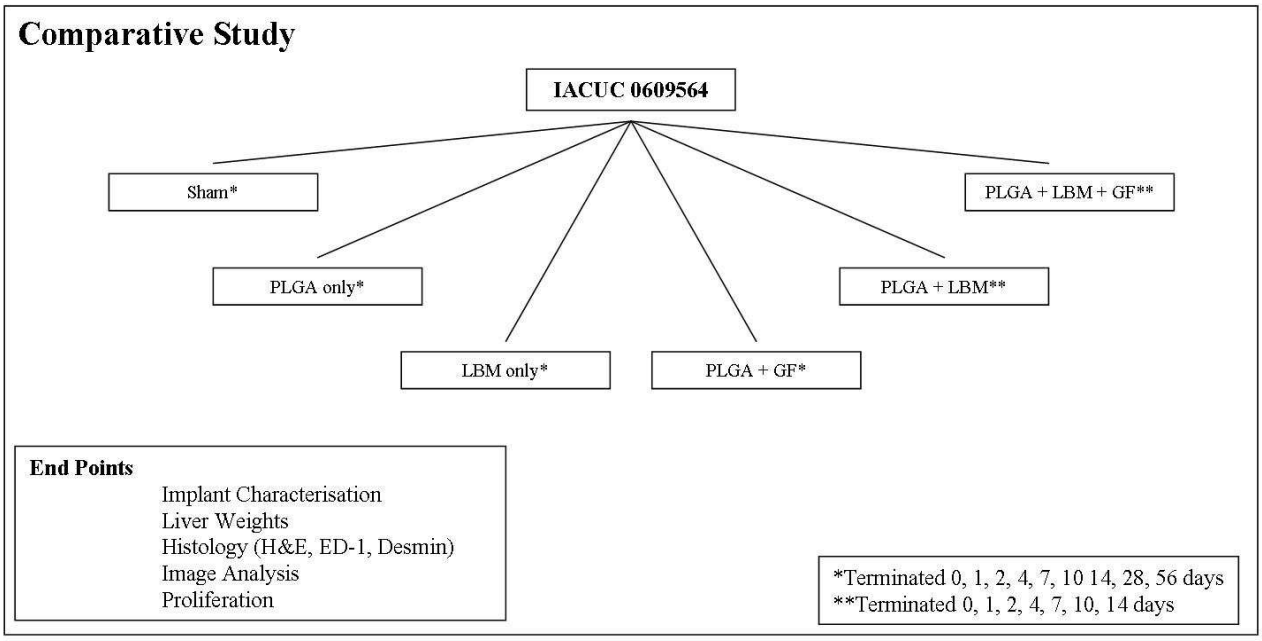

Figure 3.9 Comparative study design

3.7 Materials & Methods

3.7.1 Animals

The Comparative Study was approved by the University of Pittsburgh's Institutional Animal Care Use Committee (IACUC) and conducted in accordance with the protocols laid out in Licence 0609564. 150 adult male Wistar rats (Charles River) (200-250 g) were housed in the Animal Facility of the McGowan Institute for Regenerative Medicine, University of Pittsburgh, given access to standard laboratory rat chow and water *ad libitum* and maintained in a standard 12-hour light-dark cycle.

3.7.2 L-ECM Isolation

Decellularised L-ECM was isolated as previously described [38, 144]. Porcine liver was cut into 5 mm slices on a rotating blade and washed in de-ionized water. The liver slices were pressed and soaked in 0.02% trypsin / 0.05% EDTA acid (Gibco) at 37º C for 1 hour, washed in deionised water, repressed and mechanically agitated in a 3% Triton X-100 solution (Spectrum Laboratory Products Ltd). The slices were repressed and mechanically agitated in 4% sodium deoxycholic acid (Spectrum) for 1 hour followed by irrigation in water. Hydrated sheets of L-ECM were finally vacuum-pressed into a teflon mould (Appendix 2) or lyophilised at -20º C, milled into sub 225 μm microparticles using a Wiley mill and sterilised in ethylene oxide (EtO) (Sterile Technologies Inc.).

3.7.3 Polymer Implants

To manufacture the polymer only implants PLGA (50:50, Alkermes) and PEG (mw 400 Fluka) were mixed together at 95º C to produce a PLGA 5% PEG blend. This was milled and processed using a 230 bar pressure of CO_2 at 35º C for 60 min followed by a 60 min decompression. The supercritically processed PLGA + 5% PEG blend was milled to sub 250 μm microparticles, 8 mg of which was loaded into a 4 mm x 4 mm teflon mould (Appendix 2), sintered at 40º C for 3 hours and cooled for 30 min at 4º C before removal. The implants were stored at 4º C until implantation.

To manufacture the growth factor loaded implants, the milled polymer blend was mixed with a growth factor solution (per implant = 8 mg PLGA 5% PEG: 2.5 μg rh HGF, 5 μg

rh EGF, 2.5 μg rh FGF_1, 2.5 μg rh FGF_2), freeze dried, processed, milled and sintered as described above. To manufacture the L-ECM loaded implants, milled polymer blend was mixed with milled liver-ECM (20% by weight), processed, milled and sintered, and to manufacture the growth factor and liver-ECM loaded hybrid implants, milled polymer blend was mixed with milled liver-ECM and the growth factor solution (per implant = 6.4 mg PLGA 5% PEG + 1.6 mg L-ECM + 2.5 μg HGF, 5 μg EGF, 2.5 μg FGF_1, 2.5 μg FGF_2), freeze dried, processed, milled and sintered.

Table 3.3 Growth factor dosages for the comparative study

Growth Factor	Total
HGF	2.5 μg
EGF	5.0 μg
FGF_1	2.5 μg
FGF_2	2.5 μg

3.7.4 L-ECM Implants

To manufacture the L-ECM only implants, 10 sheets of hydrated L-ECM were vacuum pressed into a teflon mould (Appendix 2). Implants were sterilised with EtO and stored until use.

3.7.5 Implant Characterisation: L-ECM Distribution

To determine the distribution of L-ECM in the polymer implants, dyed, NaCl-labelled gelatine was substituted for the L-ECM. Milled PLGA + 5% PEG blend was mixed with milled dehydrated gelatin (sub 220 μm) containing red food dye and NaCl (80% polymer 20% gelatin by weight). This was processed and sintered as described above, and the implant imaged by light microscopy and μCT.

3.7.6 Implant Characterisation: Release Profiling

Growth factor loaded PLGA + 5% PEG implants were each incubated in 5 ml of PBS for 5 days at 37º C in static conditions. The PBS was then aspirated and stored at -20º C for later analysis. HGF, EGF FGF_1 & FGF_2 levels in 5 day implant-conditioned PBS were determined using HGF and EGF Quantikine® ELISA kits as previously described (DHG00, DEG00, DFA00B & DFB50, R&D Systems). In brief, standards and appropriate dilutions of samples were incubated on HGF and EGF antibody coated 96-well plates. The plates were washed, incubated with an HRP conjugated antibody, washed and incubated with a substrate solution (TMB) for 20-30 min before the reactions were terminated with 2 M H_2SO_4 and the optical density measured at 450 nm using a MRX plate reader (Dynex Technologies). Sample concentrations were determined by regression analysis of the standard curves.

To determine the bioactivity of implant-conditioned PBS, hepatocytes were cultured with implant-conditioned media, unconditioned media or media containing a known concentration of growth factors and the culture morphology compared. Hepatocytes were isolated from adult male Wistar rats as previously described (section 2.2.1) [177]. Viable hepatocytes were plated at a density of 15000 cells/cm^2 in T40 culture flasks for 2 hours in Williams E media containing 10% FCS. The cells were then washed with warmed PBS and the media replaced with 15 ml of either 2:1 hepatocyte culture media: unconditioned PBS, 2:1 hepatocyte culture media: conditioned PBS or 2:1 hepatocyte culture media: growth factor solution (PBS containing 2.5 μg rh HGF, 5 μg rh EGF, 2.5 μg rh FGF_1, 2.5 μg rh FGF_2). The cultures were maintained in 5% CO_2 at 37º C and imaged at 0, 12, 24, 48 and 72 hours (representative images shown).

3.7.7 Anaesthetic Protocol & Operative Technique

The anaesthetic and operative protocols were the same for the pilot and comparative studies, with the addition of one pre-operative and two post-operative doses of gentamicin (5 mg/kg) for each animal.

3.7.8 Necropsy Protocol

A sterile intraperitioneal injection of 5-bromo-2-deoxyuridine BrdU (100 mg/kg) (Sigma) was given 24 hours prior to sacrifice. At allocated time points the animals were anaesthetised (as above) and weighed. Blood samples were collected by cardiac puncture and the animals sacrificed with an intra-cardiac bolus of potassium chloride. After death

was confirmed (loss of light reflex and heart beat), a full length midline abdominal incision was made, the liver dissected from surrounding tissue and removed. The total liver and middle lobe weights were recorded and the livers prepared for histology.

3.7.9 Liver Weight Analysis

In addition to the LBW, the growth of liver tissue was assessed using the following equation:

Equation 2

$$\text{Middle: total liver weight ratio (MTR)} = \frac{\text{Middle Lobe Weight}}{\text{Total liver weight}}$$

3.7.10 Processing & Histology

At sacrifice the livers were removed, cut into 1 cm x 1 cm squares, fixed in 10% phosphate buffered formalin for 24 hours in a vacuum at 37º C and stored for up to 1 month. Livers were then processed on a vacuum tissue processor as for the pilot study (Appendix 3). 3 μm paraffin sections were stained with H&E for routine histology and Masson's Trichrome to assess of ECM deposition (Appendix 4).

3.7.11 ED-1 Immunohistochemistry

ED-1 positive cells were detected as previously described (Appendix 5) [200]. 3 µm paraffin sections were de-waxed in histoclear, quenched in H_2O_2 and rinsed in dH_20. The sections were incubated in 0.05 Tris for 5 min and in trypsin (1 mg/ml) for 15 min at 37º C. The sections were blocked, drained and incubated for 1hour at room temperature in a 1:200 primary ED-1 antibody solution (MCA341R, Serotec). The sections were rinsed in 0.1 M phosphate buffer saline containing 0.3% Triton X-100 and 0.1% sodium azide (PBST) and incubated in a 1:500 secondary antibody solution (AP192B, Chemicon) for 30 min. The sections were rinsed in PBST and labelled with an Avidin-biotin complex (ABC) Vector Elite kit (Vector Laboratories) for 30 min and the sections were rinsed in PBST. Chromogen was applied for 10 min, rinsed in dH_2O and counterstained in aqueous haematoxylin (Biomeda). Adult male Wistar rat spleen acted as the control.

3.7.12 Desmin Immmunohistochemitry

Desmin positive cells were detected as previously described (Appendix 6) [201, 202]. 3 µm paraffin sections were dewaxed in histoclear, quenched in 3% H_20_2 and rinsed in dH_20. The sections were steamed for 20 min in retrieval buffer (Dako) cooled and rinsed in dH_2O. Sections were blocked, drained and incubated in a 1:50 primary desmin antibody solution (SC-7559, Santacruz) for 1 hour at room temperature, rinsed in PBST and incubated for 30 min in a 1:500 secondary antibody solution (AP180B, Chemicon). The sections were rinsed in PBST labelled with ABC Vector elite kit for 20 min and rinsed in

PBST. Chromogen was applied for 10 min, rinsed in dH_2O and counterstained in aqueous haematoxylin (Biomeda).

3.7.13 BrdU Immunohistochemistry

BrdU positive cells were detected as previously described (Appendix 8) [202]. 3 μm paraffin sections were dewaxed in histoclear, washed, rinsed in dH_2O and incubated in 10 mM sodium citrate solution pH 6.0 for 23 min in a 650 W microwave. Sections were washed and incubated in a H_2O_2 blocking solution for 15 min, washed, incubated in buffer for 20 min, drained and incubated in a 1:200 primary BrdU antibody solution (M0744, Dako). The sections were then washed in 0.005 M TRIS/HCl pH 7.6 buffered saline, incubated in secondary antibody (K5001, Dako) for 30 min, jet washed in TBS, incubated in Dako HRP streptAvidin for 30 min, jet-washed in TBS, incubated in DAB solution for 10 min, washed and counterstained with haematoxylin. Rat spleen acted as the control.

3.7.14 Imaging and Analysis

Histological evaluation was undertaken by a blinded independent pathologist (G Michalopoulos & A. Zaitoun). H&E, Masson's Trichrome and IHC slides were imaged using a digital nanozoomer (Hamamatsu). Representative images were selected for presentation. Liver tissue in growth into the scaffolds (cell migration and ECM deposition) on H&E staining was measured using Image J image analysis software (Rasband, W.S., Image J, U. S. National Institutes of Health, Bethesda, Maryland, USA,

http://rsb.info.nih.gov/ij/ version 1.38, 1997-2007). The percentage of liver tissue migration was calculated by subtracting the area of transparent polymer from the total implant area (Figure 3.10). This value was adjusted for the L-ECM containing implants. The peri-implant inflammatory band thickness was measured using the Nanozoomer Digital Pathology software (NDP viewer Version 1.06, Hamamatsu Photonics) and is expressed relative to the widest diameter of the implant on H&E staining. Where tissue had detached this was not included in the analysis.

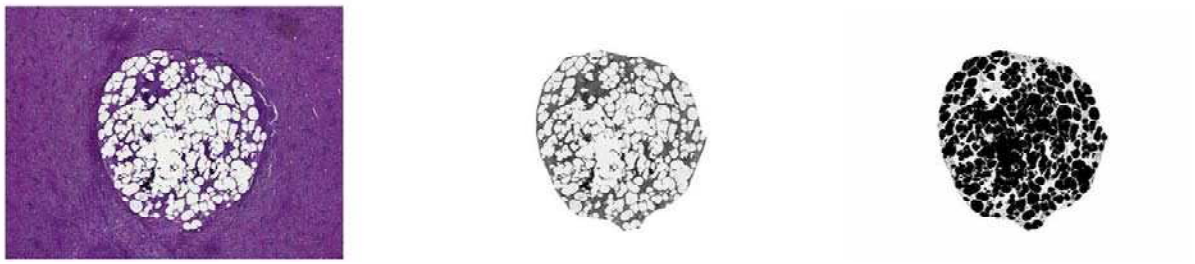

Figure 3.10 shows the data sequence generated by Image J analysis software that was used to measure liver in growth (cell migration and ECM deposition) in a porous scaffold. The implant area was first cut from a x 2.5 jpeg file (*left*). This was converted into an 8-bit file (*middle*), thresholding and inversion of which allowed calculation of the total implant area and non-polymer area respectively (*right*).

3.7.15 BrdU Count

The proportion of BrdU-labelled hepatocytes on an individual sample was determined from counting the number of positively stained hepatocyte nuclei within a 0.04 mm^2 peri-portal area using the NDP viewer software at x40 magnification. The peri-implant parenchyma was subdivided into 3 bands each 1.5 mm thick, moving peripherally from

the implant edge (Figure 3.11). At least 6 peri-portal fields were counted per band. For samples with no scaffold implanted at least 6 random 0.04 mm^2 peri-portal areas were counted. Hepatocyte nuclei were differentiated from other BrdU-labelled cells by their size and shape. Only cells with a circular morphology and nuclear diameter > 7 μm were counted. The number of BrdU-labelled hepatocytes per band is expressed as a percentage. To compare the BrdU-labelled non-parenchymal cells within the pores of different scaffolds representative images are shown.

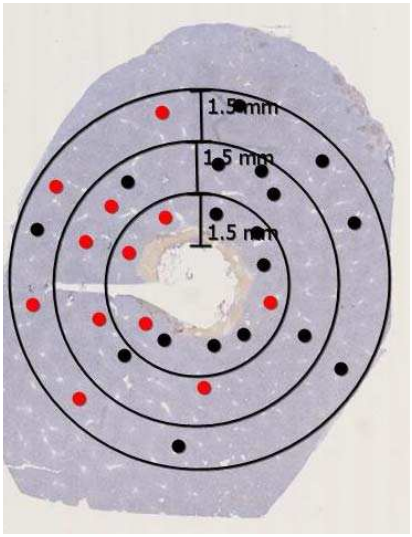

Figure 3.11 Example of an image map used to count BrdU positive nuclei in peri-implant parenchyma. A minimum of 6 0.04 mm^2 peri-portal squares are sampled per band. A total of 3 bands are sampled per block. More detailed validation of the BrdU count protocol is presented in section 4.2.8.

3.7.16 Statistical Analysis

Data was analysed using SPSS. Data are expressed as the mean +/- standard deviation. Liver weights were assessed by one-way ANOVA with Tukey's post-test. Liver tissue migration and inflammatory band thickness were analysed using independent student t-

tests. BrdU counts were analysed using independent student t-tests. P values less than 0.05 were regarded as statistically significant.

3.8 Results

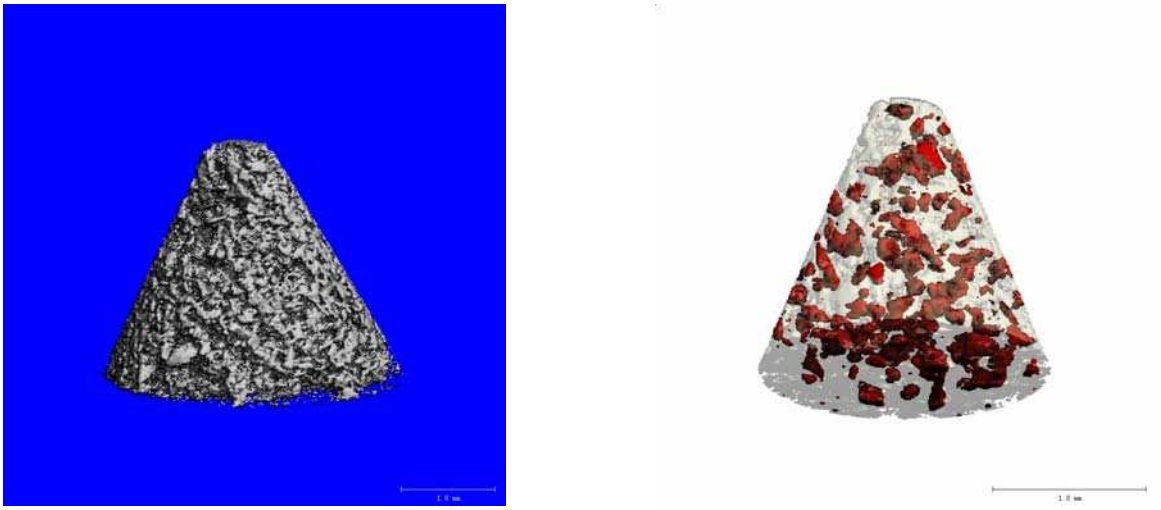

Figure 3.12 μCT reconstructions of the 4 mm x 4 mm conical implants used in the comparative study. Sub-250 μm PLGA + 5% PEG microparticles were sintered in a teflon mould to yield scaffolds with a porosity of 34.8% and a mean pore diameter of 80 μm (*left*). At 20% loading by weight the salt-labelled gelatin microparticles (*in red*) were distributed uniformly throughout the scaffold (*right*).

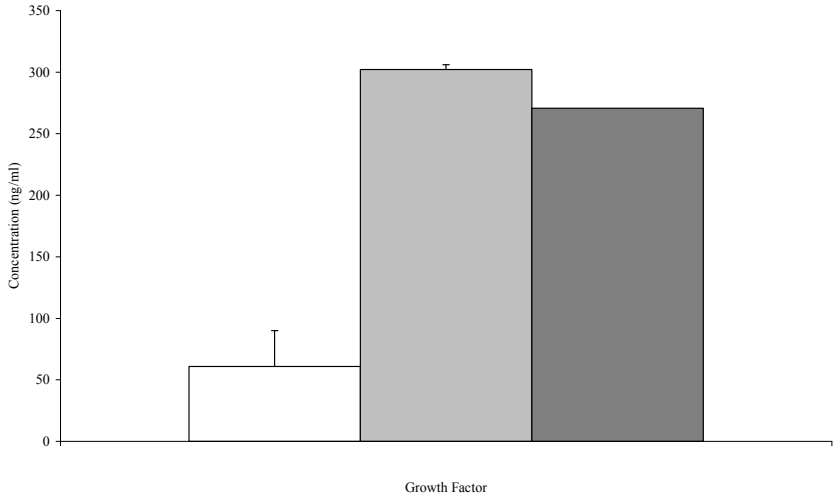

Figure 3.13 Average concentrations of HGF, EGF and FGF_2 detected in 5 ml of PBS following a 5 day static incubation with a growth factor loaded PLGA + 5% PEG cone (+/- SD of mean) (n=2). HGF (*white*), EGF (*light grey*) and FGF_2 (*dark grey*). The FGF_1 ELISA failed to detect FGF_1 in the standard, the cone incubation or an FGF_1 control solution.

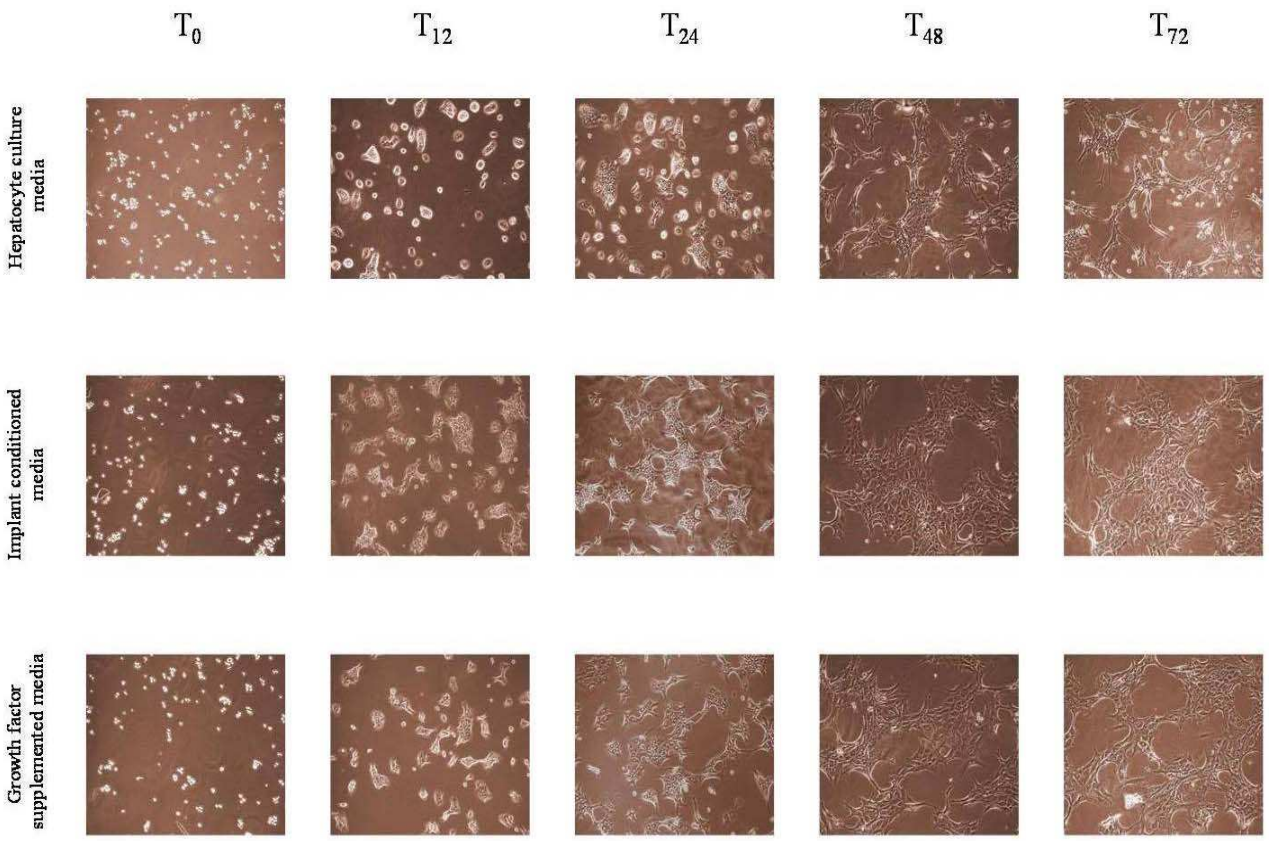

Figure 3.14 Hepatocyte culture morphology in unconditioned hepatocyte culture media, implant conditioned media and growth factor supplemented media at 0, 12, 24, 48 and 72 hours after addition of trial media. 12 hours after seeding, the hepatocytes in the implant-conditioned and growth factor supplemented media attached to the surface, flattened and had made contact with other cells. Hepatocytes in unconditioned media were rounded and there was no evidence of spreading. At 24, 48 and 72 hours after seeding, cultures in the conditioned and supplemented media contained interconnected colonies of hepatocytes with large nuclei. In the unconditioned media, hepatocyte spreading was less extensive, colonies were smaller and at 72 hours the hepatocytes had begun to detach and die. Original magnification 20X.

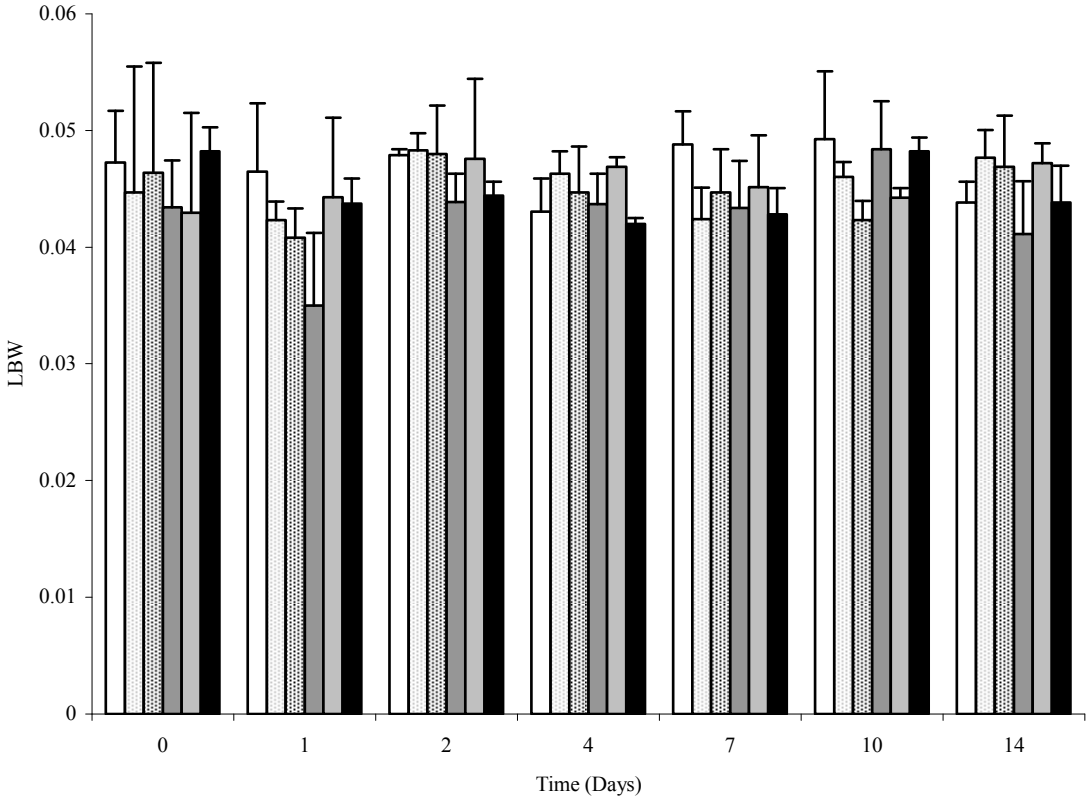

Figure 3.15 LBWs (calculated using equation 1) for the comparative study up to 14 days after implantation (+/- SD of mean) (n=3). Sham (*white*), polymer only (*grey spot*), L-ECM only (*black spot*), growth factor loaded (*dark grey*), L-ECM loaded (*light grey*) and hybrid (*black*). There were no significant differences detected between matched study groups for the duration of the study.

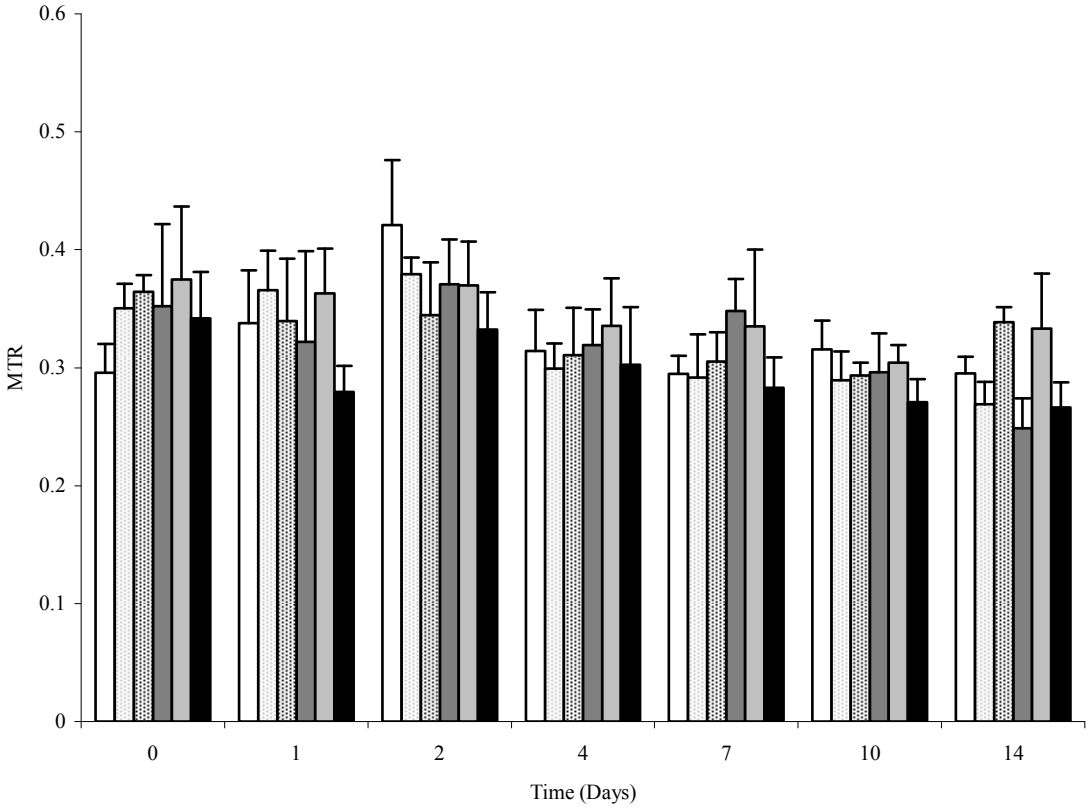

Figure 3.16 MTRs (calculated using equation 2) for the comparative study up to 14 days after implantation (+/- SD of mean) (n=3). Sham (*white*), polymer only (*grey spot*), L-ECM only (*black spot*), growth factor loaded (*dark grey*) L-ECM loaded (*light grey*), and hybrid (*black*). There were no significant differences detected between matched study groups for the duration of the study.

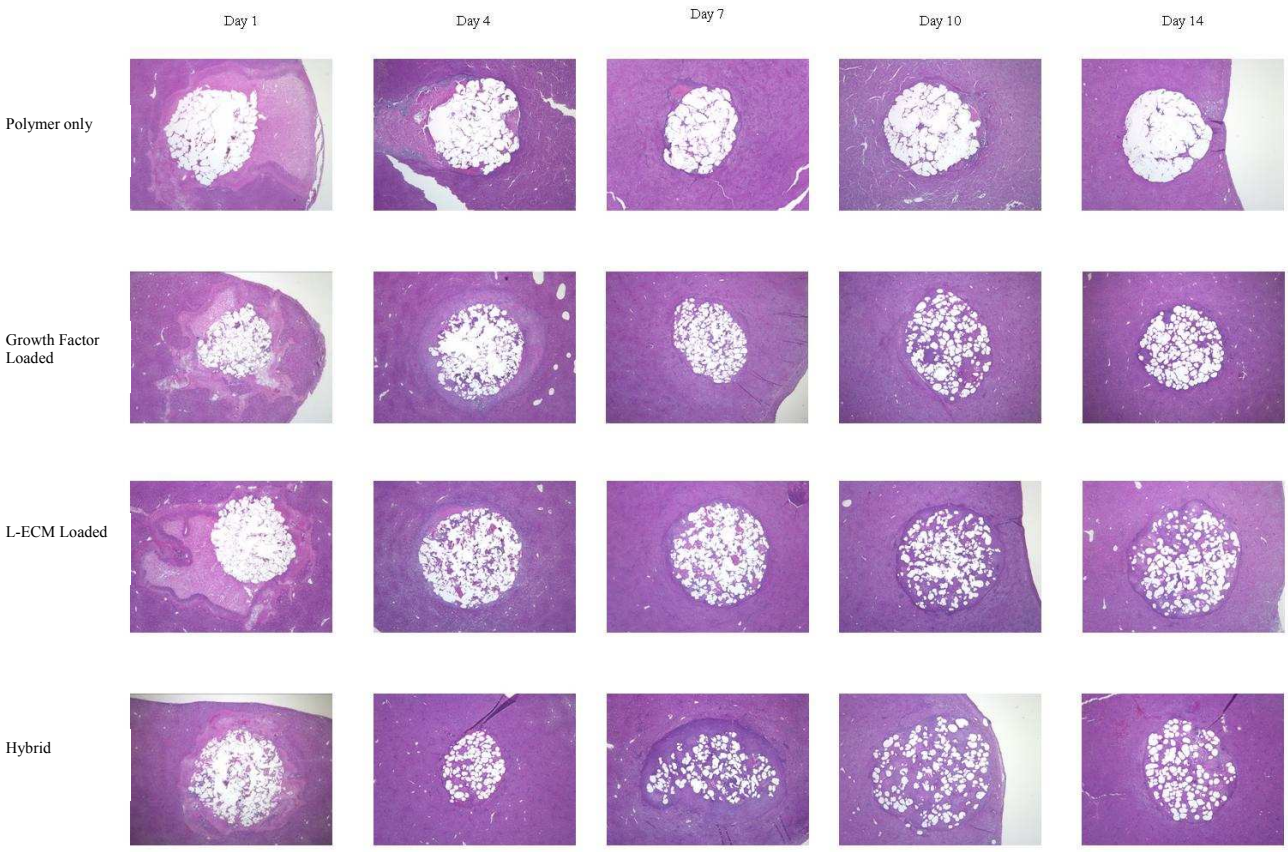

Figure 3.17 H&E for the 4 polymer-based scaffolds (polymer only, growth factor loaded, L-ECM loaded & hybrid) up to 14 days after implantation. By day 4 the pattern of ECM deposition, cell migration and the thickness of the band of inflammation around each scaffold differed between groups. There was limited interaction between the liver and the plain polymer cones. In the growth factor loaded, L-ECM loaded and hybrid scaffold implanted livers, liver-scaffold interaction was more pronounced, with greater rates of cell migration and ECM deposition and more prolonged peri-implant inflammation compared with the plain polymer implants. Original magnification 2.5X.

T_0 Day 2

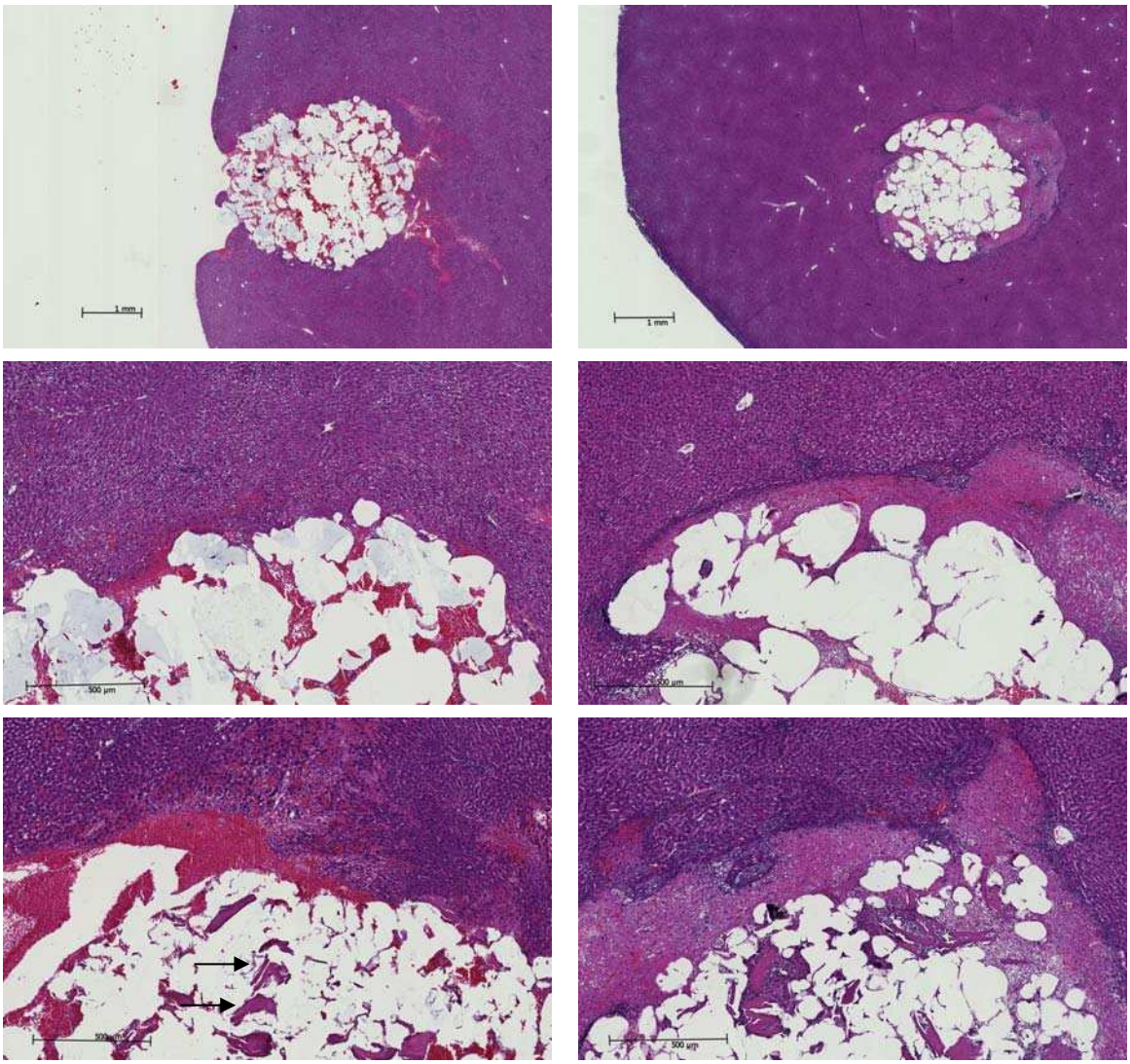

Figure 3.18 H&E of polymer based scaffold implanted livers at T_0 (*left*) & day 2 (*right*). At T_0 erythrocytes filled the pores of the scaffolds and there was venous congestion and compression of the surrounding parenchyma (polymer only T_0 *top & middle left*). In the L-ECM containing scaffolds the L-ECM microparticles stained with haematoxylin and could be easily visualised (L-ECM loaded T_0 *bottom left, arrowed*). By day 2 there was a clearly defined band of inflammation and resolving necrosis surrounding all scaffolds. There was evidence of liver tissue migration in all scaffolds (polymer only day 2 *top & middle right* and L-ECM loaded *bottom right*)

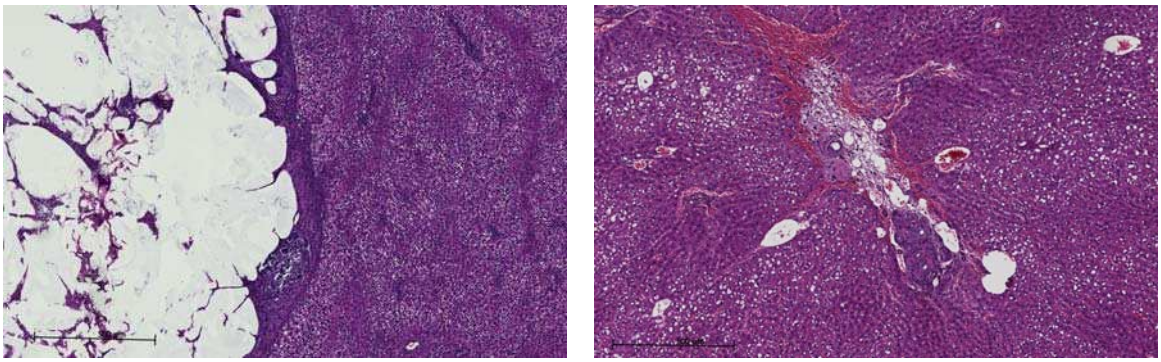

Figure 3.19 H&E of plain-polymer implanted livers at days 7 and 56. By day 7 the band of necrosis surrounding the scaffold had resolved and only a thin band of fibrous tissue remained (polymer only day 7 *left*). By day 56 the PLGA + 5% PEG had biodegraded with only residual fibrous tissue remaining at the implantation site (polymer only day 56 *right*).

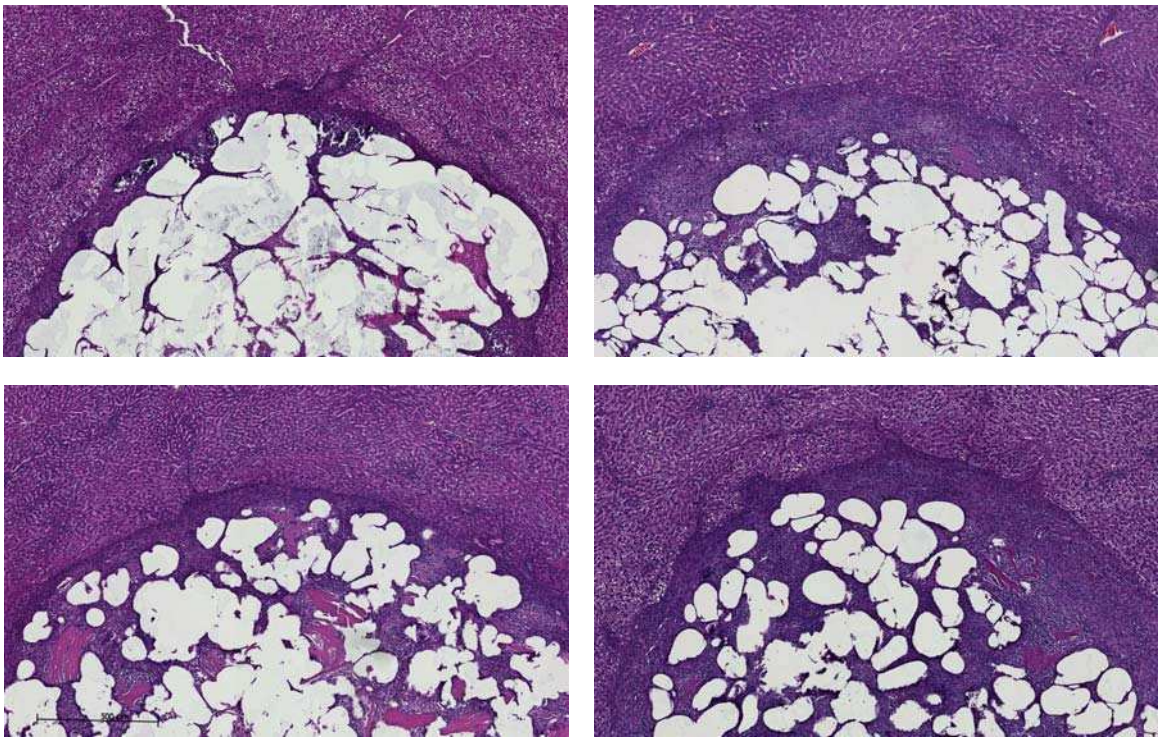

Figure 3.20 H&E of the polymer-based implants at day 7, demonstrating the patterns of tissue in growth (cell migration & ECM deposition) and inflammatory reaction around each scaffold. In the plain polymer scaffolds (*top left*) there was limited tissue in growth and the peri-implant inflammatory reaction had resolved by day 7. The presence of growth factors (*top right*) and L-ECM (*bottom left*) increased tissue migration into the scaffolds and prolonged the peri-implant inflammatory reaction. When delivered together via a hybrid scaffold they had an additive effect resulting in a faster rate of tissue migration and a more prolonged peri-implant inflammatory reaction (*bottom right*).

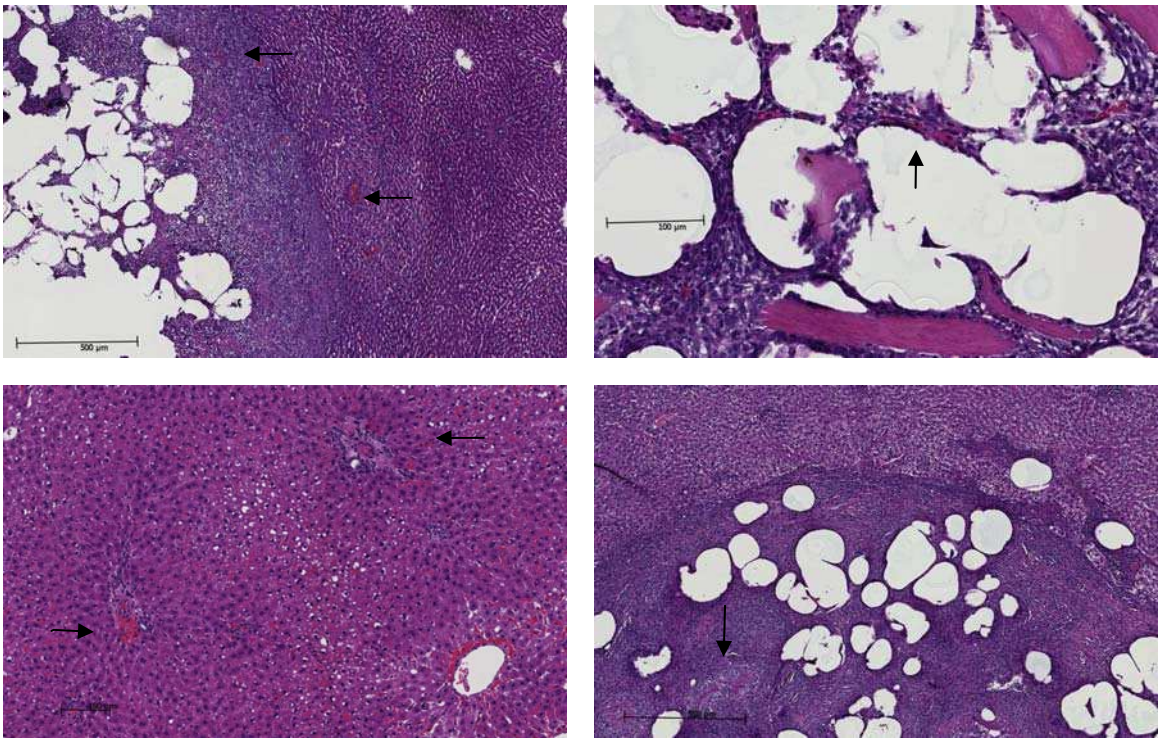

Figure 3.21 H&E of polymer-based implants demonstrating the neovascular and inflammatory changes occurring within the pores of the scaffold and in the surrounding parenchyma. In the growth factor loaded, L-ECM loaded and hybrid scaffold implanted livers there was angiogenesis (arrowed) in the band of inflammation surrounding the scaffolds by day 4 (growth factor loaded day 4 *top left*) and within the pores of the scaffolds by day 7 (L-ECM loaded day 7 *top right*). Angiogenesis was seen throughout the medial lobe of the L-ECM loaded implant at day 28 (L-ECM loaded day 28 *bottom left*). Granulomas *(arrowed)* were present in all the polymer based implants by day 14 (hybrid day 10 *bottom right*).

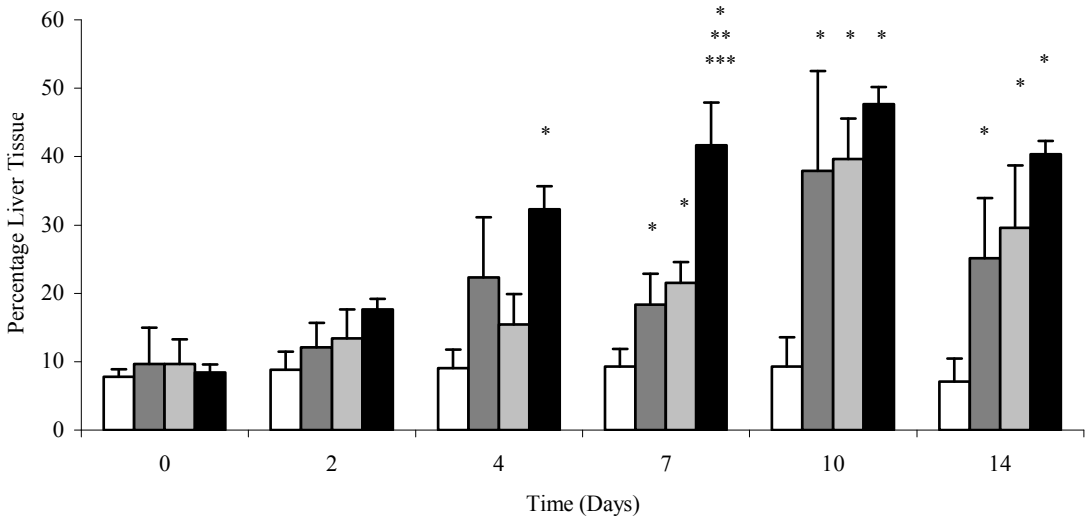

Figure 3.22 Results of image analysis (as described in section 3.7.14) used to quantify cell migration and ECM deposition for the different polymer-based scaffolds up to 14 days after implantation. The values are expressed as a percentage of the total implant area (+/- SD of mean) (n=3) and were adjusted for the L-ECM containing implants. Polymer only (*white*), growth factor loaded (*dark grey*), L-ECM loaded (*light grey*) and hybrid (*black*). For each polymer the percentage of tissue present within the implant area increased with time up to day 10. The proportion of tissue present in the L-ECM and growth factor loaded implants exceeded the polymer only implants by day 7. The amount of tissue present in the hybrid implant exceeded the polymer only by day 4 and L-ECM loaded implants and the growth factor loaded implants by day 7. There were no significant differences detected between the growth factor and L-ECM loaded polymer implanted livers. *$P < 0.05$ compared with the polymer only scaffolds, **$P < 0.05$ compared with the growth factor loaded scaffolds and ***$P < 0.05$ compared with the L-ECM loaded scaffolds.

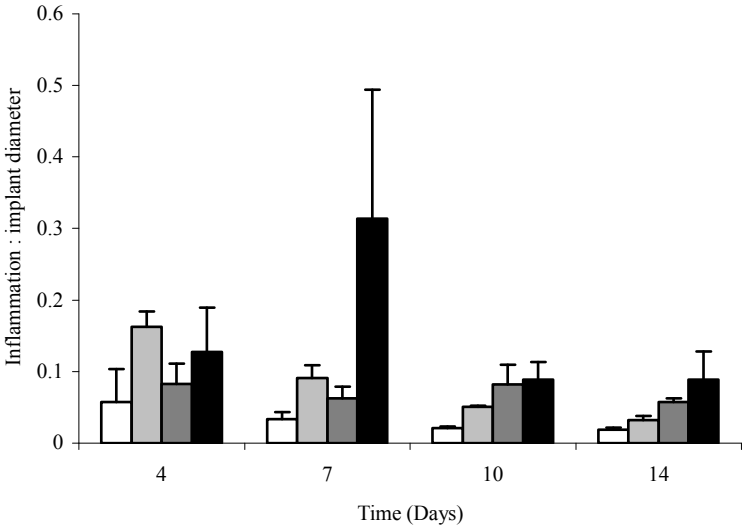

Figure 3.23 Peri-implant inflammatory band thickness for the different polymer-based scaffolds at days 4, 7, 10 and 14 after implantation. The values are expressed as an index relative to the maximum implant diameter of that section (+/- SD of mean) (n=3). Polymer only (*white*), growth factor loaded (*light grey*), L-ECM loaded (*dark grey*) and hybrid (*black*). There was no significant difference detected between the 4 groups.

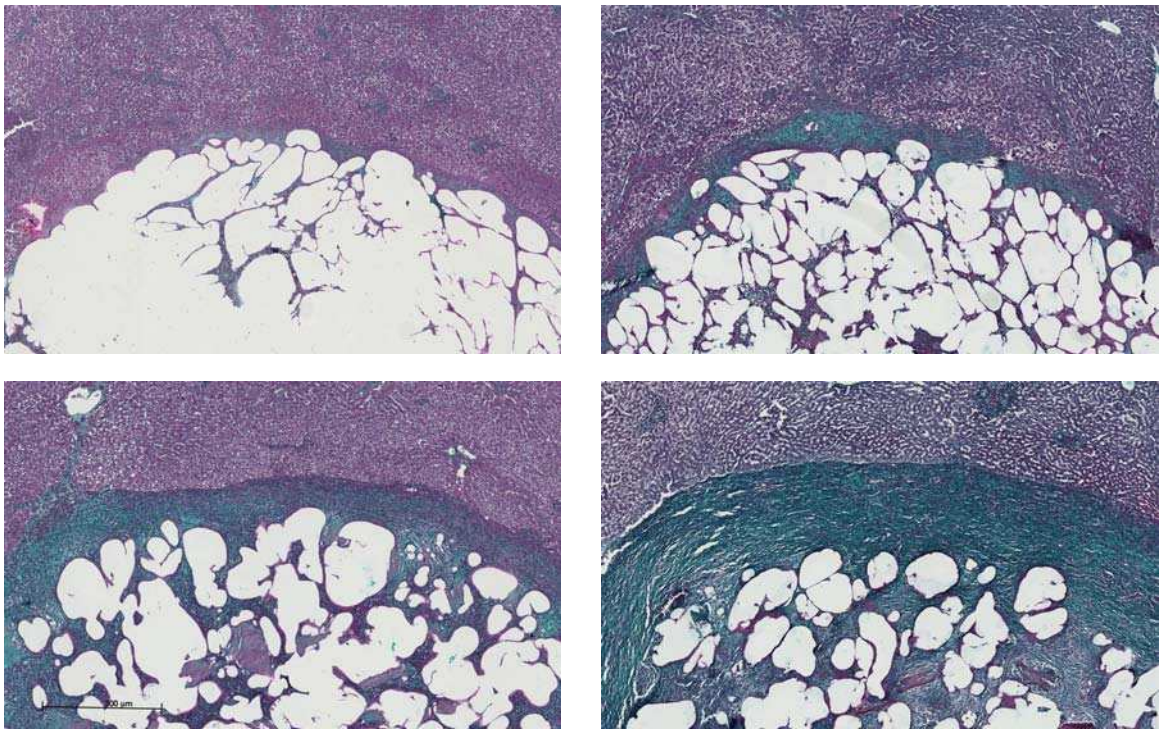

Figure 3.24 Masson's trichrome staining of the scaffold implanted livers at day 7. Collagen is stained green, cytoplasm, muscle and erythrocytes are stained red and nuclei are stained blue / black. Polymer only (*top left*), growth factor loaded (*top right*), L-ECM loaded (*bottom left*) and hybrid (*bottom right*). Collagen staining was greatest in the L-ECM containing scaffolds (L-ECM loaded & hybrid).

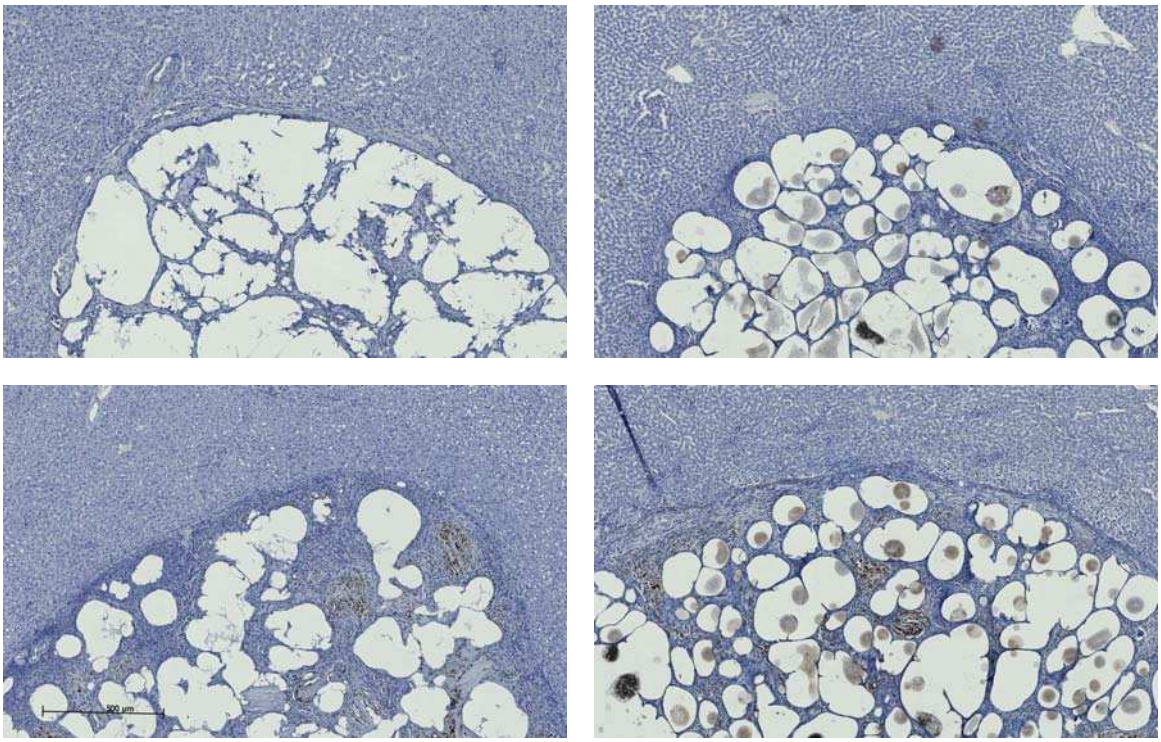

Figure 3.25 ED-1 IHC of the polymer based scaffolds in the polymer only day 28 (*top left*), growth factor loaded day 14 (*top right*), L-ECM loaded day 28 (*bottom right*) and hybrid day 14 (*bottom right*) scaffold implanted livers. ED-1 positive nuclei stain brown. ED-1 positive cells were seen in the band of inflammation surrounding all implants at day 4 and within the pores of the L-ECM containing implants from day 7. After day 7 Few ED-1 positive cells were identified within the polymer only or growth factor-loaded implants. In the L-ECM containing implants, ED-1 positive cells accumulated around the L-ECM microparticles. More ED-1 positive cells were seen in the hybrid implants than in the L-ECM only implants at day 7. Control tissue (rat spleen) not shown.

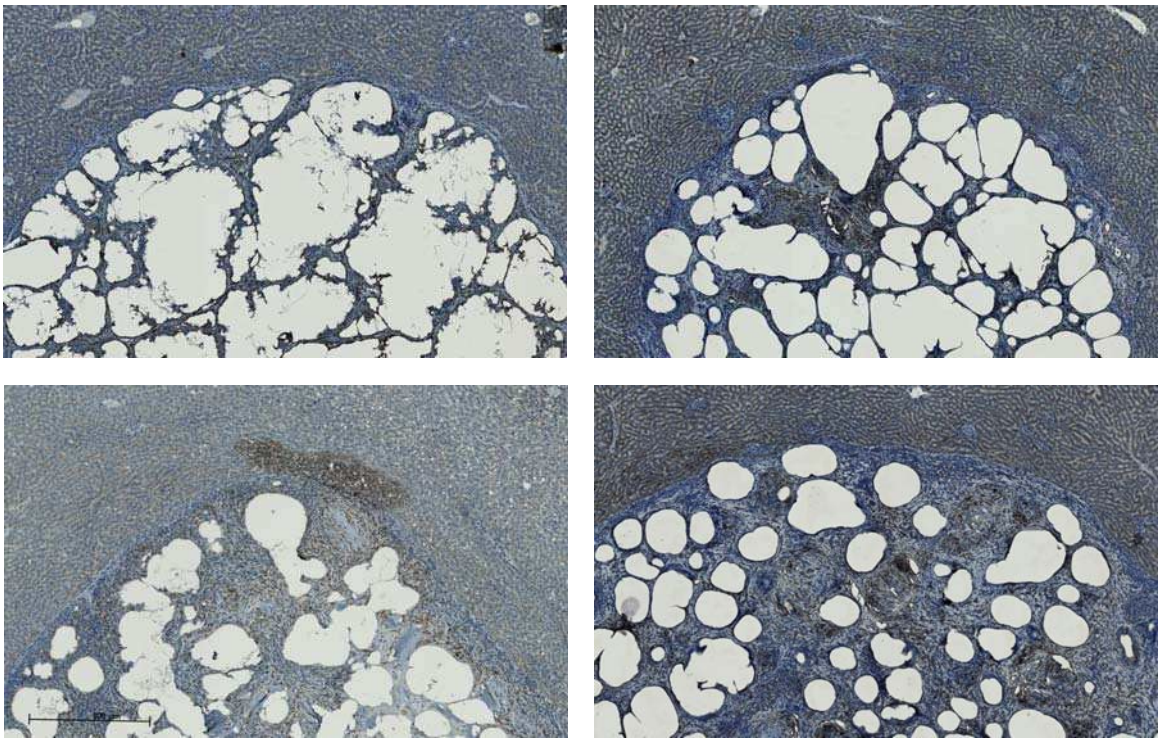

Figure 3.26 Desmin IHC of the polymer based scaffolds in the polymer only day 28 (*top left*), growth factor loaded day 14 (*top right*), L-ECM loaded day 28 (*bottom right*) and hybrid day 14 (*bottom right*) scaffold implanted livers. Desmin positive cells stain brown. Desmin positive cells were seen in the band of inflammation surrounding all implants at day 4 and within the pores of all the implants by day 7. More desmin positive cells were seen in the growth factor loaded and L-ECM loaded implants than in the polymer only implants. Desmin positive cells were distributed uniformly throughout the pores of the growth factor and L-ECM loaded implants. More desmin positive cells were seen in the hybrid implants than in the growth factor or L-ECM loaded implants at day 7.

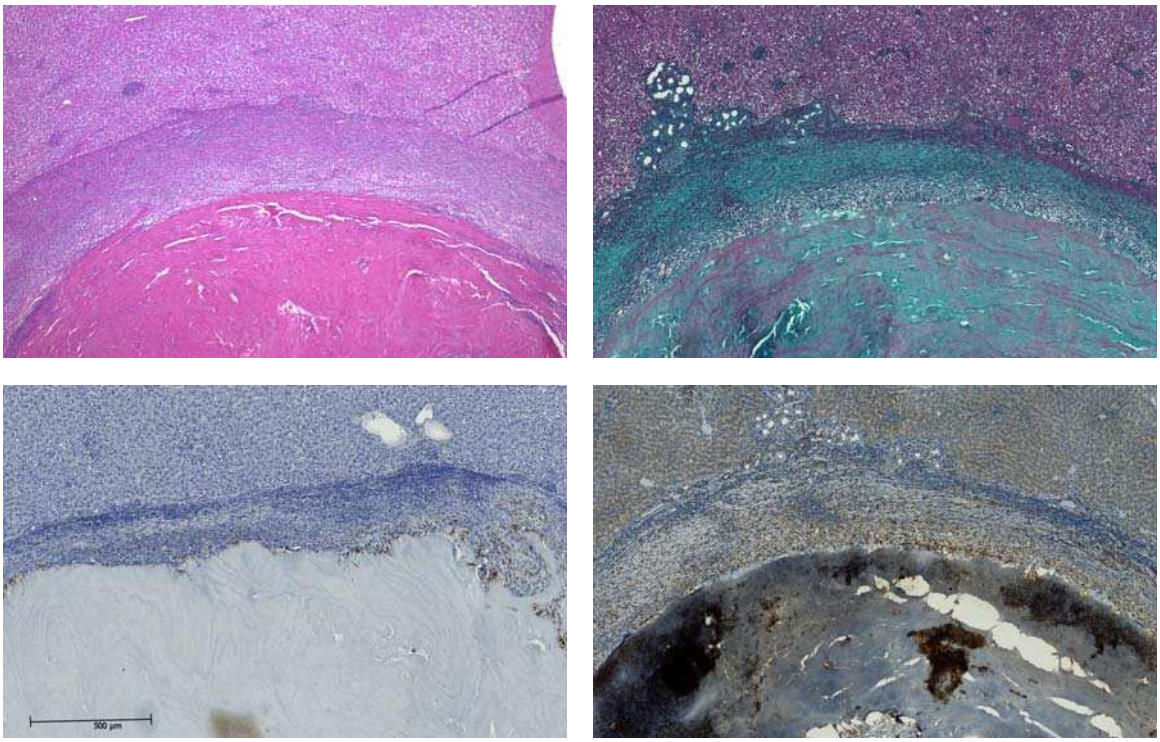

Figure 3.27 H&E (*top left*), Masson's trichrome staining (*top right*), ED-1 IHC (*bottom left*) and desmin IHC (*bottom right*) staining for the non-porous L-ECM only implant. The L-ECM only cones were non-porous and as a result behaved differently to the porous polymer based scaffolds. Collagen fibres were present around the implant up to day 56. ED-1 positive cells were found at the implant surface. Desmin positive cells were found at the implant surface and throughout the peri-implant band of inflammation. From day 1 a band of inflammation and necrosis surrounded the implants (*top left*). ECM was deposited in the peri-implant parenchyma (*top right*). ED-1 (*bottom left*) and desmin positive cells *(bottom right*) were found at the interface between the liver and the implant, but the non-porous nature of the scaffold prevented rapid migration (*bottom*).

3.8.1 BrdU IHC: Implant *versus* Sham

Implantation of polymer only cones caused a significant increase in the number of BrdU-labelled hepatocytes around the implant at day 1. Implantation of the L-ECM cones caused a significant increase in BrdU-labelled hepatocytes at day 2, day 4 and day 10. There was no significant difference detected in the proportion of BrdU-labelled hepatocytes around the L-ECM loaded and growth factor loaded polymer cones compared with sham at each time point. Implantation of the hybrid cones caused a significant increase in BrdU-labelled hepatocytes at day 1 and day 4.

3.8.2 BrdU IHC: Implant *versus* Control Scaffold

There was no significant difference detected in the proportion of BrdU-labelled hepatocytes around the L-ECM loaded and growth factor loaded polymer cones compared with the polymer only implants at each time point. L-ECM only cones produced a significant increase in the number of BrdU-labelled hepatocytes compared with the L-ECM loaded polymer cones at day 4. Implantation of the hybrid cones produced a significant increase in the number of BrdU-labelled hepatocytes compared with the polymer only implants at day 4, and compared with the L-ECM loaded polymer implants at day 1 and day 4. When the parenchymal tissue distant to the implant was examined, no increase in the proportion of BrdU-labelling of hepatocytes could be detected for each of the study groups. At days 28 and 56 no increase in the proportion of BrdU-labelled hepatocytes could be detected around the polymer only, L-ECM only or L-ECM loaded polymer implants.

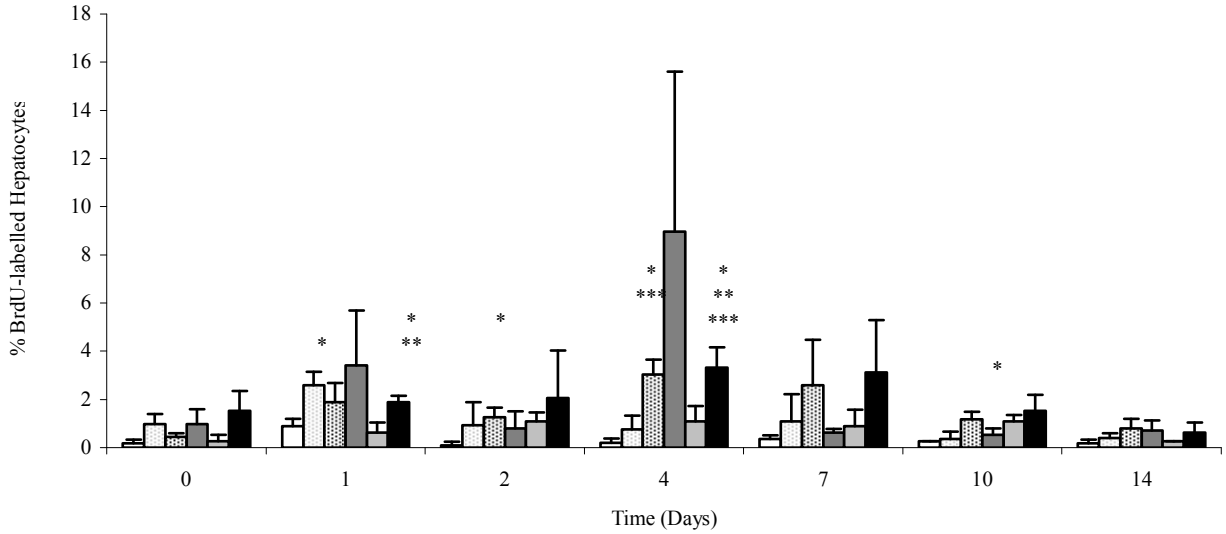

Figure 3.28 Percentage of BrdU-labelled hepatocytes in band A of the peri-implant parenchyma up to 14 days after implantation +/- SD of mean (n=3). Sham procedure (*white*), polymer only (*grey spot*), L-ECM only (*black spot*), growth factor loaded (*dark grey*), L-ECM loaded (*light grey*) and hybrid (*black*). *P < 0.05 compared with the sham group, **P < 0.05 compared with the polymer only group and ***P < 0.05 compared with the L-ECM loaded group.

Table 3.4 Percentage of BrdU positive hepatocytes in band A of the peri-implant parenchyma up to 14 days after implantation +/- SD of mean (n=3)

	0	1	2	4	7	10	14
Sham	0.18+/-0.16	0.89+/-0.31	0.09+/-0.16	0.20+/-0.17	0.36+/-0.16	0.27+/-0.00	0.18+/-0.16
Polymer Only	0.98+/-0.41	2.60+/-0.56	0.94+/-0.95	0.75+/-0.57	1.07+/-1.14	0.36+/-0.31	0.40+/-0.19
L-ECM Only	0.45+/-0.16	1.88+/-0.81	1.25+/-0.41	3.04+/-0.62	2.60+/-1.89	1.16+/-0.31	0.81+/-0.38
Growth Factor Loaded	0.98+/-0.62	3.40+/-2.28	0.81+/-0.71	8.97+/-6.64	0.63+/-0.16	0.54+/-0.27	0.72+/-0.41
L-ECM Loaded	0.27+/-0.27	0.63+/-0.41	1.07+/-0.38	1.07+/-0.65	0.89+/-0.68	1.07+/-0.27	0.27+/-0.00
Hybrid	1.52+/-0.82	1.88+/-0.27	2.06+/-1.98	3.33+/-0.83	3.13+/-2.15	1.52+/-0.68	0.63+/-0.41

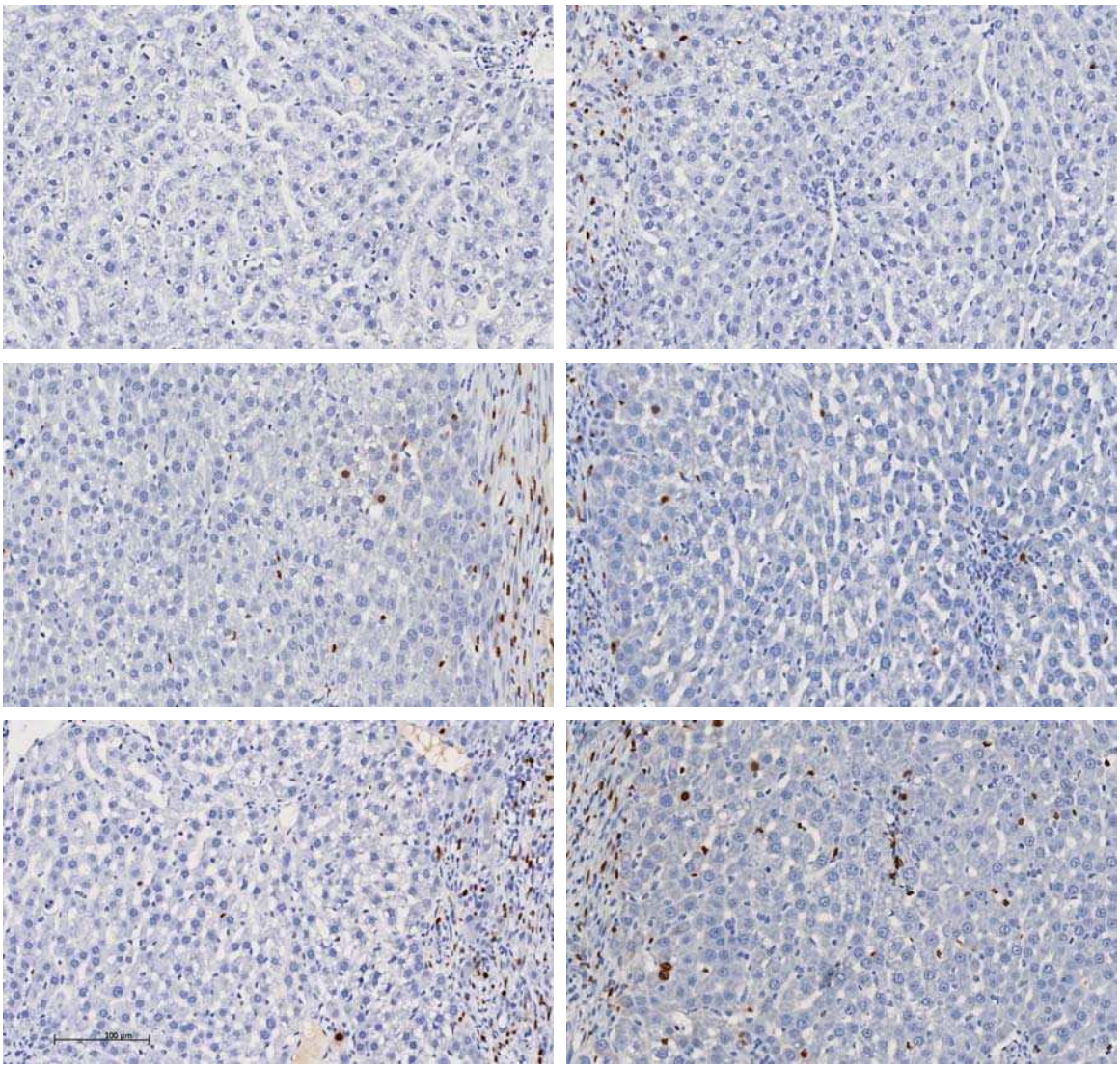

Figure 3.29 BrdU IHC of sham (*top left*), polymer only (*top right*), L-ECM only (*middle left*), growth factor loaded (*middle right*), L-ECM loaded (*bottom left*) and hybrid (*bottom right*) livers 4 days after implantation. BrdU positive nuclei stain brown, peroxidase activity stains blue. There were significant numbers of BrdU stained hepatocytes at day 4 in the L-ECM only and hybrid scaffolds. BrdU positive hepatocytes were also observed in 2 of the 3 growth factor loaded scaffold implanted livers.

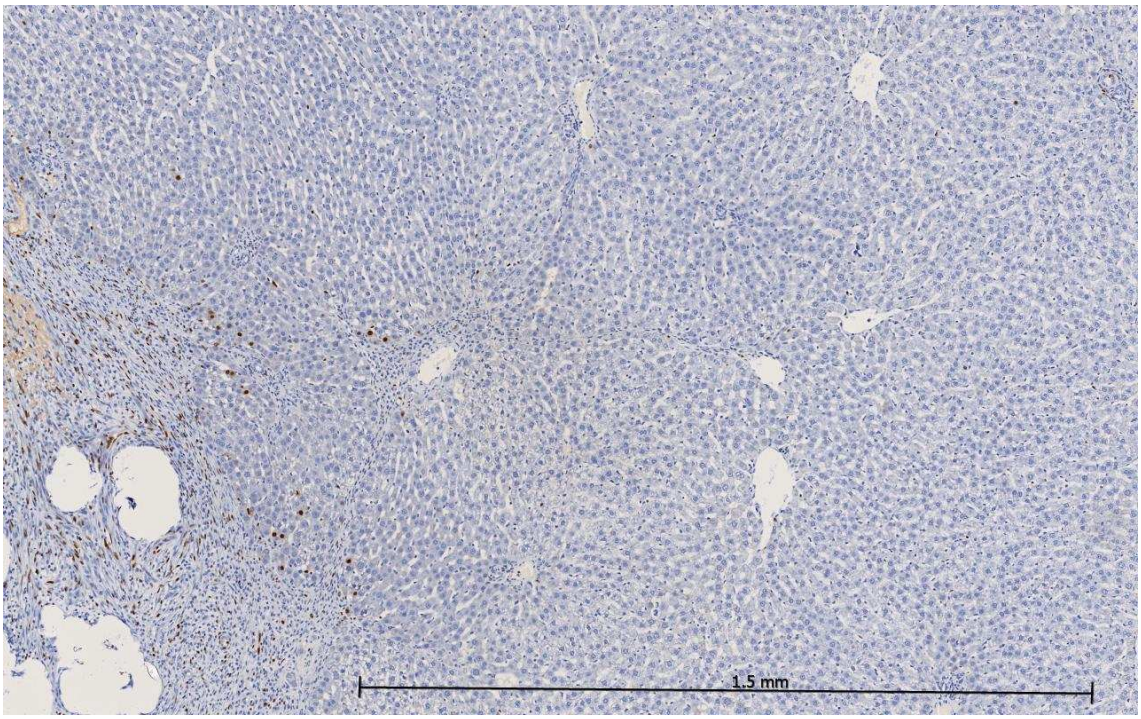

Figure 3.30 BrdU IHC of a hybrid scaffold implanted liver 4 days after implantation demonstrating that BrdU staining of hepatocytes and non-parenchymal cells was limited to band A adjacent to the implant.

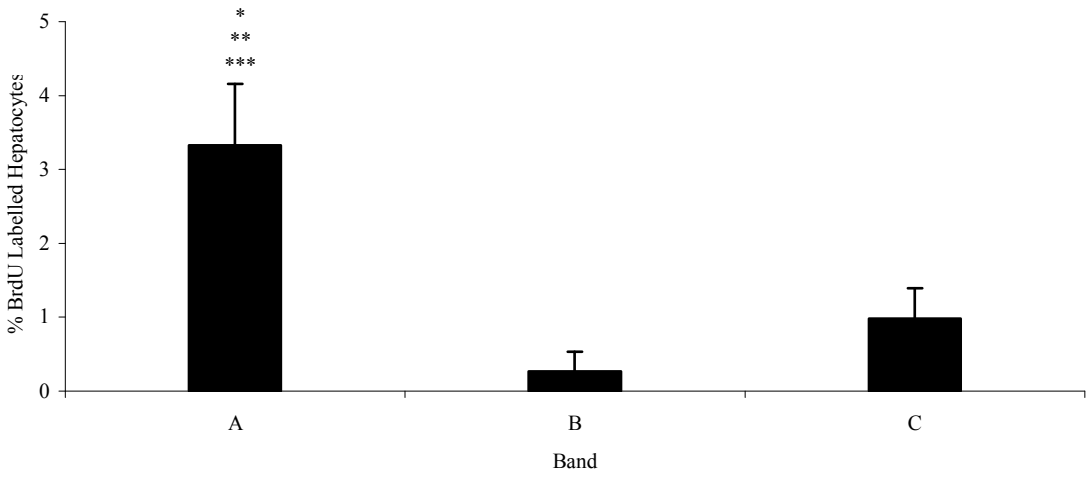

Figure 3.31 Percentage of BrdU-labelled hepatocytes in bands A, B & C of the peri-implant parenchyma of a hybrid scaffold implanted liver 4 days after implantation +/- SD of mean (n=3). *P < 0.05 compared with the sham group, **P < 0.05 compared with the polymer only group and ***P < 0.05 compared with the L-ECM loaded group.

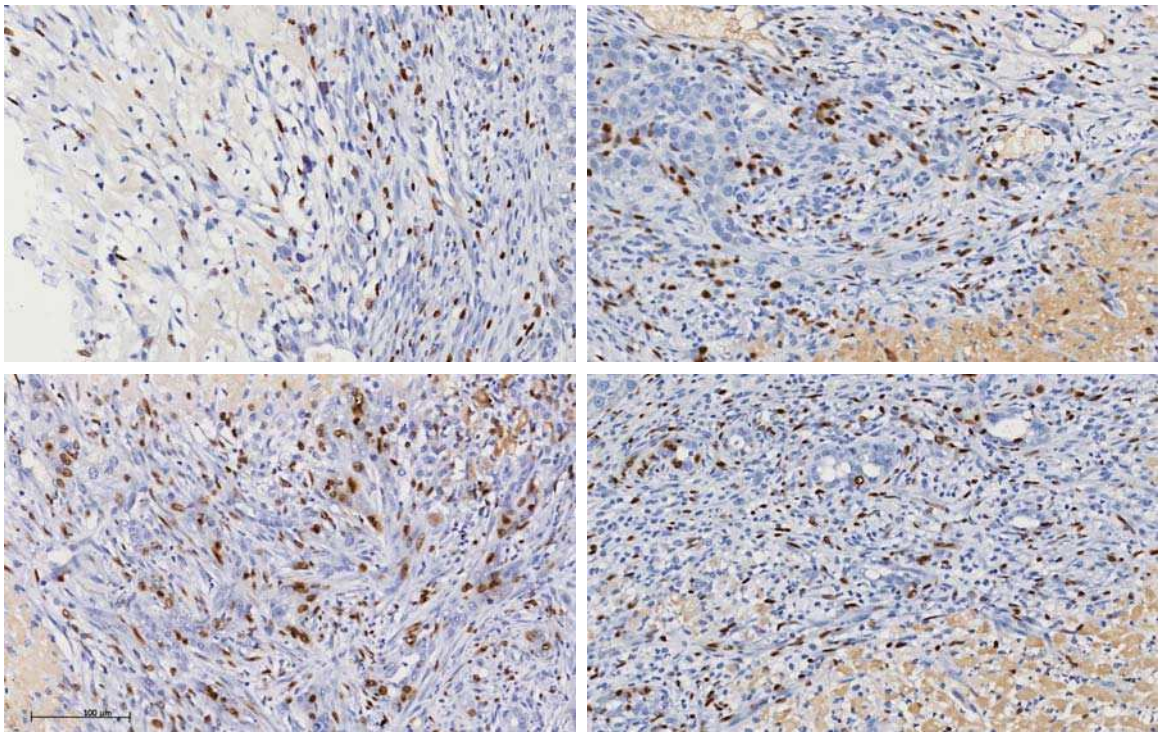

Figure 3.32 BrdU-labelled cells in the peri-implant band of inflammation at day 4. Polymer only (*top left*), growth factor loaded (*top right*), L-ECM loaded (*bottom left*) and hybrid (*bottom right*). Non-parenchymal cells with BrdU positive nuclei were present in the peri-implant parenchyma of each polymer based scaffold. Non-parenchymal cell proliferation was not quantified.

3.9 Discussion

HGF, EGF, FGF_1 and FGF_2 are all mitogenic to liver tissue and play a key role in the restoration of functional liver mass following PH [59, 64, 74]. ECM remodelling is another important component in this regenerative cascade, acting as both a reservoir for growth factors and as template for tissue assembly [74, 121]. To mimic the release profile of growth factors and remodelling of ECM proteins that occurs following PH, HGF, EGF, FGF_1, FGF_2 and L-ECM were delivered into the liver via intrahepatic biodegradable delivery devices.

3.9.1 Implant Characterisation

Sintered PLGA + 5% PEG cones loaded with 2.5 μg HGF, 5 μg EGF, 2.5 μg FGF, 2.5 μg FGF and 20% L-ECM by weight were implanted into the liver of rats. The sintered cones had a porosity of 34.8% and a mean pore diameter of 80 μm. In the pilot study the implants had a porosity of 30.8% and a mean pore diameter of 104 μm. By substituting L-ECM microparticles with NaCl labelled gelatin microparticles, it was possible to model the distribution of L-ECM in the sintered scaffolds. Because NaCl has a different density to the polymer and the gelatin, its can be identified on three-dimensional reconstruction of the micro x-ray analysis. This demonstrated that the sub-220 μm gelatin microparticles were well distributed throughout the scaffolds at 20% loading by weight. It is not known how inclusion of L-ECM or gelatin impacted on the porosity or pore diameter of the cones.

The implant size was increased from the pilot study. Sintering microparticles in a 3 mm x 4 mm mould produced cones that were fragile and difficult to implant. The cone size was increased to 4 mm diameter x 4 mm height producing cones that were more robust. When this 4 mm x 4 mm cone design was trialled in cadaveric rat liver, it could be implanted without capsule fracture. It was not necessary to undertake further terminal anaesthetic studies.

To confirm that growth factors were present in the scaffolds and that they had retained their bioactivity, an *in vitro* release study was undertaken. Growth factor loaded cones were incubated in 5 ml of PBS at 37ºC for 5 days under static conditions. A total of 304.9 ng of HGF and 1511.0 ng of EGF and 1353.6 ng of FGF_2 were detected by ELISA in the 5 ml of PBS, which equated to 12%, 30% and 54% of the estimated total growth factor incorporated per cone. The FGF_1 ELISA did not detect FGF_1 in the control or test samples. These values were less than predicted, but more detailed profiling is required to accurately assess the variation in growth factor loading per scaffold.

To determine whether the growth factors released *in vitro* had retained their bioactivity, primary hepatocytes were incubated in implant conditioned media and the culture morphology compared with a negative (unconditioned media) and a positive control (growth factor supplemented media) [45]. The conditioned media stimulated the same proliferative response in the primary hepatocyte population as in the positive control media (growth factor supplemented) up to 72 hour after incubation, unlike the cells in the negative control media (unconditioned), which remained rounded, exhibited little evidence of spreading and by 72 hours had begun to loose viability and detach.

These release studies confirmed that HGF, EGF and FGF_2 were present in the implants and that the growth factors released from the cones were bioactive. In future, additional characterisation of the release kinetics will be undertaken. To quantify the total amount of each growth factor incorporated into an implant more detailed *in vitro* release studies using different extraction buffers will be performed. The biodegradation of the scaffolds and release kinetics of the growth factors *in vivo* will also be determined by radioiodinating the scaffolds and growth factors and measuring the change in radioactivity over time [203, 204].

3.9.2 Liver Weights

In the pilot study no differences in LBWs were detected between study groups. To increase the sensitivity of the weight analysis for the comparative study, MTR was measured. As in the pilot study LBW remained constant for the duration of the study and no differences were detected between groups.

There were also no differences detected in the MTRs for matched study groups. At day 14 the MTR for the L-ECM only livers exceeded the MTR for the growth factor loaded and the hybrid livers and the MTR for the L-ECM loaded livers exceeded the MTR for the growth factor loaded livers. When LBW and actual total liver and medial lobe weights for the growth factor loaded and hybrid livers at day 14 were reviewed, all were below average (n=3 per time point), however histological examination could detect no abnormality to account for this trend. In order to confirm these differences the time points should be repeated.

3.9.3 Histological Characterisation

In the pilot study, implantation of the plain and growth factor loaded porous $P_{DL}LA$ cones resulted in a peri-implant inflammatory reaction with tissue migration into the pores of the scaffold. This migration was present in the growth factor loaded implants at day 7 and in all the implants at day 14. In this study the polymer was changed to PLGA + 5% PEG, the growth factor dose was increased (at least 5 times for each growth factor) and L-ECM delivery was used for the first time. In addition the enhanced fixation and processing enabled clearer interpretation of the response and the later time points allowed characterisation of the liver scaffold interaction at 28 and 56 days after implantation.

3.9.4 ECM Deposition & Cell Migration

The potential for cells to migrate into the pores of a scaffold is influenced by the properties of the scaffold (the biomaterial, its architecture, the ligand binding capacity and its capacity for signal delivery) and the implantation site (its blood supply and migratory potential of the cells at the implantation site). In Takimoto's study of non-biodegradable porous collagen coated polypropylene scaffold implantation into normal rat liver, cells migrated into the pores of the scaffold sequentially. First HSCs migrated and deposited ECM in the pores; this was followed by neovascularisation. When a blood supply was established oval cells could migrate into the pore spaces and by 6 months differentiated liver tissue was present throughout the scaffold. In the absence of collagen the polypropylene scaffolds became surrounded in a mass of fibrous tissue and no tissue migration occurred [174].

A similar pattern of ECM deposition and cell migration was observed in this study. In the plain PLGA + 5% PEG implants, cell migration was slow in comparison to the L-ECM and growth factor loaded implants. By day 14 a narrow band of collagen surrounded the implant and only scanty cell migration had occurred. The incorporation of L-ECM and growth factors not only increased the rate and extent of cell migration into the scaffold but also influenced which cells migrated into the scaffold and the pattern of ECM deposition within the pores. When L-ECM and growth factor were used in combination, their effects were additive.

Migration of ED-1 positive cells into the pores of the scaffolds was increased in the presence of L-ECM. In liver, Kupffer cells are the most likely source of ED-1 staining, although macrophages recruited from the peripheral circulation may also be labelled [200]. PLGA and PEG are inert biomaterials and did not stimulate ED-1 positive cells to migrate. In contrast ECM breakdown products are known to exert a direct chemotactic effect on a range of cell types, including liver and inflammatory cells [28]. Whilst growth factor incorporation did increase the rate of ED-1 positive cell migration in the L-ECM containing implants, in isolation they had no effect.

Desmin positive cells migrated into all scaffolds. In liver, the HSC is the most common desmin positive cell, although fibroblasts recruited from the peripheral circulation may also have been labelled [47, 201, 202]. In the presence of L-ECM and growth factors the rate of desmin positive cell migration was increased. When growth factors and L-ECM were delivered together they had an additive effect on desmin positive cell migration.

Masson's trichrome staining demonstrated that the pattern of ECM deposition also differed between implants. The addition of growth factors alone increased the density of

collagen deposition in and around the implant, but to a lesser degree than L-ECM incorporation, which caused extensive collagen deposition. When L-ECM and growth factors were delivered together the rate of ECM deposition increased. It was not possible to quantify the collagen deposition using image analysis because the density of collagen staining varied considerably between sections. In future collagen will be stained with pico-Sirius red which provides a more consistent level of staining [205].

When the Masson's trichrome staining is viewed alongside the desmin IHC it appears that ECM deposition occurs at the same rate as desmin positive cell migration. It is likely that these desmin positive cells (activated HSC) were responsible for the ECM deposition. It is unclear from this study how the presence of growth factors or L-ECM influenced HSC phenotype, but this has implications for the regenerative medicine strategy, as in their activated state HSC produce growth factors and ECM [47].

3.9.5 The Peri-implant Parenchyma

A number of events occurred simultaneously in the band of liver tissue adjacent to the implants. These include: the resolution of the surgical wound, the local response to polymer breakdown, the regression of the implant margin as it biodegraded, the migration of cells from the peripheral circulation and different effects induced by growth factor and L-ECM release (proliferation, ECM deposition, anigiogenesis). In the plain polymer implanted livers this reaction was complete by day 7 and was not associated with significant ECM deposition or angiogenic changes. In the growth factor loaded group this reaction resolved by day 10 and in the implants that contained L-ECM (including the L-ECM only implant) the peri-implant reaction persisted for longer. H&E, IHC and Masson's trichrome staining demonstrate that this was largely an inflammatory process with ED-1 and desmin cell migration, proliferation and ECM deposition. How these events impacted on the effectiveness of the growth factor delivery system was unclear.

3.9.6 Vascular Proliferation

Vascular proliferation was observed within the pores and in the peri-implant parenchyma of all the polymer scaffold implanted livers. The presence of growth factors and L-ECM increased the rate and extent of vascular proliferation. It was not possible to determine whether the pattern of vascular proliferation was different between the L-ECM and growth factor containing scaffolds. HGF, EGF, FGF_1 and FGF_2 have all been shown to exert angiogenic effects in different tissues. The angiogenic effects of L-ECM or its breakdown products have not previously been documented. To characterise these angiogenic effects in greater detail image analysis could be undertaken to map capillary number and density and IHC could be undertaken to define the vessel morphology [169].

Vascular proliferation was also observed throughout the entire median lobe at day 28 in the L-ECM loaded polymer implanted livers. These changes were limited to the implanted lobe and were not pan-hepatic. They were not observed in the sham, polymer only or L-ECM only implants at 28 days. Again the mechanism is unclear and repetition of the time point is required.

3.9.7 The L-ECM Only Implant

The L-ECM only implant was not porous. It was therefore not possible to study migration into an L-ECM only scaffold or make a direct comparison with the porous polymer implants of its effects on the peri-implant parenchyma. Porosity was likely to enhance the level of liver-implant interaction by increasing the surface area available for ECM and growth factor mobilisation and by providing a route for cell migration. As a result in the L-ECM only implants there was no significant migration into the implants and the implants were still present at day 56. In the parenchyma adjacent to the implants there was an inflammatory reaction for the duration of the study, this band was made up of ED-1 and desmin positive cells, collagen fibres and vascular tissue.

3.9.8 Proliferation

BrdU incorporation detected by immunohistochemistry was used to measure the number of hepatocytes in the S-phase of proliferation. Work by Michlalopoulos et al [96] demonstrated that hepatocyte proliferation following HGF infusion or PH occurs predominantly in the peri-portal regions of the lobule. In this study examination of the hepatocyte population therefore focused on the peri-portal regions adjacent to the implants. If there was a proliferative response detected in the peri-implant tissue then bands distant to the implant were also examined. The proliferative count was validated by a blinded liver histopathologist.

Following capsule incision and cone implantation an increase in the number of proliferating hepatocytes was observed between time zero and day 1 for all study groups. This increase was restricted to the parenchyma adjacent to the capsule incision or cone implantation sites and was likely to be a direct response to the controlled liver injury. In the sham, plain polymer and L-ECM loaded polymer groups the number of proliferating hepatocytes then returned to baseline. In the L-ECM only implanted livers the number of proliferating hepatocytes continued to increase up to day 4 and then returned to baseline by day 14. In the hybrid implants there was an increase in proliferating cells up to day 4 followed by a return to baseline by day 14. In all samples this proliferative response was limited to the band of parenchyma adjacent to the implant. The number of BrdU positive cells in the peripheral bands was not increased.

The proliferative response that occurs in normal liver following HGF or EGFR ligand infusion is dose dependent. At lower doses HGF and EGFR ligand infusion can stimulate

an increase in proliferation but only sustained delivery of large doses of HGF has been shown to stimulate an increase in functional liver mass [95].

When HGF or EGFR ligands are infused into liver that has been "primed" by chemical injury or by PH, lower doses of growth factor may achieve an increase in the proliferative rate of the hepatocyte population. In this study relatively low doses of HGF EGF, FGF_1, FGF_2 together with L-ECM were delivered directly into the liver parenchyma at the site of a controlled liver injury. This injury was associated with an inflammatory response that could have "primed" the hepatocyte population to the action of the growth factors being released. This may explain the increase in proliferating hepatocytes observed in the L-ECM only and hybrid implants at day 4 and day 7, and is supported by the peak in peri-implant inflammation at that time point. As the peri-implant band of inflammation decreased in size, so did the proliferative count. When the inflammatory band was present in the absence of growth factors the proliferative response did not increase significantly and when growth factors were present in the absence of a modest inflammatory response no increase in proliferation was detected.

The pattern of proliferation in the non-parenchymal cells within the scaffold followed a similar time course. The non-parenchymal cells present within the pores of the scaffold corresponded to the ED-1 and desmin positive cells labelled by IHC. As with the hepatocytes in the surrounding parenchyma the non-parenchymal cells proliferation peaked at day 4 and then decreased.

3.9.9 MIB-5 Immunohistochemistry

In the pilot study MIB-5 IHC was used to identify hepatocyte and non-parenchymal cell proliferation. MIB-5 stained nuclei were present in the control tissue but despite changes that were consistent with proliferation, no MIB-5 staining was observed in the liver tissue. This led to concerns that proliferating cells were not being detected.

Table 3.5 Proliferative markers in rat liver [194, 195, 206]

Proliferative Marker	Mechanism	Limitations
BrdU IHC	BrdU is incorporated into DNA during S-phase and then detected by IHC	-it requires pre-treatment with BrdU -The mutagenic properties of BrdU preclude use in survival studies - may be expressed by non cycling cells
MIB-5 / Ki-67 IHC	Ki-67 nuclear antigen is expressed in G1, S and G2 of the cell cycle (not G_0) and then detected by IHC	-there is variation in expression & localization -the half life varies -lost with different fixation and staining protocols
proliferating cell nuclear antigen (PCNA) IHC	PCNA is an auxiliary protein of DNA polymerases δ and ε. Expression increases during the G_1, peaks in S and declines during G_2 & M-phases of the cell cycle. It is detected by IHC	-it has variable expression - lost with different fixation and staining protocols -may be expressed by non cycling cells
In situ hybridization (ISH) for histone mRNA	Detects histone mRNA, the synthesis of which is restricted to the S phase of the cell cycle	-Contamination & over fixation can reduce accuracy of detection

A range of techniques have been developed to identify proliferation in rat tissue (table 3.5). Of these the gold standard for detecting DNA synthesis *in vivo* is labeling of DNA by the modified pyrimidine analogue, a halogenated derivative of thymidine, BrdU [194, 207, 208]. BrdU is incorporated into DNA during the S-phase of DNA synthesis which can then be detected by IHC [194]. The main disadvantage to this approach is that BrdU has to be administered prior to animal sacrifice. MIB-5 and PCNA IHC do not require pre-treatment, however both antigens have variable expression and the sensitivity of the detection can vary with different fixation, processing and retrieval protocols. Similarly

mRNA ISH accurately detects cells in the S-phase of the cell cycle but the technique is less widely available and has variable sensitivity [194].

In the comparative study BrdU IHC was used as the primary proliferative marker. In addition modifications were made to the fixation and processing protocols to ensure optimal fixation and processing. These modifications enabled successful detection of DNA synthesis in the control (rat spleen) and liver tissue. When samples that had stained positive for BrdU were then examined for MIB-5 no proliferation could be detected. This suggests that the hepatocyte and non-parenchymal cell MIB-5 / Ki-67 antigens were lost during fixation or processing. Further evaluation is required.

3.9.10 Summary

HGF, EGF, FGF_1 and FGF_2 are all mitogenic to liver cells [56, 74]. In addition they exert chemotactic, motogenic and angiogenic effects in a range of tissues [89, 102, 103, 107]. The release studies demonstrated that the growth factors are present within the scaffolds and that they had retained their bioactivity. As the polymer biodegrades these growth factors are mobilised and can bind to cell receptors. The growth factors also increase the ligand binding capacity of the biomaterial, allowing cells to attach and migrate into the scaffold pores.

L-ECM may act in a number of ways. When present within the polymer scaffold it increases the ligand binding capacity, allowing cells to attach and migrate. The breakdown products of ECM are known to exert a direct chemotactic effect and in protein extraction studies, L-ECM has also been shown to contain a number of growth factors (HGF, EGF, VEGF, FGF_2), although these levels varied considerably between

preparations (unpublished). As a result when L-ECM is broken down growth factors as well as ECM degradation products are mobilised and can act within the scaffold or on the surrounding liver parenchyma. Since this study was completed a porous L-ECM scaffold has been developed. Implantation of this scaffold would give a clearer idea of how L-ECM influences cell specific migration.

The limitations in this study relate to release profiling. Whilst this study demonstrated that growth factors were present in the growth factor loaded scaffolds and that the growth factors released from them *in vitro* had retained their bioactivity, data interpretation would be improved by more detailed characterisation of *in vivo* release from all implants. It is not known how the presence of L-ECM affects the release kinetics of the growth factors contained within the scaffolds (ECM proteins can bind growth factors and as a result they may delay the release of growth factors). This may explain the different patterns seen when growth factors and L-ECM are delivered alone and in combination. It is also unclear from this data how collagen deposition and cell migration affects the release of the growth factors. In future studies it would be useful to study the intra-hepatic and systemic concentrations of individual growth factors.

This study has demonstrated that:

1. Intrahepatic implantation of porous $P_{DL}LA$ & PLGA + 5% PEG scaffolds is feasible

2. Intrahepatically implanted PLGA + 5% PEG and L-ECM biodegrade with time

3. Growth factor and L-ECM incorporation into porous PLGA + 5% PEG scaffolds enhances the rate of liver cell migration and ECM deposition with the pores of the scaffold and together they have an additive effect

4. L-ECM incorporation promotes the migration of desmin positive cells and may exert a chemotactic affect on ED-1 positive cells into porous PLGA + 5% PEG scaffolds

5. Growth factor incorporation promotes the migration of desmin positive cells and in the presence of L-ECM accelerates the migration of ED-1 positive cells into porous PLGA + 5% PEG scaffolds

6. Intrahepatic implantation of a growth factor & L-ECM loaded PLGA + 5% PEG scaffold stimulates a proliferative and inflammatory response in the adjacent peri-implant parenchyma

3.10 Conclusions

Incorporation of growth factors and L-ECM into a PLGA + 5% PEG scaffold promotes liver cell migration and ECM deposition within the pores of the scaffold and stimulates a proliferative response in the hepatocyte and non-parenchymal cell population in the immediate peri-implant parenchyma.

Chapter 4 Intrahepatic Growth Factor Delivery Following Partial Hepatectomy

4.1 Introduction

The rapid restoration of liver mass that occurs after PH is achieved by pan-hepatic hepatocyte proliferation. After 2/3 hepatectomy 95% of the hepatocyte population enters the cell cycle. This occurs in a wave of proliferation from the peri-portal to the peri-central zone of each lobule. In the rat liver this wave of hepatocyte proliferation peaks after 24 hours and is largely complete by 72 hours [59, 64, 74].

Table 4.1 summarises the results of previous studies that have examined the impact of growth factor delivery on hepatocyte proliferation following PH. Webber demonstrated that infusion of HGF and EGFR ligands into the portal circulation after a 1/3 hepatectomy led to an increase in hepatocyte DNA synthesis [97]. Work by Ishii and Fujiwara showed similar effects when HGF was infused into the systemic circulation after 2/3 hepatectomy [98, 99]. In Ishii's study HGF infusion was associated with faster restoration of liver mass.

Fausto hypothesised that the impact of exogenous HGF or EGFR ligand infusion on hepatocyte proliferation in hepatectomised liver was greater than that seen when infused into normal liver because the hepatocyte population had been "primed" for growth factor receptor binding either by TNF and IL-6 receptor binding or another start signal [64].

Table 4.1 summarises the results of 4 studies exploring the impact of intrahepatic growth factor delivery following partial hepatectomy. Where response to growth factor delivery was not stated the section is blank

Study	Species & Strain	Growth Factor	Route	Dose	Outcome				
					Proliferation			Liver weight	
					Measure	Response			
Ishii *et al* 1995[99]	Rat ♂ *Wistar*	HGF + 70% hepatectomy	Jugular Vein	100 µg/kg/day up to 5 days	BrdU	↑	-	↑	x1.3
Webber *et al* 1994[97]	Rat ♂ *Sprague-Dawley*	rh HGF + 33% hepatectomy	Portal Vein	80 µg	3H-thymidine	↑	x5	-	-
Fujiwara *et al* 1993[98]	Rat ♂ *Sprague-Dawley*	h and rh HGF + 70% hepatectomy	Femoral Vein	600 µg/kg	BrdU		-	-	-
Webber *et al* 1994[97]	Rat ♂ *Sprague-Dawley*	rh EGF + 33% hepatectomy	Portal Vein	80 µg	3H-thymidine	↑	x3-4	-	-

In chapter 3 the development of an intrahepatic growth factor delivery system that provided combined release of the liver's key mitogens was described. When this delivery system was implanted into normal liver it stimulated a proliferative response, increasing the rate of hepatocyte DNA synthesis in the parenchyma adjacent to the implant. The aim of this study was to determine how growth factor delivery from an intrahepatically implanted biodegradable scaffold affected the rate of hepatocyte DNA synthesis after PH. The study was undertaken in rats using the Higgins & Anderson model for 2/3 hepatectomy [57]. The hybrid scaffold developed in chapter 3 was used to deliver the growth factors. A pilot cadaveric, terminal anaesthesia and short survival study was performed to optimise the study protocol. Scaffolds were implanted into 2 groups. In the first group the scaffold was implanted at the time of PH (Simultaneous PH). In the second group the scaffold was implanted 2 days before the PH (Delayed PH). Animals were then maintained for up to 2 weeks after PH. Control animals underwent a PH and capsule incision or a sham procedure (laparotomy and capsule incision). Liver function was assessed by measuring serum AST and bilirubin. H&E staining was used to assess basic histology and proliferation was measured using BrdU incorporation detected by immunohistochemistry. In all groups T_0 refers to the time of PH.

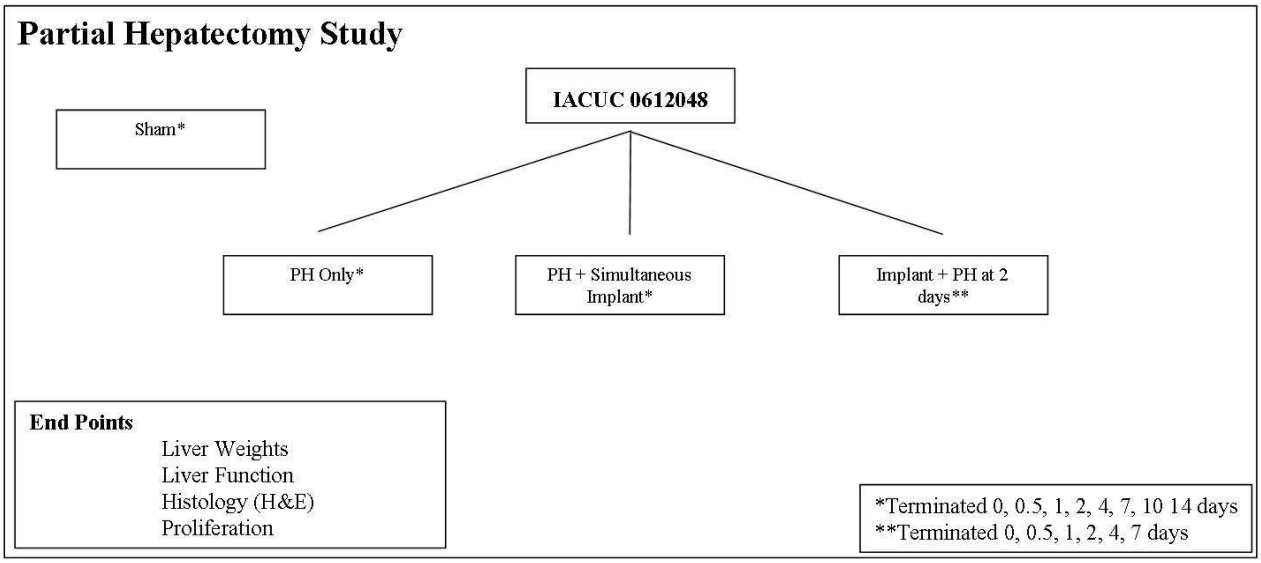

Figure 4.1 Partial hepatectomy study design

4.2 Materials & Methods

4.2.1 Animals

The study was approved by the University of Pittsburgh's IACUC and conducted in accordance with the protocols laid out in Licence 0612048. 78 adult male Wistar rats (Charles River) (150-250 g) were housed in the Animal Facility of the McGowan Institute for Regenerative Medicine, University of Pittsburgh, given access to standard laboratory rat chow and water *ad libitum* and maintained in a standard 12-hour light-dark cycle.

4.2.2 PH Study Implant Manufacture

To manufacture the hybrid scaffolds for the PH study PLGA (50:50) and PEG (mw 400) were mixed together at 95º C to produce a PLGA 5% PEG blend. This was milled mixed with milled L-ECM and the growth factor solution (per implant = 6.8 mg PLGA 5% PEG + 1.2 mg liver-ECM + 2.5 μg HGF, 5 μg EGF, 2.5 μg FGF_1, 2.5 μg FGF_2), freeze dried and processed using a 230 bar pressure of CO_2 at 35º C for 60 min followed by a 60 min decompression. The supercritically processed hybrid blend was milled to sub 250 μm microparticles, 8 mg of which was loaded into a 4 mm x 4 mm teflon mould, sintered at 40ºC for 3 hours and cooled for 30 min at 4º C before removal. The implants were stored at 4º C until implantation.

Table 4.2 Growth factor dosages for the PH study

Growth Factor	Total
HGF	2.5 μg
EGF	5.0 μg
FGF_1	2.5 μg
FGF_2	2.5 μg

4.2.3 Anaesthetic Protocol

See Section 3.2.4

4.2.4 Operative Technique

The abdomen was shaved, cleaned with 10% aqueous betadine and draped. In those animals undergoing PH, a 4cm upper midline abdominal incision was made, the falciform ligament divided and using bilateral subcostal compression the middle lobe and left lobe were delivered. The middle and left lobes were ligated with 1/0 silk, divided, weighed and discarded. To implant the scaffold delivery device into the right lateral lobe, the lobe was held between the thumb and index finger, a 1 mm capsular incision was made on the surface of the lobe to a depth of 0.5 mm using a number 11 scalpel blade, and the cone was implanted so that its edges sat below the capsule. Haemostasis was achieved where necessary by gentle compression with a cotton bud. The abdominal cavity was inspected and the abdominal wall closed in layers with 3/0 vicryl on a cutting needle. The animal was recovered on a warming mat, weighed and housed under standard conditions with buprenorphine given for 2 days post-operatively. In those animals undergoing a

sham procedure an upper midline incision, right lateral lobe mobilisation and liver capsule incision was performed.

4.2.5 Necropsy Protocol

A sterile intraperitioneal injection of BrdU (100 mg/kg) was given 24 hours prior to sacrifice. At allocated time points the animals were anaesthetised and weighed. Blood samples were collected by cardiac puncture and the animals sacrificed with an intra-cardiac bolus of potassium chloride. After death was confirmed (loss of light reflex and heart beat), a full length midline abdominal incision was made, the liver dissected from surrounding tissue and removed. The total liver and implanted lobe weights were recorded before the livers were prepared for histology.

4.2.6 Liver Weight Analysis

In addition to the LBW (Equation 1), the growth of liver tissue was assessed using the following equation:

Equation 3

$$\text{Implanted to total liver weight ratio (ITW)} = \frac{\text{Implanted lobe weight}}{\text{Total liver weight}}$$

4.2.7 Histology, H & E and BrdU Immunohistochemistry

Samples were processed and stained for H&E and BrdU as described in sections 3.7.10 & 3.7.13.

4.2.8 BrdU Count

As in chapter 3 the proportion of BrdU-labelled hepatocytes on an individual sample was determined by counting the number of positively stained hepatocyte nuclei within a 0.04 mm^2 peri-portal area using the NDP viewer software at x40 magnification. The peri-implant parenchyma was subdivided into 3 bands (Figure 4.2) and only cells with a circular morphology and nuclear diameter > 7 μm were counted. The cumulative mean of hepatocytes per field in bands A, B & C for a sample block are shown in figure 4.3. The final number of BrdU-labelled hepatocytes per band is expressed as a percentage.

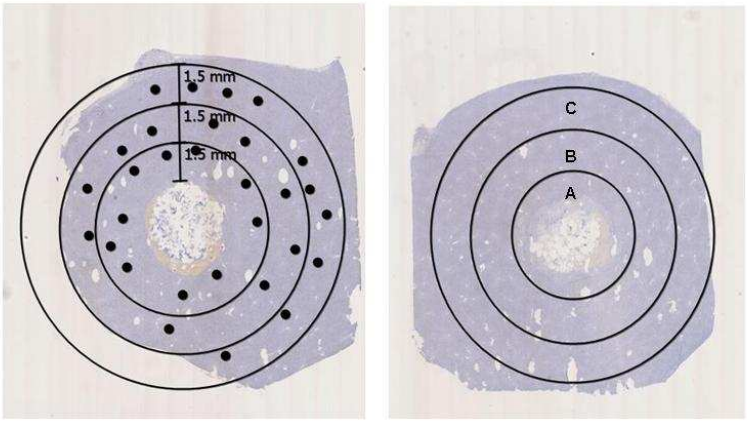

Figure 4.2 Image map for the BrdU scoring. Each block was divided into 3 bands (A, B and C). Each band was 1.5 mm thick beginning at the implant edge, with up to 10 0.04 mm^2 peri-portal squares sampled per band.

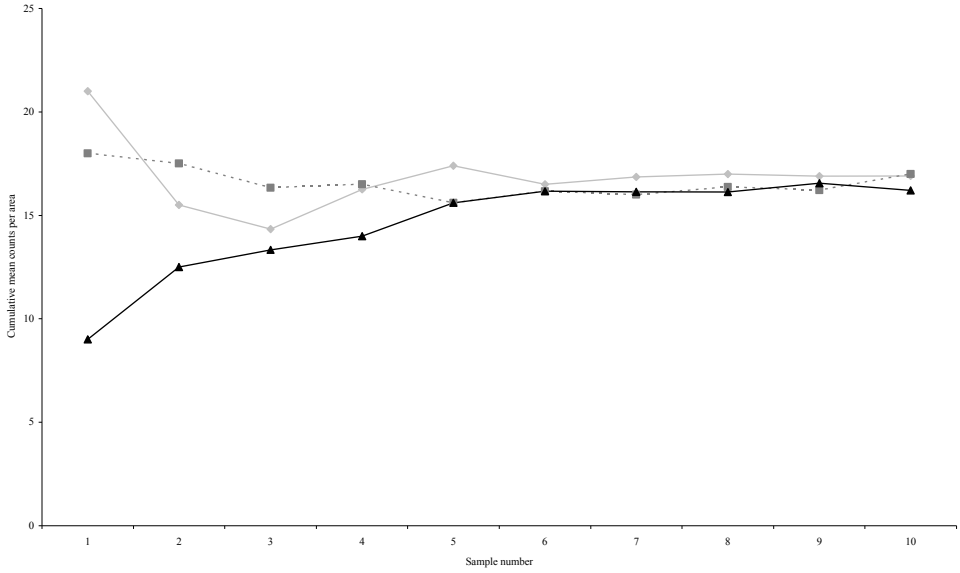

Figure 4.3 Cumulative mean of BrdU positive hepatocytes in a scaffold implanted liver (implant + PH) at day 2 post PH in bands A (♦), B (■) & C(▲) per field. At least 6 peri-portal fields were counted per band (n=3 per time point). For samples with no scaffold implanted at least 6 random 0.04 mm^2 peri-portal areas were counted.

4.2.9 Liver Function

Serum AST and total bilirubin were measured on a plate analyser in the Clinical Chemistry Department of the Children's Hospital, University of Pittsburgh Medical Centre.

4.2.10 Statistical Analysis

Data was analysed using SPSS. Data are expressed as the mean +/- standard deviation. Liver weights and liver function were assessed by one-way ANOVA with Tukey's post-test. BrdU counts were analysed using independent student t-tests. P values less than 0.05 were regarded as statistically significant.

4.3 Results

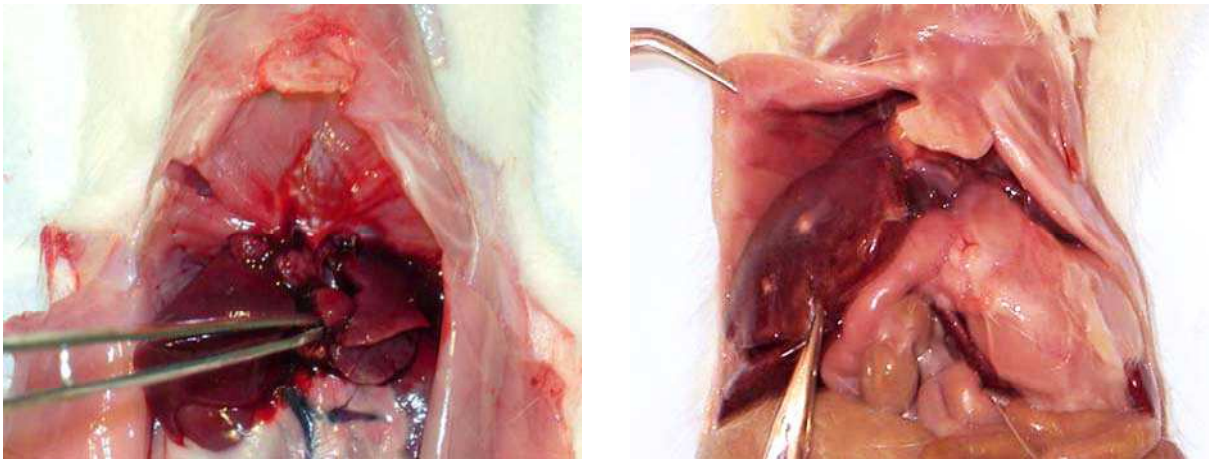

Figure 4.4 Photographs of rat abdomens at necropsy following PH (*left*) and with a scaffold implanted 5 days after PH (*right*). The anterior abdominal wall has been excised and the scaffold implanted into the right lateral lobe.

Table 4.3 Average resected lobe to total body weight ratio and percentage hepatectomy for the 3 study groups. There was no significant difference in size of hepatectomy between groups.

	Resected Lobe : total body weight ratio	Percentage average sham LBW (0.044)
PH	0.030 +/- 0.003	68.0%
PH + Implant	0.030 +/- 0.004	68.7%
Implant + PH	0.028 +/- 0.004	65.4%

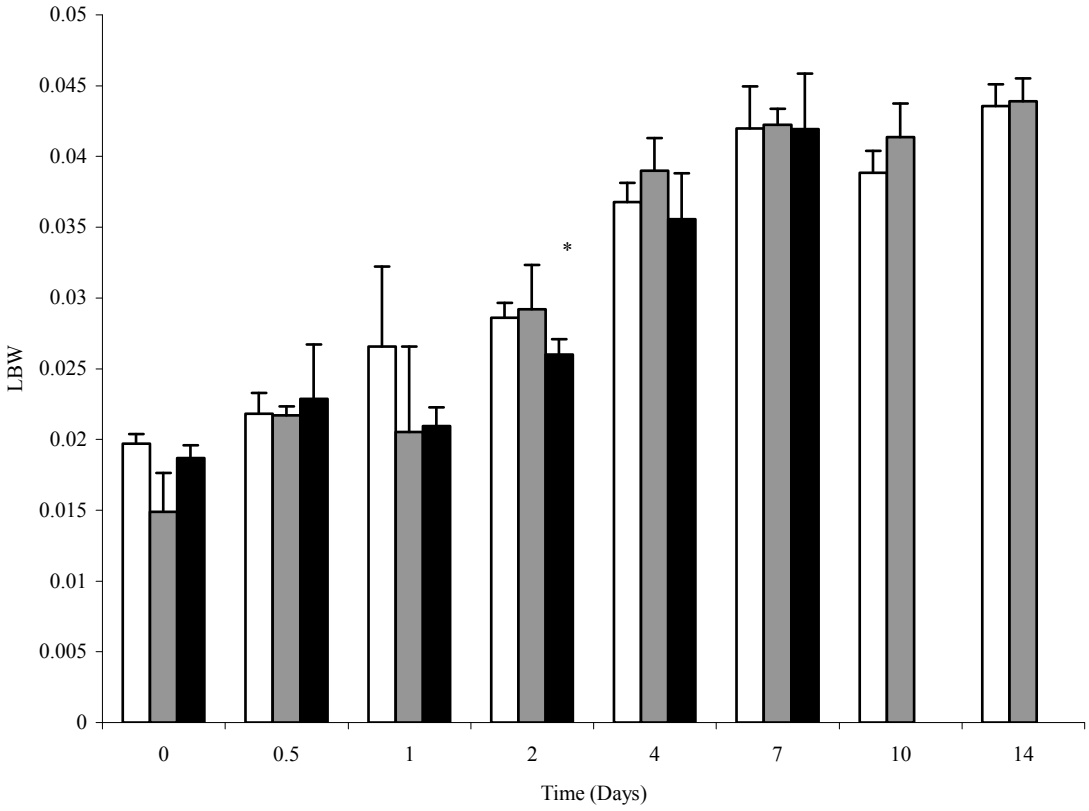

Figure 4.5 LBW (calculated using equation 1) up to 14 days after PH (+/- SD of mean) (n=3). PH (*white*), PH + implant (*grey*) and implant + PH (*black*). The average LBW in normal liver is 0.044 +/- 0.005. At T_0 (After PH) the average LBW was 0.018 +/- 0.003. In all groups LBW increased with time. By day 7 LBW was equal to the average sham LBW in all groups. The LBW in the PH animals was significantly greater than the LBW of the implant + PH animals at day 2. There were no other differences in LBW detected. *P < 0.05 compared with PH alone.

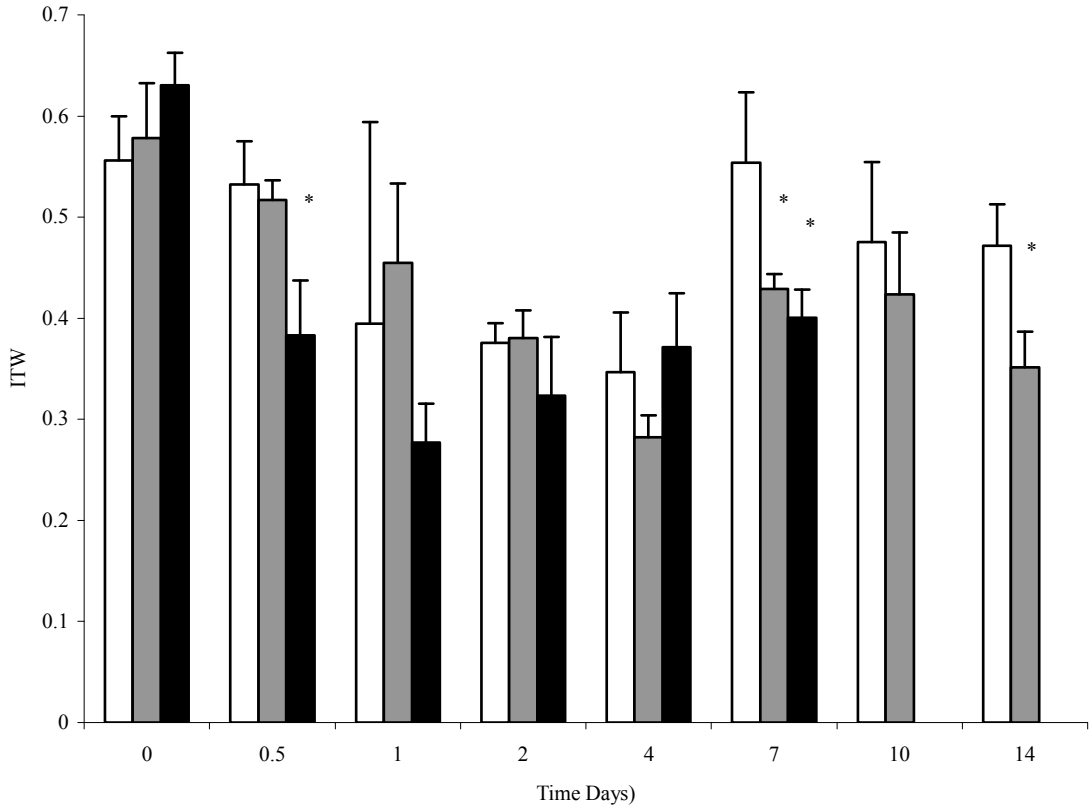

Figure 4.6 ITWs (calculated using equation 3) up to 14 days after PH (+/- SD of mean) (n=3). PH (*white*), PH + implant (*grey*) and implant + PH (*black*). In all groups ITW initially decreased after PH and then increased. At 12 hours the ITW for the PH only animals was significantly greater than the ITW for the implant + PH animals. At day 7 the ITW for the PH animals was significantly greater than the ITW for the PH + implant and the implant + PH animals. At day 14 the ITW for the PH animals was significantly greater than the ITW for the PH + implant animals. *$P < 0.05$ compared with PH alone.

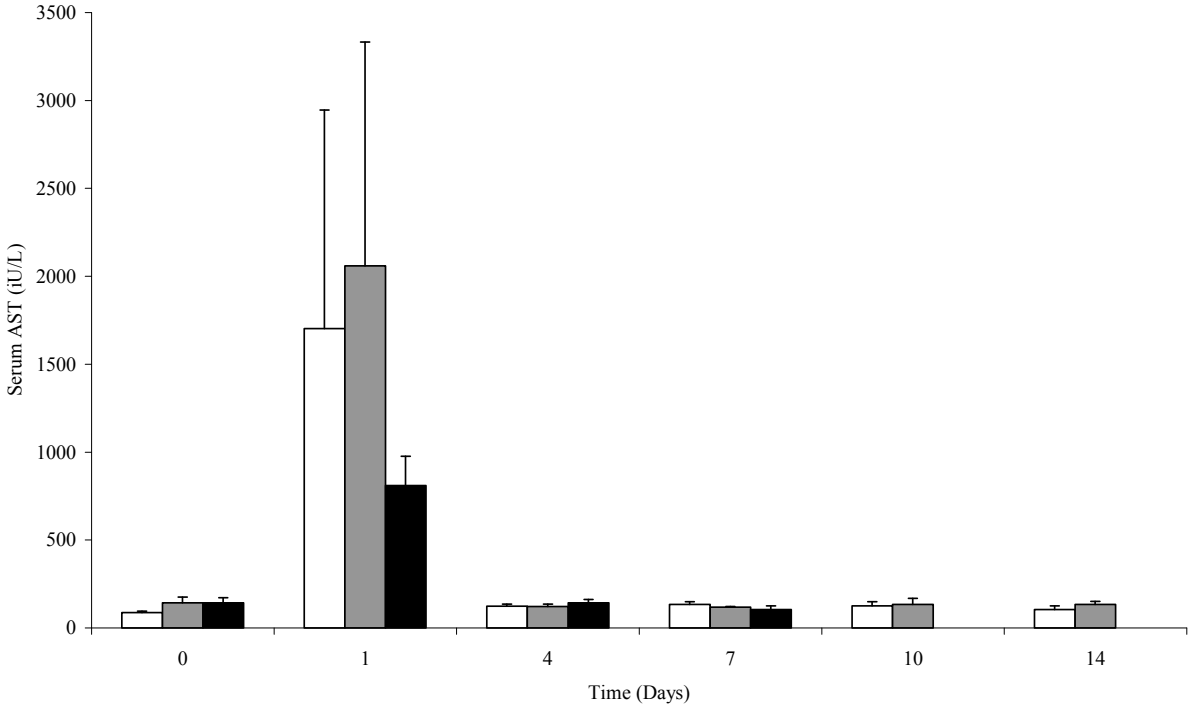

Figure 4.7 Serum AST up to 14 days after PH (+/- SD of mean) (n=3). PH (*white*), PH + implant (*grey*) and implant + PH (*black*). In all animals serum AST rose significantly following PH and returned to baseline levels in all animals by day 4. There was no significant difference in serum AST detected between groups for the duration of the study. No increase in serum bilirubin was detected for the duration of the study.

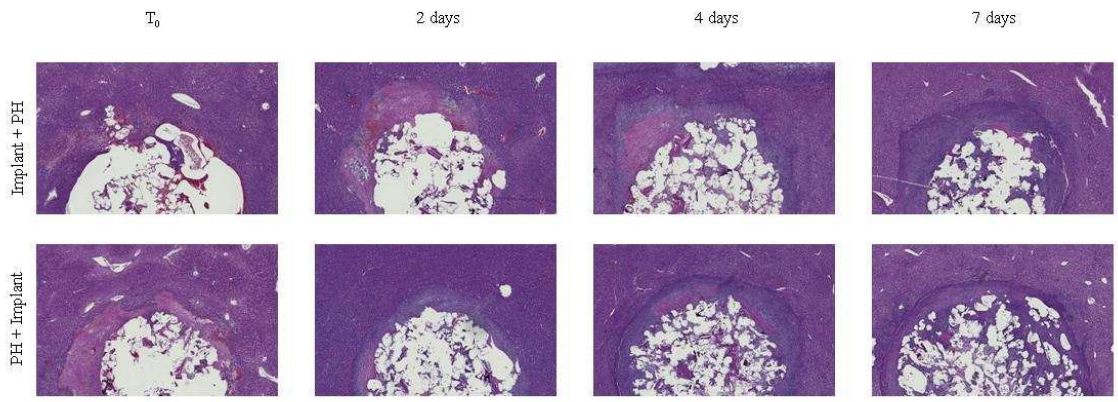

Figure 4.8 H&E of the PH + implant (*top*) and implant + PH (*bottom*) livers at T_0, 2, 4 and 7 days after PH. In the PH + implant group: at T_0 erythrocytes filled the pores of the scaffold and the surrounding parenchyma was compressed; at day 2 the scaffolds were surrounded by a band of inflammation and necrosis; at day 4 the band of necrosis had resolved and the band of inflammation was well demarcated.; by day 7 there was a dense peri-implant inflammatory reaction and marked ECM deposition and liver tissue migration in the pores of the scaffold. In the implant + PH group: at T_0 the scaffolds were surrounded by a band of inflammation and necrosis; at day 2 the band of necrosis had resolved and the band of inflammation was well demarcated; at day 4 a dense band of inflammation surrounded the scaffold, there was ECM deposition and liver tissue migration in the pores of the scaffold; by day 7 the peri-implant band of inflammation was resolving. Original magnification 2.5X.

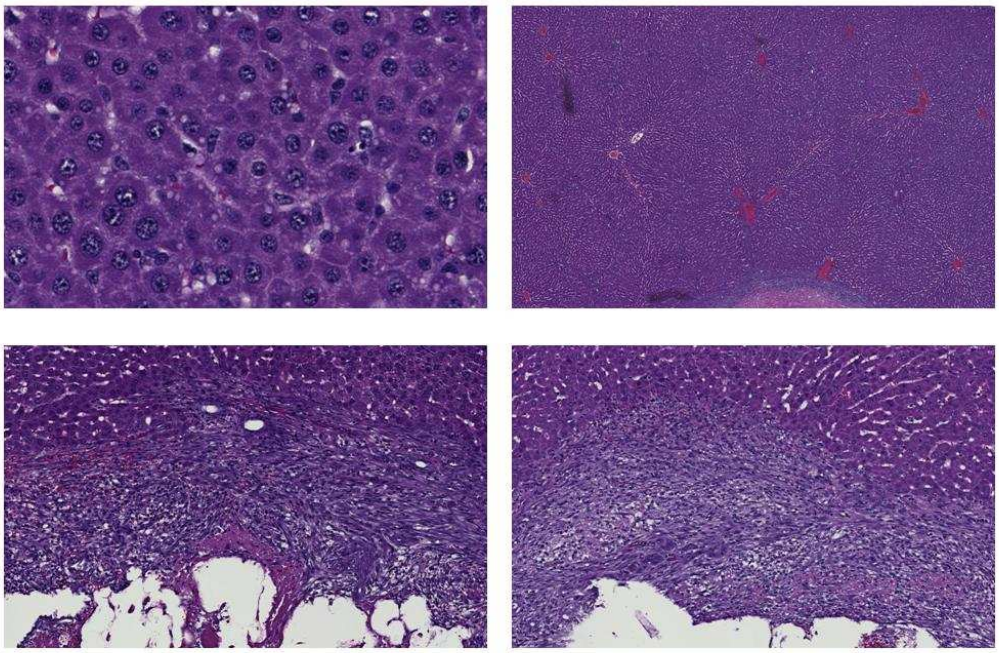

Figure 4.9 H&E demonstrating mitotic, neovascular and inflammatory changes after PH. Hepatocyte mitosis was visible 12 hours after PH in all groups and remained visible for up to 7 days (PH + implant day 2*, top left*). Vascular proliferation was present in the implanted and non-implanted residual liver tissue 2 days after PH (implant + PH day 2, *top right*). A well demarcated band of inflammation surrounded the PH + implant group of scaffolds from day 4 (PH + implant day 4 , *bottom left*) and the implant + PH group of scaffolds from day 2 (implant + PH day 2, *bottom right*). Original magnifications top left 20X, top right 2.5X and bottom 10X.

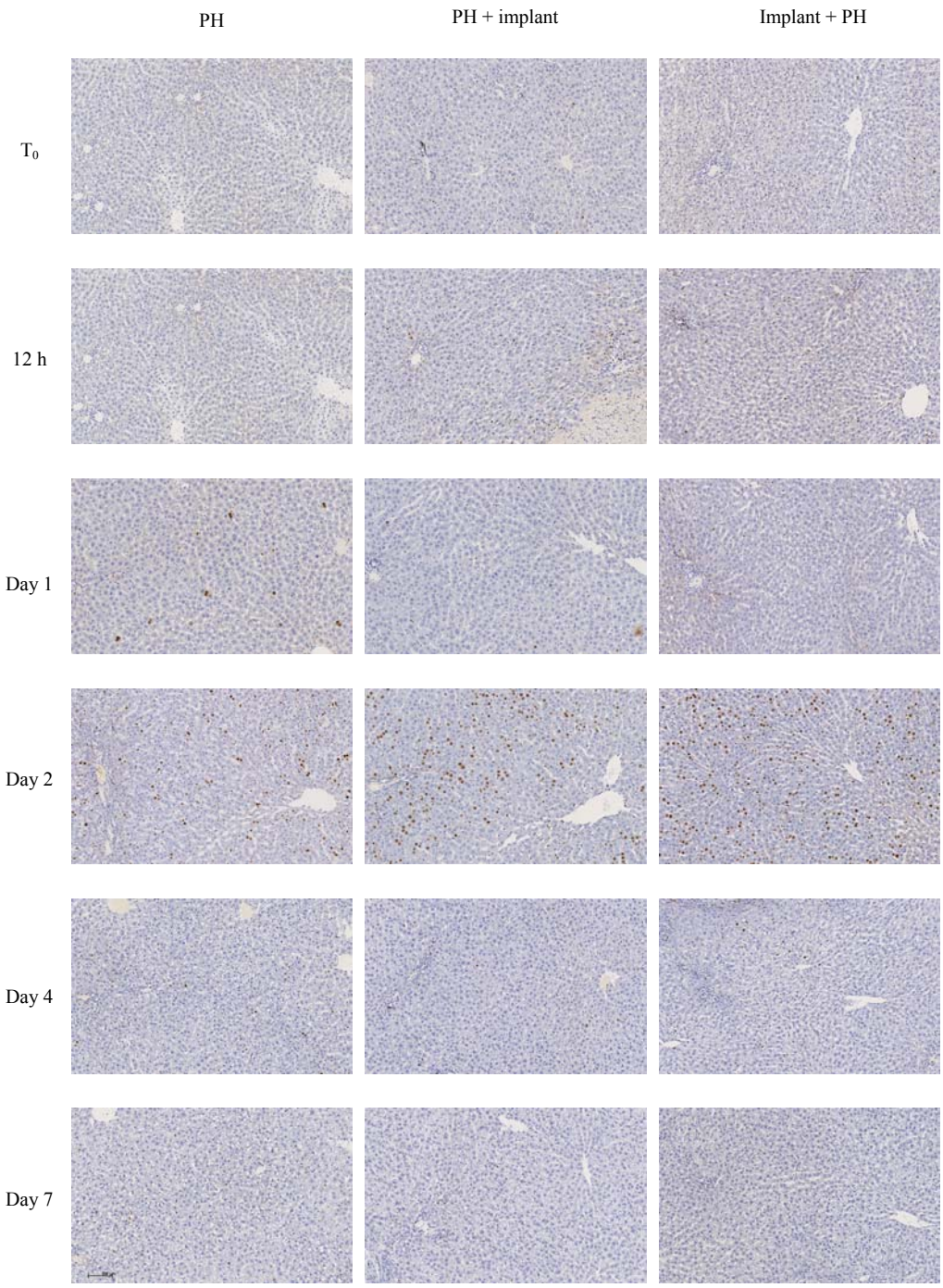

Figure 4.10 BrdU IHC of single liver lobules in implanted and non-implanted lobes up to 7 days after PH. BrdU positive nuclei are stained brown. PH (*left*), PH + implant (*middle*) and implant + PH (*right*). The images are orientated so that the portal tracts are on the left and central veins are on the right. In the scaffold implanted livers the images are taken from band B. In all groups the number of BrdU stained cells increased up to 2 days after PH and then decreased. There were more BrdU positive cells in the non-implanted group at day 1 and in the implanted groups at day 2.

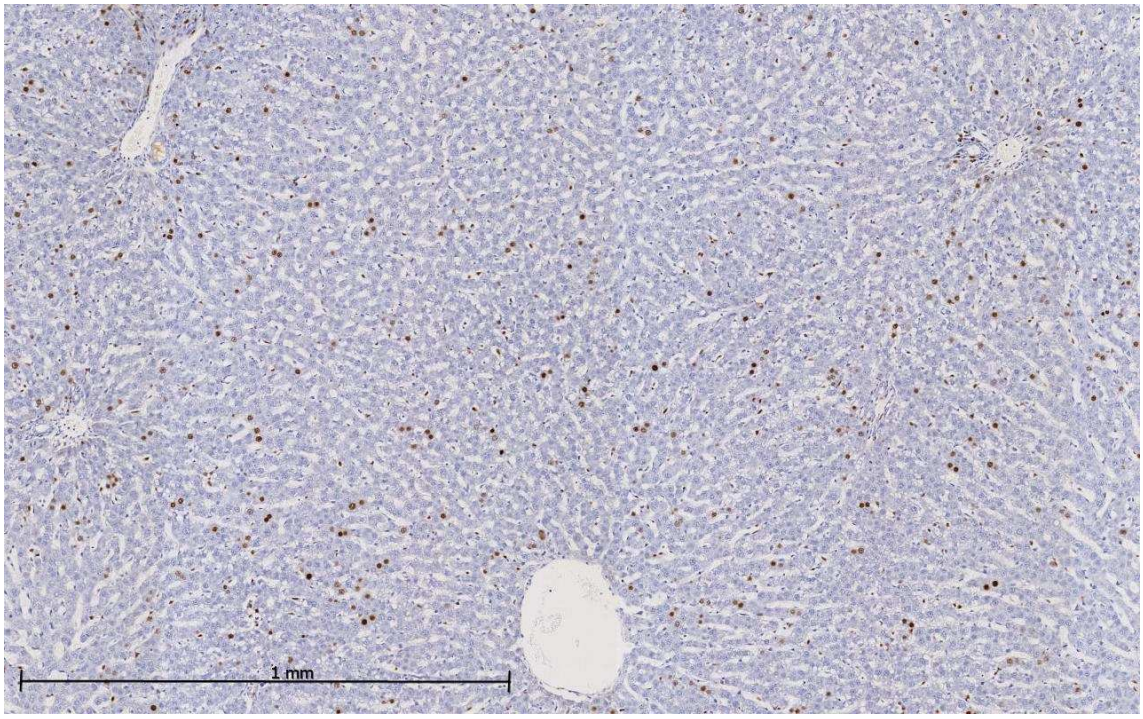

Figure 4.11 BrdU IHC of a non-implanted section of liver tissue 2 days after PH demonstrating the distribution of BrdU positive nuclei in relation to portal tracts and central vein. Hepatocyte proliferation advances in a wave from the peri-portal to the peri-central region. At each time 0.04 mm^2 area of tissue lying between a portal tract and a central vein was sampled.

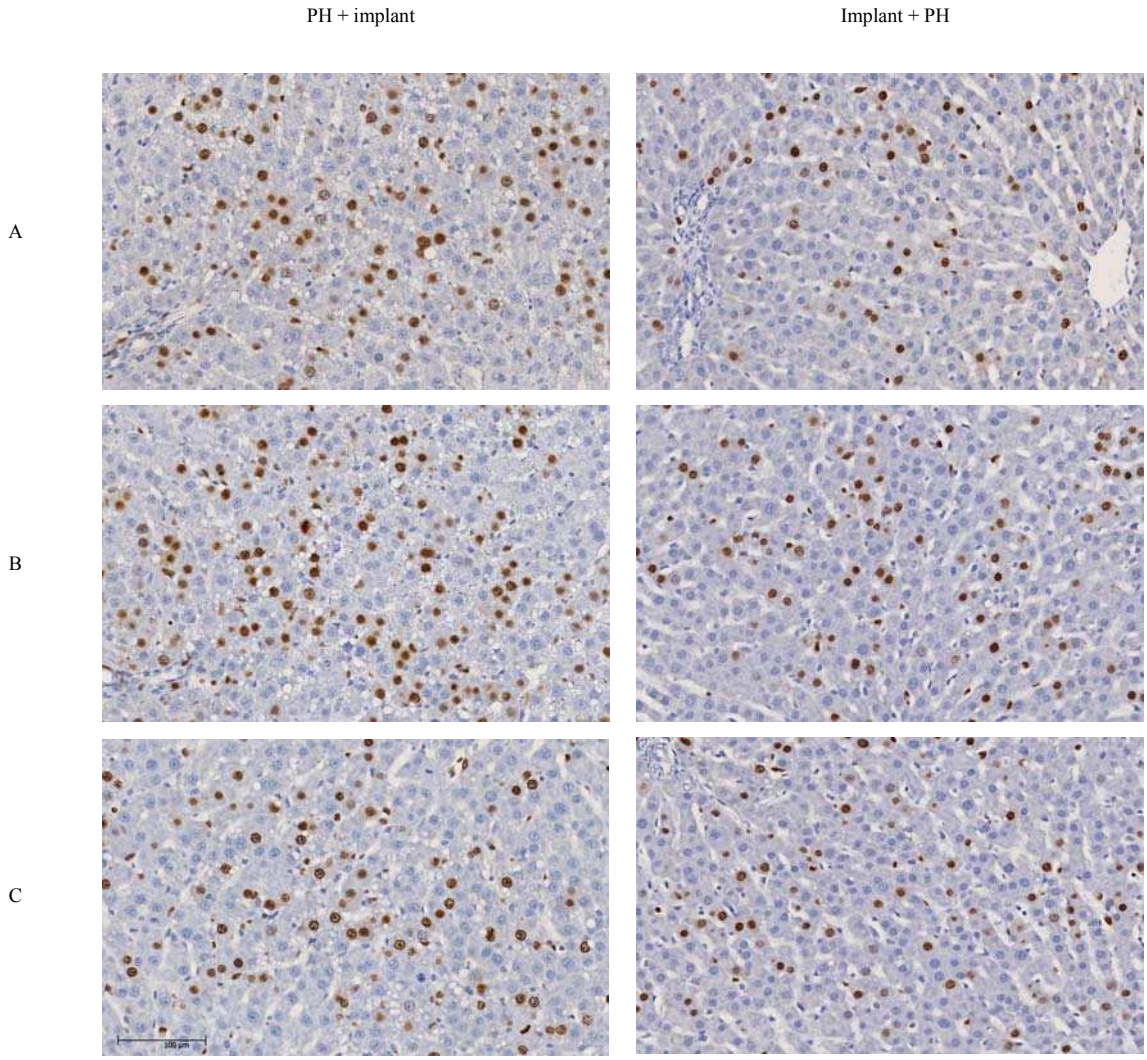

Figure 4.12 BrdU IHC of peri-implant liver parenchyma from the PH + implant (*left*) and implant + PH (*right*) peri-implant parenchyma 2 days after PH in bands A, B and C. There were more BrdU positive hepatocytes in the bands closest to the implant.

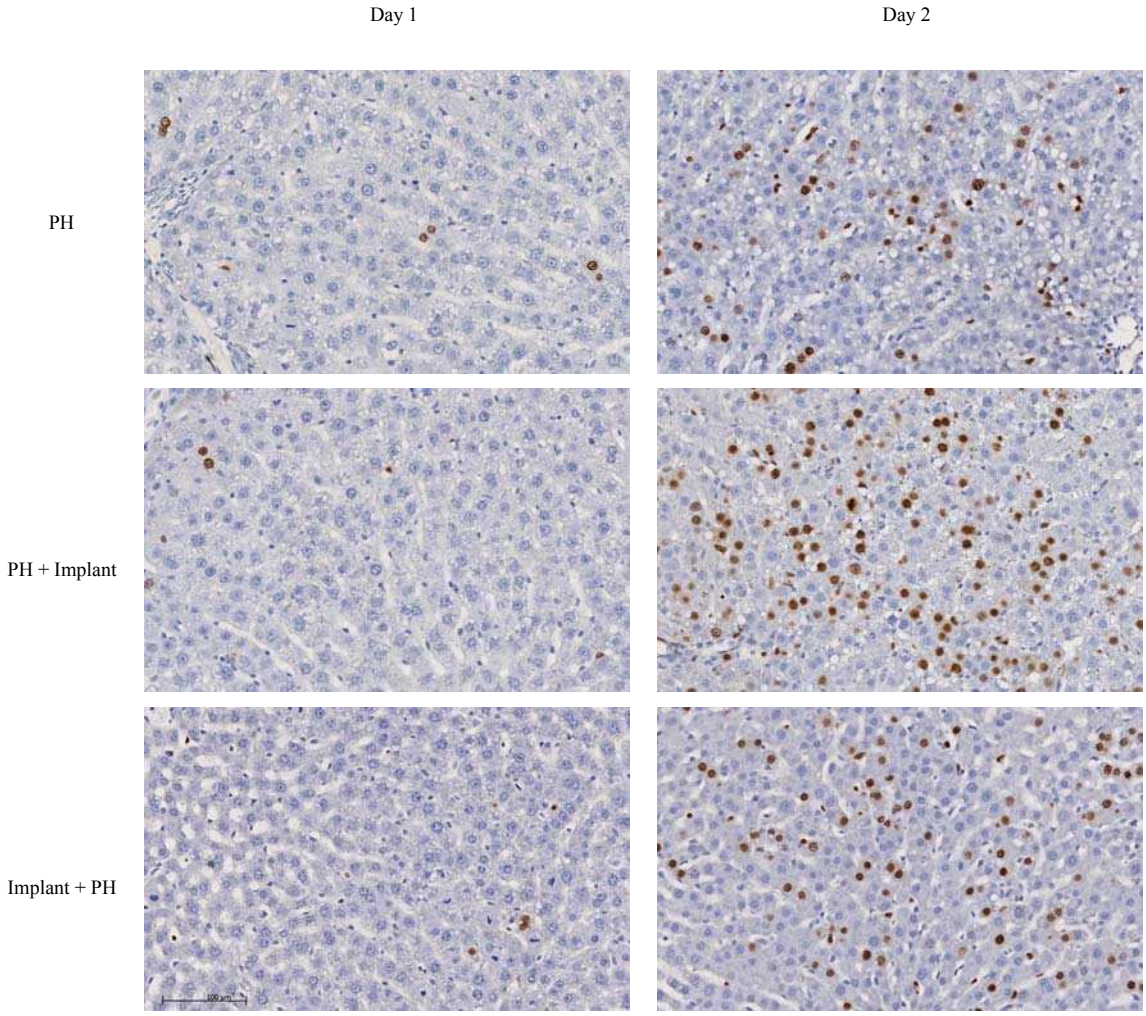

Figure 4.13 BrdU staining of PH (*top*), PH + implant (*middle*) and implant + PH (*bottom*) at day 1 (*left*) and 2 (*right*) after PH. In the scaffold implanted livers the images are taken from band B. The peak of hepatocyte BrdU staining occurred 2 days after implantation. There were more BrdU stained hepatocytes in the non-implanted livers (PH) at day 1 and in band B of the implanted livers (PH + implant & implant + PH) at day 2.

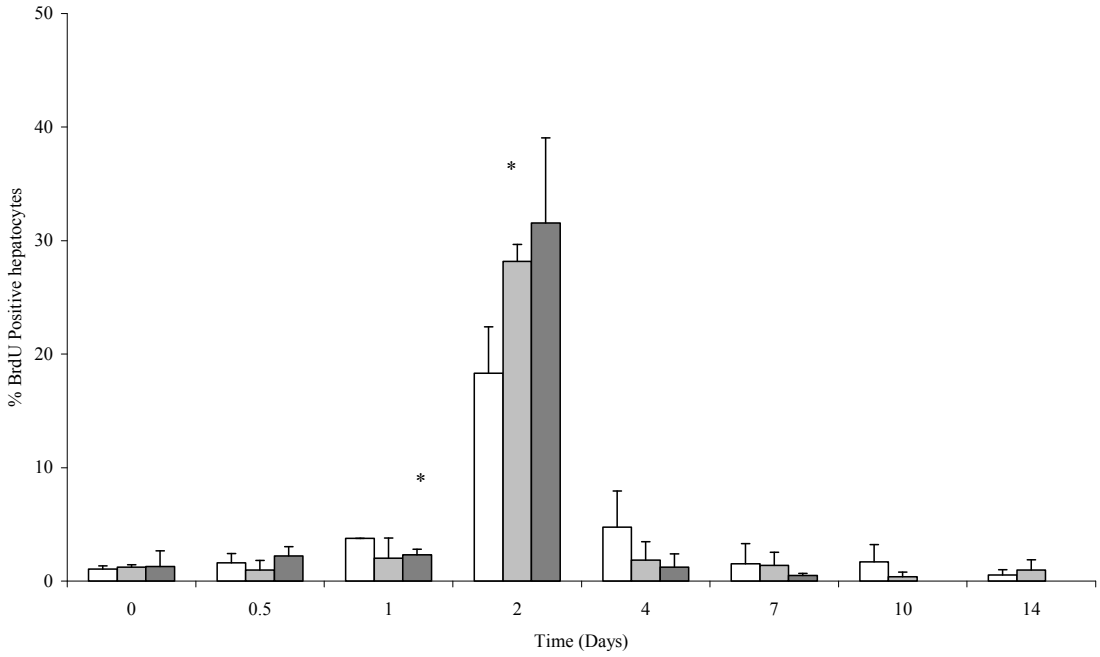

Figure 4.14 Percentage of BrdU-labelled hepatocytes for the PH study up to 14 days after PH (+/- SD of mean) (n=3). PH only (*white*), PH + implant (*grey*) and implant + PH at 2d (*black*). The value stated for the implanted livers is the average for the 3 bands. At day 1 the percentage of BrdU positive hepatocytes in the non-implanted liver was significantly greater than implant + PH. At day 2 the percentage of BrdU positive hepatocytes in PH + implant group was significantly greater than the PH only group. There were no differences detected between groups for the remainder of the study. *$p < 0.05$ compared with the PH only group.

Table 4.4 Percentage of BrdU positive hepatocytes in the peri-implant parenchyma up to 14 days after partial hepatectomy +/- SD of mean (n=3)

	0	0.5	1	2	4	7	10	14
Sham	0.18+/-0.16	0.89+/-0.82	0.89+/-0.31	0.09+/-0.16	0.18+/-0.16	0.45+/-0.16	0.27+/-0.00	0.18+/-0.16
PH only	1.07+/-0.27	1.61+/-0.81	3.76+/-0.00	18.31+/-4.10	4.74+/-3.20	1.52+/-1.79	1.70+/-1.53	0.54+/-0.47
PH + implant	1.22+/-0.23	0.98+/-0.85	2.03+/-1.77	28.17+/-1.50	1.85+/-1.62	1.40+/-1.13	0.39+/-0.40	0.98+/-0.91
Implant + PH	1.28+/-1.40	2.21+/-0.83	2.33+/-0.47	31.55+/-7.51	1.22+/-1.17	0.49+/-0.19		

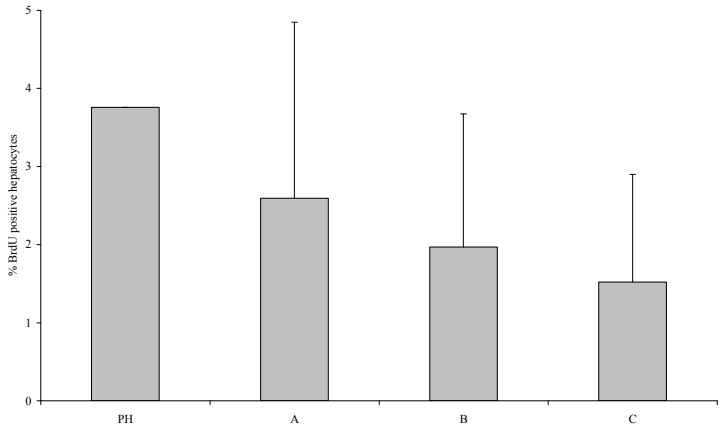

Figure 4.15 Percentage of BrdU labelled hepatocytes in bands A, B & C of the PH + implant group at day 1. There were no significant differences detected.

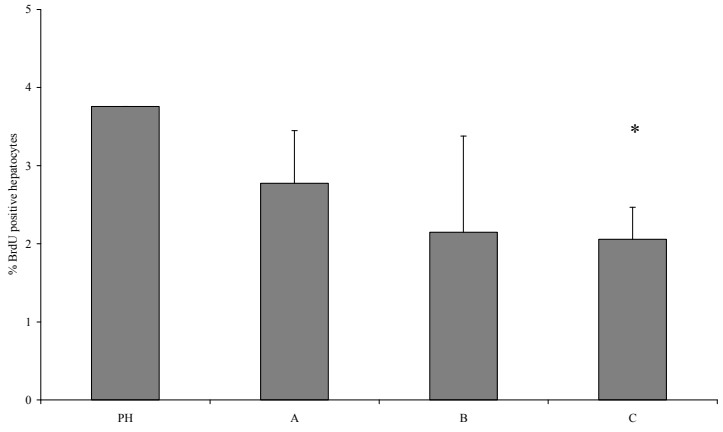

Figure 4.16 Percentage of BrdU labelled hepatocytes in bands A, B & C of the implant + PH group at day 1. In band C the number of BrdU labelled hepatocytes was significantly less than the PH only livers. There was no significant difference between band A or B and the PH only livers. *P < 0.05 compared with the PH only group.

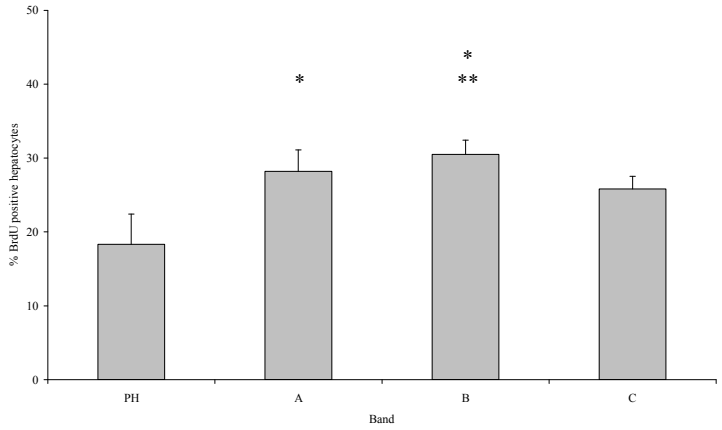

Figure 4.17 Percentage of BrdU labelled hepatocytes in bands A, B & C of the PH + implant group at day 2. In bands A & B the number of BrdU labelled hepatocytes was significantly greater than the PH only livers at day 2. There was no significant difference between band B and the PH only livers. In addition band B was significantly greater than band C. *P < 0.05 compared with the PH only group and **P < 0.05 compared with band C.

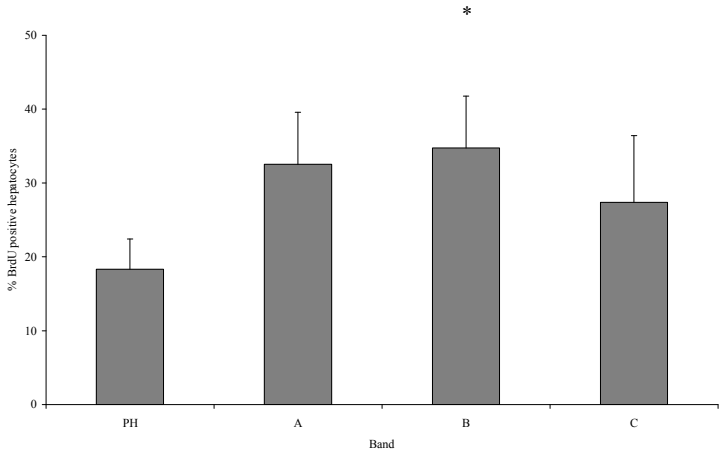

Figure 4.18 Percentage of BrdU labelled hepatocytes in bands A, B & C of the implant + PH group at day 2. In band B the number of BrdU labelled hepatocytes was significantly greater than the PH only livers. There was no significant difference between band A or C and the PH only livers. *P < 0.05 compared with the PH only group.

4.4 Discussion

When exogenous HGF and EGF receptor-ligands are infused into liver that has been "primed" for regeneration, they induce an increase in hepatocyte DNA synthesis [96-99]. The aim of this study was to determine if delivery of HGF, EGF, FGF_1 and FGF_2 from an intrahepatically implanted PLGA + 5% PEG + 15% L-ECM scaffold could increase hepatocyte proliferation and enhance liver regeneration in liver "primed" by 2/3 hepatectomy.

4.4.1 Study Design & Pilot

In chapter 3 the development of an intrahepatic growth factor delivery device was described. In order to establish how intrahepatic growth factor delivery impacted on liver regeneration after PH, several modifications to the scaffold design and implantation technique were required. First the implantation site was changed. In chapter 3 the scaffolds were implanted into the medial lobe of the rat liver. Because the left and medial lobes of the rat liver are resected in the Higgins 2/3 hepatectomy model, the scaffold had to be implanted at an alternative site [57]. The right lateral lobe was the largest and most accessible of the remnant lobes and following a series of cadaveric and terminal anaesthetic studies was identified as the best site for scaffold implantation for the PH study.

The polymer: L-ECM ratio was also modified. In order to implant the scaffold into liver tissue the sintered cone must not deform. The T_g of PLGA + 5% PEG is between 35-40º C as a result when is handled for long periods it softens. The rate of softening is increased when protein is incorporated into the scaffold blend because this reduces the total polymer per implant. Scaffold

softening was not a problem in the comparative study because the implants could be implanted into the medial lobe of the rat liver quickly with minimal handling. Scaffold softening was a problem when implantation of the 20% L-ECM scaffold into the right lateral lobe was piloted. To overcome this, the proportion of L-ECM loaded per scaffold was reduced to 15% by weight. This adjustment increased scaffold strength and allowed implantation without deformation. In future to preserve the L-ECM loading capacity of the scaffolds, alternative implantation and delivery systems could be developed.

Younger animals were used for the PH study; as a result the average pre-operative body weight for the PH study was 187.3 +/- 22.1 g *versus* 260.1 +/- 32.0 g for the comparative study. This reduction in body weight made PH and right lateral lobe mobilisation easier. The sex, strain and husbandry conditions were the same in both studies. When the implantation regimes were piloted, the animals tolerated both PH and scaffold implantation well. There were 2 intra-operative deaths. One was due to an anaesthetic complications and the other was due to uncontrolled liver haemorrhage from a large liver capsule tear. There were no post-operative deaths.

4.4.2 Liver Weight Analysis

In the Higgins & Anderson model for PH, three of the five liver lobes are excised. The remaining lobes then grow to restore liver mass. The majority of liver mass is restored by day 3 and regeneration is usually complete by day 7. This model provides a highly reproducible surgical resection [74] and this was confirmed in the resected lobe weight analysis.

In all groups LBW returned to pre-PH levels by day 7. A significant difference was detected between the LBW of the PH only group and the simultaneous PH group at day 2. Review of the liver and body weights for this time point demonstrated that there was no significant difference between the average liver weight for the simultaneous PH group and the other groups, but that the average body weight for the simultaneous PH group was greater. It is unclear whether this reduction in LBW reflects impaired regeneration in the implanted lobe. Repetition of this time point is therefore required.

A change in inter-lobe weight distribution after PH occurs as the liver regenerates and reorganises. How the liver mass redistributes after PH has not previously been described. In this study the pattern of ITW change was consistent between study groups; initially dropping after PH and then rising to a plateau by day 7. Implantation of a scaffold into the right lateral lobe was associated with a rightward shift in the growth curve (figure 4.19). This shift was statistically significant at 12 hours, 7 and 14 days after PH. It is unclear whether this reflects impaired regeneration or whether the scaffold implantation caused a change in the inter-lobe weight distribution. Again repetition of the time points is required.

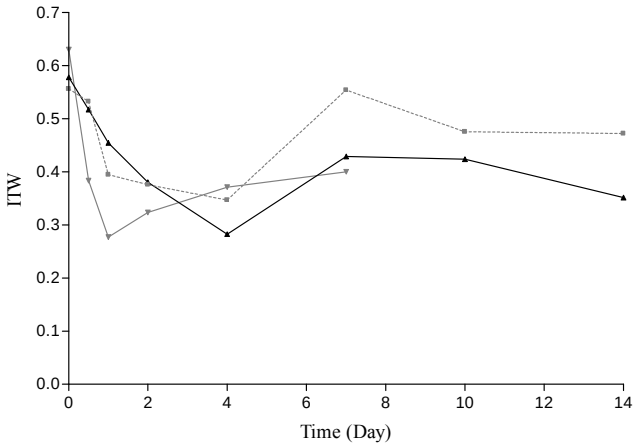

Figure 4.19 ITW curves for the different study groups up to 14 days after PH. PH only (■), PH + Implant (▲) and Implant + PH at 2d (▼). Note the rightward shift and reduced plateau of the scaffold implanted right lateral lobes.

4.4.3 Liver Function

After PH, AST rose significantly in all groups and serum bilirubin remained constant. The increase in AST at day 2 was expected and reflected the timing and extent of the parenchymal injury. Whilst there was no difference in AST levels detected between study groups, AST reached its highest levels in the simultaneous PH group and was lowest in the delayed PH group.

4.4.4 Basic Histology

The appearances of the H&E stained scaffold implanted liver after PH mirrored that of the H&E staining of hybrid scaffolds implanted into normal liver (chapter 3). The scaffolds were initially surrounded by a peri-implant band of inflammation and necrosis, which resolved with time. At the same time cells migrated and ECM was deposited in the pores of the scaffold. There were some minor differences secondary to the PH. Numerous mitotic bodies were observed

throughout the lobe at day 2 after PH and the rate of migration and ECM deposition appeared faster than in the normal liver. This trend could be confirmed by image analysis (section 3.7.14).

4.4.5 Proliferation

Following 2/3 hepatectomy, hepatocyte DNA synthesis increases as liver mass is restored. In rat liver, this begins within 12 hours of PH and normally peaks around 24 hours [59]. In this study the peak in hepatocyte DNA synthesis occurred after 24 hours in both the scaffold implanted and non-scaffold implanted livers. Otherwise the pattern of hepatocyte DNA synthesis in this PH study was consistent with the literature. The reason for the later peak is unclear. The rate of DNA synthesis after PH can vary between rodent species and strains and in response to circadian rhythm [74]. To define it more clearly the number of time points in the first 72 hours after PH and the number of animals per time point should be increased.

A number of differences in hepatocyte DNA synthesis were observed between the scaffold implanted and non-scaffold implanted livers. At day 1 the number of BrdU positive hepatocytes in the PH only group was significantly greater than in band C of the implant + PH group, whilst at day 2 there were significantly more BrdU positive hepatocytes in bands A and B of the PH + implant group and in band B of the implant + PH group than in the PH only livers. The differences in hepatocyte DNA synthesis observed between the non-implanted and scaffold implanted livers after PH suggests that the scaffolds are influencing liver regeneration. Further evaluation is required to determine if these differences represent an increase or decrease in the overall rate of liver regeneration.

When the growth factor loaded scaffolds were implanted into normal liver tissue the proliferative response that they induced was limited only to the liver parenchyma adjacent to the scaffolds. A similar gradient of proliferation was observed in the scaffold implanted livers after PH. Because growth factors are rapidly cleared by the liver, their direct release into the liver parenchyma from a scaffold was unlikely to stimulate proliferation beyond the adjacent peri-implant parenchyma. In future studies hepatocyte DNA synthesis at other sites in the residual liver tissue should be assessed.

The timing of scaffold implantation did not impact on the rate of DNA synthesis after PH in this study. The highest rates of hepatocyte DNA synthesis were seen in the delayed PH group but overall the proliferative response seen in the parenchyma surrounding the scaffolds implanted at the time of PH was more consistent. A better understanding of the release kinetics of growth factors from the scaffold and of the pathways that initiate, regulate and terminate liver regeneration will allow the development of more targeted growth factor delivery regimes.

4.4.6 Summary

This study set out to characterise how intrahepatic delivery of HGF, EGF, FGF_1 and FGF_2 from a PLGA +5% PEG + 15% L-ECM scaffold impacts on liver regeneration following 70% hepatectomy. It demonstrated that scaffold implantation at the time of PH in the rat was feasible and that growth factor delivery was associated with an increase in hepatocyte DNA synthesis after PH. However it failed to demonstrate faster restoration of functional liver mass although scaffold implantation did impact on inter-lobar redistribution of liver mass.

The limitations in this study relate to the study design (the number of animals per time point, the time points used and the control groups) and release profiling. To make a preliminary assessment of intrahepatic growth factor delivery at the time of PH, 3 animals were used per time point at intervals up to 14 days after PH. In order to provide a more accurate assessment of the proliferative response after PH, future studies should focus on the first 7 days after PH with more animals per time point.

In order to determine the impact of PLGA + 5 % PEG + 15% L-ECM implantation into the liver at the time of PH an additional control group should be incorporated into the study design. Implantation of a non-growth factor loaded scaffold into the liver at the time of PH would determine if the scaffold alone can induce a proliferative response.

As in the comparative study more detailed *in vitro* and *in vivo* release profiling is required to characterise the release kinetics of growth factors from the scaffold at the time of PH; in particular how growth factor release was affected by the haemodynamic changes that occur following PH and how the reduction in L-ECM loading impacted on growth factor release. In addition it would be beneficial to have a measure of the systemic and hepatic serum growth factor concentrations in non-implanted and scaffold implanted livers after PH.

4.5 Conclusion

Intrahepatic implantation of a PLGA + 5% PEG scaffold loaded with growth factors and L-ECM is associated with an increase in the rate of hepatocyte proliferation following PH. Further evaluation of growth factor delivery at the time of PH is warranted.

Chapter 5 General Discussion

This thesis set out to review the expanding role of scaffolds in the field of liver tissue engineering and to describe the development and evaluation of two scaffold based liver tissue engineering strategies. In the first study the scaffold was used as a supportive template for parenchymal and non-parenchymal cell co-culture with the aim of offsetting hepatocyte de-differentiation and improving long term hepatocyte viability and function *in vitro*. In the second study the scaffold was used as an intrahepatic delivery device for growth factors and ECM proteins with the aim of stimulating growth and enhancing regeneration *in vivo*.

5.1 *In Vitro* Study

The objectives of the *in vitro* study were to evaluate hepatocyte-HSC co-culture on a $P_{DL}LA$ scaffold, determine the impact of polymer surface modification on culture morphology and function and compare this approach with existing hepatocyte culture strategies. Previous work had demonstrated that hepatocyte-HSC co-culture produced viable cultures with differentiated hepatic ultrastructure and function [32-34]. The aim of this study was to determine if hepatocyte-HSC co-culture on a microporous $P_{DL}LA$ scaffold could induce additional functional benefits.

Preliminary studies demonstrated that seeding of hepatocytes and HSC unto a $P_{DL}LA$ scaffold was feasible, that in the short term the hepatocytes remained viable and that culture morphology varied in response to variations in ligand binding capacity of the scaffold. A series of large scale long term comparative studies were therefore undertaken. Overall the results of these were disappointing. It was not possible to sustain a viable hepatocyte population beyond 3 days post-

seeding. When hepatocytes were seeded onto the unmodified scaffolds in mono-culture there was limited interaction with the scaffold and functionality was poor. Modification of the scaffold surface properties by NaOH treatment or allylamine plasma deposition increased surface binding of hepatocytes but did not enhance their synthetic or metabolic functionality.

Seeding HSC unto the scaffolds in mono-culture demonstrated that the ligand binding capacity of the scaffold could influence the phenotype of the HSC. When HSC were co-cultured with hepatocytes on $P_{DL}LA$ they acted as an interface between the scaffold surface and the hepatocytes but no benefit in terms of viability and function could be demonstrated. When hepatocyte-HSC co-culture on $P_{DL}LA$ was compared with hepatocyte monoculture on collagen or an alginate scaffold the functionality of the hepatocyte-HSC co-culture on $P_{DL}LA$ was significantly lower.

The hypothesis "co-culture of hepatocytes with HSC on a three-dimensional $P_{DL}LA$ scaffold would enhance hepatocyte viability and function compared with traditional hepatocyte culture systems" was therefore not proven. There are elements of the strategy that warrant further evaluation. Specifically how the HSC acts as an interface between parenchymal cells and the scaffold and how it directs liver tissue assembly. By studying the interaction between the HSC-ECM and HSC-hepatocyte in this deconstructed micro-environment a better understanding of the properties of the activated HSC could be obtained and used to modulate HSC activity in specific disease states or harnessed in future *in vitro* or *in vivo* liver tissue engineering enterprises.

5.2 *In Vivo* Study

The objectives of the *in vivo* study were to develop an intrahepatic growth factor and ECM delivery device and evaluate its impact on liver growth in normal liver and liver following PH. Infusion of growth factors into the liver had previously been shown to stimulate growth and enhance regeneration [95-99]. The aim of this study was to determine if intrahepatic growth factor delivery from a biodegradable scaffold had real therapeutic potential.

A poly (α hydroxy acid) polymer scaffold was used as the delivery device. A series of cadaveric and terminal anaesthetic studies allowed optimisation of the scaffold design and implantation technique before the first survival pilot was undertaken. This pilot study confirmed that intrahepatic scaffold implantation was feasible and provided preliminary characterisation of the liver scaffold interaction highlighting modifications to the study design that would be required for a larger scale comparative study.

When the growth factor delivery device was implanted into normal liver tissue a number of observations were made. As expected the biomaterials (PLGA, PEG & L-ECM) biodegraded with time. The presence of growth factors and L-ECM enhanced the rate of liver cell migration and ECM deposition into the pores of the scaffold and increased the duration and extent of the inflammatory response in the parenchyma surrounding each implant. When the growth factor delivery device was implanted into liver tissue at the time of PH similar patterns of cell migration, ECM deposition and peri-implant inflammation were observed. In addition the redistribution of liver mass between lobes was influenced by the presence of an implanted growth factor delivery device.

The hypothesis "intrahepatic growth factor & L-ECM delivery from a porous PLGA + 5% PEG scaffold could stimulates a proliferative response in the peri-implant parenchyma of normal liver and liver tissue following PH" was proven, although the proliferative response was limited only to the immediate peri-implant parenchyma of normal and partially hepatectomised liver and was not associated with an increase or faster restoration of liver mass.

These results suggest that there is a potential therapeutic application for intrahepatic growth factor delivery. If it were possible to stimulate liver growth prior to or to enhance regeneration after resection it may become possible to improve the outcome of those patients with pre-existing parenchymal liver disease or those requiring radical resection for cure. However before this approach is developed, more detailed characterisation of the release kinetics and dose responses for individual growth factors must be undertaken, and the work must be trialled in appropriate disease models.

5.3 The Future of Liver Tissue Engineering for Liver Surgery

The rapid evolution that has occurred in liver surgery over the last 30 years has presented a new set of challenges for the surgeon and the scientist. *In vitro* and *in vivo* tissue engineering may provide solutions on many of these new frontiers. Stem cell technology should eventually provide a renewable source of regeneration competent liver cells for *in vitro* and *in vivo* strategies. Developments in scaffold fabrication including natural-synthetic hybrid constructs may enable more effective signal delivery and rather than targeting growth factor signalling cascades, it may become possible to focus on specific intracellular signalling pathways. The liver

has a remarkable regenerative capacity perhaps future liver tissue engineering strategies will focus on harnessing this capacity rather than trying to generate new liver tissue *de novo*.

Bibliography

1. Fortner J, Blumgart L. A historic perspective of liver surgery at the end of the millenium. J Am Coll Surg 2001;193:210-22.

2. McCarter M, Fong Y. Metastatic liver tumours. Semin Surg Oncol 2000;19(2):177-88.

3. Burroughs A, Hochhauser D, Meyer T. Systemic treatment and liver transplantation for hepatocelluar carcinoma: two ends of the therapeutic spectrum. Lancet Oncol 2004;5:409-18.

4. Bramhall S, Minford E, Gunson B, Buckalls J. Liver transplantation in the UK. World J Gastroenterology 2007;7(5):602-11.

5. Parkin D, Bray F, Ferlay J, Pisani P. Estimating the world cancer burden: GLOBOCAN. Int J Cancer 2001;94:153-6.

6. West J, Woods H, Logan R, Quinn M, Aithal G. Trends in the incidence of primary liver and biliary tract cancers in England and Waales 1971-2001. B J Cancer 2006;94:1751-8.

7. Ryder S. Guidelines for the diagnosis and treatment of hepatocellular carcinoma (HCC) in adults. Gut 2003;52((S III)):iii1-iii8.

8. Molmenti E, Klintmalm G. Liver transplantation in association with hepatocellular carcinoma: an update of the International Tumor Registry. Liver Transpl 2002;8:736-48.

9. Kavolius J, Fong Y, Blumgart L. Surgical Resection of metastatic liver tumours. Surgical Onc Clinics of North Am 1996;5:337-52.

10. Wagner J, Adson M, Van Heerden J. The natural history of hepatic metastases from colorectal cancer. A comparison with resective treatment. Ann Surg 1984;199:502-8.

11. Fong Y, Fortner J, Sun R. Clinical score for predicting recurrence after hepatic resection for metastatic colorectal cancer: analysis of 1001 consecutive cases. Ann Surg 1999;230:309-21.

12. ONS. Deaths by age, sex and underlying cause, 2004 registrations: Office for National Statistics; 2004.

13. Schindl M, Redhead D, Fearon K, Garden O, Wigmore S. The value of residual liver volume as a predictor of hepatic dysfunction and infection after major liver resection. Gut 2005;54:289-96.

14. Belghiti J, Hiramatsu K, Benoist S, Massault P, Sauvanet A, Farges O. Seven hundred forty-seven hepatectomies in the 1990s: an update to evaluate the actual risk of liver resection. Am Coll Surg 2000;191(1):38-46.

15. Bosetti C, Levi F, Lucchini F, Zatonski W, Negri E, La Vecchia C. Worldwide mortality from cirrhosis: an update to 2002. J Hepatol 2007;46(5):827-39.

16. Jalan R, Sen S, Williams R. Prospects for extracorporeal liver support. Gut 2004;53:890-8.

17. Bismuth H, Samuel D, Castaing D, Williams R, Pereira S. Liver transplantation in Europe for acute liver failure. Semin Liver Dis 1996;16:415-25.

18. UK.Transplant. Transplant Activity Report; 2007.

19. Nerem R. Tissue Engineering: the hope, the hype and the future. Tissue Engineering 2006;12:1143-50.

20. Heath C. Cells for Tissue engineering. Trends in Biotechnology 2000;18:17-9.

21. Pearson R, Bhandari R, Quirk R, Shakesheff K. Recent advances in tissue engineering: an invited review. J of Long Term Effects of Medical Implants 2002;12(1):1-33.

22. Williams H. The value of continuous electrical muscle stimulation using a completely implantable system in the preservation of muscle function following motor nerve injury and repair; an experimental study. Microosurgery 1996;17:589-96.

23. Black J. Biological Performance of Materials: Fundamentals of Biocompatibility. New York: Marcel Dekker; 1992.

24. Whitaker M, Quirk R, Howdle S, Shakesheff K. Growth factor release from tissue engineering scaffolds. J Pharm Pharmacol 2001;53:1427-37.

25. Woods H, Silva M, Nouvel C, Shakesheff K. Materials processing in cupercritical carbon dioxide: surfactants, polymers and biomaterials. J Mater Chem 2004;14(11):1663-78.

26. Bosman F, Stamenkovic I. Functional structure and compsition of the extracellular matrix. J Pathol 2003;200:423-8.

27. Stamenkovic I. Extracellular matrix remodelling: the role of the matrix metalloproteinases. J Pathol 2003;200:448-64.

28. Li F, Li W, Johnson S, Ingram D, Yoder M, Badylak S. Low -molecular weight peptides derived from extracellular matrix as cheoattractants for primary endothelial cells. Endothelium 2004;11:199-206.

29. Michalopoulos G, Pitot H. Primary culture of parenchymal liver cells on collagen membrances. Exp Cell Res 1975;94:70-5.

30. Sellaro T, Ravindra A, Stolz D, Badylak S. Maintenance of hepatic sinusoidal endothelial cell phenotype in vitro using organ-specific extracellular matrix scaffolds. Tissue Engineering 2007;13(9):2310-10.

31. Badylak S. The extracellular matrix as a biologic scaffold material. Biomaterials 2007;28(25):3587-93.

32. Riccalton-Banks L, Liew C, Bhandari R, Shakesheff K. Long-term culture of functional liver tissue: Three-dimensional co-culture of primary hepatocytes and stellate cells. Tissue Engineering 2000 9 (3):401-10.

33. Thomas R, Bennett A, Thomson B, Shakesheff K. Hepatic Stellate cells on poly(DL-lactic acid) surfaces control the formation of 3D hepatocyte co-culture aggregates in vitro. European Cells and Materials 2006;11:16-26.

34. Thomas R, Bhandari R, Barratt D, et al. The effect of three-dimensional co-culture of hepatocytes and hepatic stellate cells on key hepatocyte functions in vitro. Cells, Tissues and Organs 2005;181(2):67-79.

35. Csete M. Oxygen and stem cell fate. Annals of the New York Academy of Sciences 2005;1049:1-8.

36. Csete M. Oxygen in the cultivation of stem cells. Ann NY Acad Sci 2005;1049:1-8.

37. Allen J, Khetani S, Bhatia S. In vitro zonation and toxicity in a hepatocyte bioreactor. Toxicol Sci 2005;84(1):110-9.

38. Brown R, Wiseman M, Chuo C-B, Cheema U, Nazhat S. Ultrarapid engineering of biomimetic materials and tissues: fabrication of nano- and microstructures by plastic compression. Advanced Functional Materials 2005;15(11):1762-70.

39. Vozzi G, Flaim C, Ahluwalia A, Bhatia S. Fabrication of PLGA scaffolds using soft lithography and microsyringe deposition. Biomaterials 2003;24(14):2533-40.

40. Brown R, Prajapati R, McCrouther D, Yannas I, Eastwood M. Tensional homeostasis in dermal fibroblasts: mechanical responses to mehanical loading in three-dimensional substrates. J Cell Physiol 1998;175:323-32.

41. Ming G, Henley J, Tessier-Lavigne M, Song H, Poo M. Electrcal activity modulates growth cone guidance by diffusible factors. Neuron 2001;29:441-52.

42. Borgens R, Bohnert D. Responses to pinal axons to an applied DC voltage gradient. Exp Neurol 1997;145:376-89.

43. Brown B, Lindberg K, Reing J, Stolz D, Badylak S. The basement membrane component of biologic scaffolds derived from extracellular matrix. Tissue Engineering 2006;12(3):519-26.

44. Lumelsky N. Commentary: engineering of tissue healing and regeneration. Tissue Engineering 2007;13(7):1393-8.

45. Lewis A. Flow cytometric analysis of hepatocyte proliferation in vitro. PhD Thesis 2003.

46. Jones A, Schmuker D. Electron Microscopy of the liver. 2 ed. Oxford: OUP; 1999.

47. Sato M, Suzuki S, Senoo H. Hepatic Stellate Cells: Unique Characteristics in Cell Biology and Phenotype. Cell Structure and Function 2003;28:105-12.

48. Guillouzo A. Liver cell models in in vitro toxicology. Environmental Health Perspectives 1998;106(Supp 2):511-32.

49. Wisse E, Braet F, Luo D, et al. Sinusoidal Liver Cells. Oxford: OUP; 1999.

50. Lee D, Yoon H, Lee J, et al. Enhanced liver-specific functions of endothelial cell-covered hepatocyte hetero-spheroids. Biochemical Eng J 2004;20(2-3):181-7.

51. Morin O, Normand C. Long term maintenance of hepatocyte functional activity in co-culture: requirements for sinusoidal endothelial cells and dexamethasone. J Cell Physiol 1986;129:103-10.

52. Mabuchi A, Mullaney I, Sheard P, et al. Role of hepatic stellate cell/hepatocyte interaction and activation of hepatic stellate cells in the early phase of liver regeneration in the rat. J Hepatol 2004;40(6):910-6.

53. Higashi N, Kojima N, Miura M, Imai K, Sato M, Senoo H. Cell-cell junctions between mammalian (human and rat) hepatic stellate cells. Cell Tissue Res 2004;317(1):35-43.

54. Bedossa P, Paradis V. Liver extracellular matrix in health and disease. J Pathol 2003;200:504-15.

55. Michalopoulos G, DeFrances M. Liver Regeneration. Science 1997;276(4):60-6.

56. Michalopoulos G, DeFrances M. Liver Regeneration. Advances in Biochemical Engineering and Biotechnology 2005;93:101-34.

57. Higgins G, Anderson R. Experimental pathology of the liver. Archives of Pathology 1931;12:186-202.

58. Koniaris L, McKillop I, Schwartz S, Zimmers T. Liver Regeneration. Journal Am Coll Surgeons 2003;197(4):634-59.

59. Taub R. Liver Regeneration: from myth to mechanism. Nature Reviews Molecular cell biology 2004;5:836-47.

60. Rabes H, Wirsching R, Tuczek H, Iseler G. Analysis of cell cycle compartments of hepatocytes after partial hepatecomy. Cell Tissue Kinetics 1976;9(6):517-32.

61. Fabrikant J. The kinetics of cellular proliferation in regenerating liver. J Cell Biol 1968;36(3):551-65.

62. Grisham J. A morphologic study of deoxyribonucleic acid synthesis and cell proliferation in regenerating rat liver; autoradiography with thymidine-H3. Cancer Res 1962 22:842-9.

63. Fausto N. Liver Regeneration and Repair: Hepatocytes, progenitor cells, and stem cells. Hepatology 2004;39(6):1477-87.

64. Fausto N. Liver Regeneration. J Hepatology 2000;32(S1):19-31.

65. Lambotte L, Saliez A, Triest S, Barker A, Baranski A. Control of the rate and extent of proliferative response after partial hepatectomy. Am J Physiol 1997;46:G905-12.

66. Mann F. The portal circulation and restoration of the liver after partial removal. Surgery 1940;8:225-38.

67. Thomson R, Clarke A. Role of portal blood supply in liver regeneration. Nature 1965;208:392-3.

68. Markiewski M, DeAngelis R, Lambris J. Liver inflammation and regeneration: two distinct biological phenomena or parallel pathophysiologic processes? Mol Immunol 2006;43(1-2):45-56.

69. Taylor B, Alarcon L, Billiar T. Inducible nitric oxide synthase in the liver: regulation and function. Biochem (Mosc) 1998;63:766-81.

70. Li J, Billiar T. Nitric Oxide. IV. Determinants of nitric oxide protection and toxicity in liver. Am J Physiol GI 1999;276(5):1069-73.

71. Obolenskaya M, Vanin A, Mordvintcev A, Mulsch A, Decker K. EPR evidence of nitric oxide production by the regeneration rat liver. Biochem Biophys Res Comm 1994;202(1):571-6.

72. Hortelano S, Dewez B, Genaro A, Diaz-Guerra M, Bosca L. Nitric oxide is released in regenerating liver after partial hepatectomy. Hepatology 1995;21:776-86.

73. Macedo M, Lautt W. Shear-induced modulation of vasoconstriction in the hepatic artery and portal vein by nitric oxide. Am J Physiol 1998;274:G253-60.

74. Michalopoulos G. Liver Regeneration. J Cell Physiol 2007;9999:1-16.

75. Schoen, Smith J, Lautt W. The role of prostoglandins in triggering the iver regeneration cascade. Nitric Oxide 2005;13:111-7.

76. Cornell R. Gut-derived endotoxin elicits hepatotrophic factor secretion of liver regeneration. Am J Physiol 1985;249:R551-62.

77. Cornell R. Restriction of gut-derived endotoxin impairs DNA synthesis for liver regeneration. Am J Physiol 1985;249:R563-9.

78. Mastellos D, Papadimitriou J, Franchini S, Tsonis P, Lambris J. A novel role of complement: mice deficient in the fifth component of complement (C5) exhibit impaired liver regeneration. J Immunol 2001;166:2479-86.

79. Strey C, Markiewski M, Mastellos D, et al. The proinflammatory mediators C3a andC5a are essential for liver regeneration. J Exp Med 2003;198 913-23.

80. Selzner N, Selzner M, Odermatt B, Tian Y, Rooijen N, Clavien A. ICAM-1 triggers liver regeneration through leukocyte recruitment and Kupffer cell–dependent release of TNF-α/IL-6 in mice. 2003;3:692-700.

81. Malik R, Selden C, Hodgson H. The role of non-parenchymal cells in liver growth Sem Cell Dev Biol 2002;Volume 13(6): 425-31

82. Taub R, Greenbaum L, Peng Y. Transcriptional regulatory signals define cytokine dependent and independent pathways in liver regeneration. Sem Liver Dis 1999;19:117--27.

83. Yamada Y, Kirillova I, Peschon J, Fausto N. Initiation of liver growth by tumor necrosis factor: deficient liver regeneration in mice lacking type I tumor necrosis factor receptor. Proc Natl Acad Sci 1997;94:1441-6.

84. Webber E, Bruix J, Pierce R, Fausto N. Tumor necrosis factor primes hepatocytes for DNA replication in the rat Hepatology 1998;28(5):1226-34.

85. Akerman P, Cote P, Yang S, et al. Antibodies to tumor necrosis factor-alpha inhibit liver regeneration after partial hepatectomy Am J Physiol GI 1992;263(4):579-85.

86. Heinreich P, Behrmann I, Haan S, Hermanns H, Schaper F. Principles of interleukin 6 type cytokine signalling and its regulation Biochem J 2003;374:1-20.

87. Zimmers T, McKillop I, Pierce R, Koniaris L. Massive liver growth in mice induced by systemic interleukin 6 administration. Hepatology 2003;38:326-34.

88. Zimmers T, Pierce R, McKillop I, Koniaris L. Resolving the role of IL-6 in liver regeneration. Hepatology 2003;38:1590-1.

89. Funakoshi H, Nakamura T. Hepatocyte growth factor: from diagnosis to clinical applications. Clinica Chimica Acta 2003;327 1 -23.

90. Ponzetto C, Bardelli A, Zhen Z. A multifunctional docking site mediates signalling and transformation by the hepatocyte growth factor / scatter factor receptor family. Cell Structure and Function 1994;77:261-71.

91. Pediaditakis P, Lopez-Talavera J, Petersen B, Monga S, Michalopoulos G. The processing and utilization of hepatocyte growth factor/scatter factor following partial hepatectomy in the rat Hepatology 2001;34(4 (Pt 1)):688-93.

92. Masumoto A, Yamamoto N. Sequestration of a hepatocyte growth factor in extracellular matrix in normal adult rat liver Biochem Biophys Res Commun 1991;174(1):90-5.

93. Schuppan D, Schmid M, Somasundarum R, et al. Collagens in the liver extracellular matrix bind hepatocyte growth factor Gastroenterology 1998;114(1):139-52.

94. Burr A, Toole K, Chapman C, Hines J, Burt A. Anti-hepatocyte growth factor antibody inhibits hepatocyte proliferation during liver regeneration. J Pathol 1998;185:298-302.

95. Patijn G, Lieber A, Schowalter D, Schwall R, M K. Hepatocte growth factor induces hepatocyte proliferation in vivo and allows for efficient retro-viral mediated gene transfer in mice. Hepatology 1998;28:707-16.

96. Liu M, Mars W, Zarneger R, Michalopoulos G. Collagenase pretreatment and the mitogenic effects of hepatocyte growth factor and tranforming growth factor in adult liver. Hepatology 1994;19:1521-7.

97. Webber E, Godowski P, Fausto N. In vivo response of hepatocytes to growth factors requires an initial priming stimulus. Hepatology 1994;19(2):489-97.

98. Fujiwara K, Nagoshi S, Ohno A, et al. Stimulation of liver growth by exogenous human hepatocyte growth factor in norma and partially hepatectomised rats. Hepatology 1993;18:1443-9.

99. Ishii T, Sato M, Sudo K, et al. Hepatocyte growth factor stimulates liver regeneration and elevates blood protein levels in normal and partially hepatectomized rats. Journal of Biochemistry 1995;117:1105-12.

100. Matsuda Y, Matsumoto K, Ichida T, Nakamura T. Hepatocyte Growth factor suppresses the onset of liver cirrhosis and abrogates lethal hepatic dysfunction in rats. J Biochem (Japan) 1995;118:643-9.

101. Matsuda Y, Matsumoto K, Yamada A. Preventative and therapeutic effects in rats of hepatocyte growth factor infusion on liver fibrosis / cirrhosis. Hepatology 1997;26:81-9.

102. Wells A. EGF receptor. International Journal of Biochemistry and cell Biology 1999;31:637-43.

103. Boonstra J, Rijken P, Humbel B, Cremers F, Verkleij A, Bergen P. The epidermal growth factor. Cell Biol Int 1995;19(5):413-29.

104. Lee D, Fenton S, Berkowitz E, Hissong M. Transforming growth factor a: expression, regulatiion and biological ativities. Pharmacological Reviews 1995;47(1):51-85.

105. Mead J, Fausto N. Transforming growth factor alpha may be a physiological regulator of liver regeneration by means of an autocrine mechanism. Proc Natl Acad Sci 1989;86(5):1558-15562.

106. Slavin J. Fibroblast growth factors: at the heart of angiogenesis. Cell Biol Int 1995;19(5):431-44.

107. Biolly B, Vercoutter-Edouart A, Hondermarck H, Nurcombe V, Bourhis X. FGF signals for cell proliferation and migration through differnt patways. Cytokine & Growth Factor Reviews 2000;11:295-302.

108. Eswarakumar V, Schlessinger L. Cellular signalling by fbroblast growth factor receptors. Cytokine & Growth Factor Reviews 2005;16:139-49.

109. Kan M, Huang JS, Mansson PE, Yasumitsu H, Carr B, McKeehan W. Heparin-binding growth factor type 1 (acidic fibroblast growth factor): a potential biphasic autocrine and paracrine regulator of hepatocyte regeneration Proc Natl Acad Sci 1989;86(19):7432-6.

110. Houck K, Zarneger R, Muga S, Michalopoulos G. Acidic fibroblast growth factor (HBGF-1) stimulates DNA synthesis in primary rat hepatocyte cultures. J Cell Physiol 1990;143(1):129-32.

111. Lee H, Cusick R, Browne F, et al. Local delivery of basic fbroblast growth factor increases bot angiogenesis and engraftment of hepatocytes in tissue engineered polymer devices. Transplantation 2002;73:1589-93.

112. Bucher N, Swaffield M. Regulation of hepatic regeneration in rats by synergistic action of insulin and glucagon. Proc Natl Acad Sci 1975;72:1157-60.

113. Hwang T, Chen M, Chen T. Augmentation of liver regeneration with glucagon after partial hepatectomy in rats. J Formos Med Assoc 1993;92:725-8.

114. Starzl T, Francavilla A, Porter K, Benchou J. The effect of splanchnic viscera removal upon canine liver regeneration. Surg Gyn Ob 1978;147:193-207.

115. Taniguchi K, Roberts L, Aderca I, et al. Mutational spectrum of beta-catenin, AXIN1 and AXIN2 in hepatocellular carcinoma and hepatoblastomas. Oncogene 2002;21:4863-71.

116. Colletti L, Green M, Burdick M, Kunkel S, Strieter R. Proliferative effects of CXC chemokines in rat hepatocytes in vitro and in vivo. Shock 1998;10(4):248-57.

117. Francavilla A, Carr B, Azzrone A, et al. Hepatocyte proliferation and gene expression induced by triiodothyronine in vivo and in vitro. Hepatology 1994;20(5):1237-41.

118. Francavilla A, Gavaler J, Makowska L, et al. Estradiol and testosterone levels in patients undergoing partial hepatectomy. A possible signal for hepatic regeneration?. Dig Dis Sci 1989;34(6):818-22.

119. Bissell D. Hepatic fibrosis as wound repair: a progress report. J Gastroenterol 1998;33(2):295-302.

120. Kresse H, Schonherr E. Proteoglycans of the extracellular matrix and growth control. J Cell Physiol 2001;189(3):266-74.

121. Mohammed F, Khokha R. Thinking outside the cell: proteases regulate hepatocyte division. Trends in Cell Biol 2005;15(10):555-63.

122. Fausto N, Mead J, Braun L, et al. Proto-oncogene expression and growth factors during liver regeneration. 1986 1986;39:69-86.

123. Sanderson N, Factor V, Nagy P, et al. Hepatic expression of mature transforming growth factor beta 1 in transgenic mice results in multiple tissue lesions. Proc Natl Acad Sci 1995;92(7):2572-6.

124. Ueberham E, Low R, Ueberham U, Schonig K, Bujard H, Gebhardt R. Conditional tetracycline-regulated expression of TGF-beta 1 in liver of transgenic mice leads to reversible intermediary fibrosis. Hepatology 2003;37(5):1067-78.

125. Russell W, Coffey RJ, Ouellette A, Moses H. Type beta transforming growth factor reversibly inhibits the early proliferative response to partial hepatectomy in the rat. Proc Natl Acad Sci 1988;85(14):5126-30.

126. Ichikawa T, Zhang Y, Kogure K, et al. Transforming growth factor beta and activin tonically inhibit DNA synthesis in the rat liver. Hepatology 2001;34(5):918-25.

127. Maher J. Primary hepatocyte culture: is it home away from home? Hepatology 1988;8:1162-6.

128. Bissell D, Arenson D, Maher J, Roll F. Support of cultured hepatocytes on laminin-rich gel. J Clin Inv 1987;79:801-12.

129. Bissell D, Hammaker L, Meyer U. Parenchymal cells from adult rat liver in nonproliferation monolayer culture. J Cell Biol 1973;59:722-34.

130. Dunn J, Yarmush M. Long-term in vitro function of adult hepatocytes in a collagen sandwich configuration. Biotech Progress 1991;7:237-45.

131. Lazar A, Peshwa M, Wu F, Chi C-M, Cerra F, Hu W-S. Formation of porcine hepatocyte spheroids for use in bioartificial liver. Cell Transplantation 1995;4:259-68.

132. Wu F, Friend J, Hsiao C, et al. Efficient assembly of rat hepatocyte spheroids for tissue engineering applications. Biotech Bioeng 1996;50:404-15.

133. Koide N, Sakaguchi K, Koide Y, et al. Formation of multicellular spheroids composed of adult rat hepatocytes in dishes with positively charged surfaces and under other nonadherent environments Experimental Cell Research 1990;186:227-35.

134. Bhandari R, Riccalton L, Lewis A, et al. Liver tissue engineering: A role for co-culture systems in modifying hepatocyte function and viability. Tissue Engineering 2001;7(3):345-57.

135. Harimoto M, Yamato M, Hirose M, et al. Novel approach for achieving double-layered cell sheets co-culture: overlaying endothelial cell sheets onto monolayer hepatocytes utilizing temperature-responsive culture dishes. J Biomed Mat Res 2002;62(3):464-70.

136. Powers J, Rodriguez R, Griffith L. Cell-Subsrtatum Adhesion Strength as a Determinant of Hepatocyte Aggregate Morphology. Biotechnology Bioengineering 1997;53(4):415-26.

137. Griffith L, Lopina S. Microdistribution of substratum-bound ligands affects cell function: hepatocyte spreading on PEO-tethered galactose. Biomaterials 1998;19:979-86.

138. Mikos A, Sarakinos G, Lyman M, Ingber D, Vacanti J, LANGER R. Pre-vascularisation of porous biodegradable polymers. Biotechnology Bioengineering 1993;42:716-23.

139. Temenoff J, Mikos A. Review: tissue engineering for regeneration of articular cartilage. Biomaterials 2000;21(5):431-40.

140. Levenberg S, Mulligan R, Langer R. Engineering vascularised skeletal muscle. Nature Biotechnol 2005;23:879-84.

141. Kim B, Mooney D. Development of biocompatible synthetic ECMs for tissue engineering. Trends in Biotechnology 1998;16 224-30.

142. Cima L, Ingber D, Vacanti J, Langer R. Hepatocyte culture on biodegradable polymeric substrates. Biotechnology Bioengineering 1991;38:145-58.

143. Davis M, Vacanti J. Toward development of an implantable tissue engineered liver Biomaterials 1996;17(3):365-72.

144. Lin P, Chan W, Badylak S, Bhatia S. Assessing porcine liver-derived biomatrix for hepatic tissue engineering. Tissue Engineering 2004;10(7-8):1046-53.

145. Petronis S, Eckert K, Gold J, Wintermantel E. Microstructuring ceramic scaffolds for hepatocyte cell culture. J Materials Science-Materials In Medicine 2001;12(6):523-8.

146. Babensee J, Anderson J, McIntire L, Mikos A. Host response to tissue engineering devices. Adv Drug Delivery Rev 1998;33:111-39.

147. Anderson J, Langone J. Issues and perspectives on the biocompatibility and immunotoxicity evaluation of implanted controlled release systems. J Controlled Release 1999;57:107-13.

148. Kaufmann P, Heimrath S, Kim B, Mooney D. Highly porous polymer matrices as a 3D culture system for hepatocytes. Cell Transplantation 1997;6(463).

149. Nam Y, Yoon J, Lee J, Park T. Adhesion behaviours of hepatocytes cultured onto biodegradable polymer surface modified by alkali hydrolysis process. J Biomaterial Sci-Polymer Ed 1999;10(11):1145-58.

150. Dehili C, Lee P, Shakesheff K, Alexander M. Comparision of primary rat hepatocyte attachment to collagen and plasma-polymerised allylamine on glass. Plasma Processes and Polymers 2006;3:474-84

151. Gutsche A, Hungnan L, Zurlo J, Yager J, Leong K. Engineering of a sugar-derivatized porous network for hepatocyte culture. Biomaterials 1996;17(3):387-93.

152. Risbud M, Karamuk E, Moser R, Mayer J. Hydrogel-coated textile scaffolds as three-dimensional growth support for human umbilical vein endothelial cells (HUVECs): Possibilities as coculture system in liver tissue engineering. Cell Transplantation 2002;11(4):369-77.

153. Risbud M, Karamuk E, Schlosser V, Mayer J. Hydrogel-coated textile scaffolds as candidate in liver tissue engineering: II. Evaluation of spheroid formation and viability of hepatocytes. J Biomaterial Sci-Polymer Ed 2003;14(7): 719- 31

154. Mayer J, Karamuk E, Akaike T, Wintermantel E. Matrices for tissue engineering-scaffold structure for a bioartificial liver support system. J Controlled Release 2000;64(1-3):81-90.

155. Takei R, Park K, Ise H, et al. Coated antireceptor antibody as an extracellular matrix for liver tissue engineering. Tissue Engineering 1997;3(3):281-8.

156. Hollister S. Porous scaffold design for tissue engineering. Nature Materials 2005;4:518-24.

157. Ranucci C, Moghe P. Polymer substrate topography actively regulates the multicellular organization and liver-specific functions of cultured hepatocytes. 1999 1999;5(5):407-19.

158. Ranucci C, Kumar S, Batra S, Moghe P. Control of hepatocyte function on collagen foams: sizing matrix pores toward selective induction of 2-D and 3-D cellular morphogenesis Biomaterials 2000;21(8):783-93.

159. Glicklis R, Merchuk J, Cohen S. Modelling Mass Transfer in hepatocyte spheroids via cell viability, spheroid size and hepatocellular functions. Biotechnology Bioengineering 2004;86(6):672-80.

160. Dvir-Ginzberg M, Gamlieli-Bonshtein I, Agbaria R, Cohen S. Liver tissue engineering within alginate scaffolds: Effects of cell-seeding density on hepatocyte viability, morphology, and function. Tissue Engineering 2003;9(4):757-66.

161. Yan Y, Wang X, Xiong Z, et al. Direct construction of a three-dimensional structure with cells and hydrogel. J Bioactive Compatible Polymers 2005;20:259-69.

162. Ostrovidov S, Jiang J, Sakai Y, Fujii T. Membrane-based PDMS microbioreactor for perfused 3D primary rat hepatocyte cultures. Biomedical MicrodevicesS 2004;6(4):279-87.

163. Gerlach J. Development of a Hybrid liver support system: a review. Int J Artficial Organs 1996;19:610-6.

164. Demetriou A, Brown R, Busuttil R, Fair J, McGuire B, Rosenthal P. Prospective, randomised, multicenter, controlled trial of bioartificial liver in treating acute liver failure. Ann Surg 2004;239:660-70.

165. Fox I, Roy-Chowdhury J. Hepatocyte Transplantation. J Hepatology 2004;40:878-86.

166. Demetriou A, Reisner A, Sanchez J, Levenson S, Moscioni A, Roy-Chowdhury J. Repalcement of liver function in rats by transplantation of micro-carrier attached hepatocytes. Science 1986;233:1190-2.

167. Demetriou A, Reisner A, Sanchez J, Levenson S, Moscioni A, Roy-Chowdhury J. Transplantation of micro-carrier attached hepatocytes into 90% partially hepatectomized rats. Hepatology 1988;8:1006-9.

168. Hansen L, Vacanti J. Hepatocyte transplantation usin artificial biodegradable polymers. Austin, Texas: Landes; 1993.

169. Kedem A, Perets A, Gamlielli-Bonshtein I, Dvir-Ginzberg M, Mizrahi S, Cohen S. VEGF-releasing scaffolds enhance vascularisation and engraftment of hepatocytes transplanted on liverr lobes. Tissue Engineering 2005;11(5-6):715-22.

170. Jaffe V, Darby H, Bishop A, Hodgson H. The growth of liver cells in the pancreas after intresplenic implantation: the effects of portal perfusion. Int J Exp Path 1991;72:289-99.

171. Mooney D, Sano K, Kaufmann P, et al. Long-term engraftment of hepatocytes transplanted on biodegradable polymer sponges. J Bio Mat Res 1996;37:413.

172. Kneser U, Kaufmann P, Fiegel H, et al. Long-term differentiated function of heterotypically transplanted hepatocytes on 3D polymer matrices. J Bio Mat Res 1999;47:494.

173. Oe S, Fukunaka Y, Hirose T, Yamaoka Y, Tabata Y. A trial on regeneration therapy of rat liver cirrhosis by controlled release of hepatocyte growth factor. Journal of Controlled Release 2003;88(2):193-200.

174. Takimoto Y, Dixit V, Arthur M, Gitnick G. De novo liver tissue formation in rats using a novel collagen-polypropylene scaffold. Cell Transplantation 2003;12(4):413-21.

175. Hammond J, Beckingham I, Shakesheff K. Scaffolds for liver tissue engineering. Expert Review of Medical Devices 2006;3(1):21-7.

176. Barry J, Silva M, Shakesheff K, Howdle S, Alexander M. Using plasma deposits to promote cell population of the porous interior of three-dimensional poly (DL-lactic acid) tissue engineering scaffolds. Advanced Functional Materials 2005;15:1134-40.

177. Seglen P. Preparation of of isolated rat liver cells. Methods in Cell Biology 1976;19:29-83.

178. Riccalton-Banks L, Bhandari R, Fry J, Shakesheff K. A simple method for the simultaneous isolation of stellate cells and hepatocytes from rat liver tissue. . Molecular and Cellular Biochemistry 2003;248 97-102

179. Barry J, Silva M, Popov V, Shakesheff K, Howdle S. Supercritical carbon dioxide:putting the fizz into biomaterials. Phil Trans R Soc 2006;364:249-61.

180. Waxman D, Lapenson D, Aoyama T, Gelboin H, Gonzalez F, Korzekwa K. Steroid hormone hydroxylase specificities of eleven cDNA-expressed human cytochrome P450s. Arch Biochem Biophys 1991;290:160-6.

181. Sonderfan A, Arlotto M, Parkinson A. Identification of the cytochrome P-450 isozymes responsible for testosterone oxidation in rat lung, kidney, and testis: evidence that cytochrome P-450a (P450IIA1) is the physiologically important testosterone 7 alpha-hydroxylase in rat testis. *Endocrinology* 1989;125::857-66.

182. Leclerc E, Sakai Y, Fujii T. Perfusion culture of fetal human hepatocytes in microfluidic environments. Biochemical Engineering J 2004;20(2-3):143-8.

183. Mars W, Kim T, Stolz D, Liu M, Michalopoulos G. Presence of urokinase in serum-free primary rat hepatocyte cultures and its role in activating hepatocyte growth factor. cancer Res 1996;56:2837-43.

184. Mars W, Liu M, Kitson R, Goldfarb R, Gabauer M, Michalopoulos G. Immediate early detection of urokinase receptor after partial hepatectomy and its implications for initiation of liver regeneration. Hepatology 1995;21:1695-701.

185. Lindroos P, Zarneger R, Michalopoulos G. Hepatocyte growth factor (hepatopoietin A) rapidly increases in plasma before DNA synthesis and liver regeneration stimulated by partial hepatectomy and carbon tetrachloride administration. Hepatology 1991;13:743-9.

186. Yu C, Wang F, Jin C, et al. Role of fibroblast growth factor type 1 and 2 in carbon tetrachloride-induced hepatic injury and fibrogenesis. Am J Pathol 2003;163:1653-62.

187. Borowaik M, Garratt A, Wustefeld T, Strehle M, Trautwein C, Birchmeier C. Met provides essential signals for liver regeneration. Proc Natl Acad Sci 2004;101:10608-13.

188. Huh C, Factor V, Sanchez A, Ucida K, Conner E, Thorgeirsson S. Hepatocyte growth factor / c-met sinalling pathway is required for efficient liver regeneration and repair. Proc Natl Acad Sci 2004;101:4477-82.

189. Gkretsi V, Mars W, Bowen W, et al. Loss of integrin linked kinase from mouse hepatocytes in vitro and in vivo results in apoptosis and hepatitis. Hepatology 2007;45:1025-34.

190. Tabata I. The importance of drug delivery systems in tissue engineering. Pharm Sci Technol Today 2000;3(3):80-9.

191. Howdle S, Watson M, Whitaker M, et al. Supercritical fluid mixing: preparation of thermally sensitive polymer composites containing bioactive materials. Chem Commun 2001:109-10.

192. Ginty P, Barry J, White L, Howdle S, Shakesheff K. Controlling protein release from scaffolds using polymer blends and composites. Eur J Pharm Biopharm 2008;68(1):82-9.

193. Yang X, Whitaker M, Clarke N, Shakesheff K, Oreffo R. In vivo human bone and cartilage formation using porous polymer scaffolds encapsulated with bone morphogenetic protein-2 J Bone Min Res 2003;18 (7):1366-.

194. Muskhelishvilli L, Latendresse J, Kodell R, Henderson E. Evaluation of cell proliferation in rat tissues with BrdU, PCNA, Ki-67 immunohistochemistry and in situ hybridisation for histone mRNA. The Journal of histochemistry and cytochemistry 2003;51(12):1681-8.

195. Gerlach R, Sakkab D, Scholzen T, Dabler R, Alison M, Gerdes J. Ki-67 Expression During Rat Liver Regeneration After Partial Hepatectomy. Hepatology 1997;26:573-8.

196. Yang X, Tare R, Partridge KA, et al. Induction of human osteoprogenitor chemotaxis, proliferation, differentiation, and bone formation by osteoblast stimulating factor-1/pleiotrophin: osteoconductive biomimetic scaffolds for tissue engineering. J Bone Min Res 20031847-57

197. Brown D, Gatter K. Ki67 protein: the immaculate deception? Histopathology 2002;40:2-11.

198. Roos F, Ryan A, Chamow S, Bennett G, Schwall R. Induction of liver growth in normal mice by infusion of hepatocyte growth factor / scatter factor. Am J Physiol GI 1995;31:G380-6.

199. Hamilton L. Ph.D Thesis. 2008.

200. Roggin K, Kim J, Kurkchubasche A, Papa E, Vezeridis A, Tracy T. Macrophage phenotype during cholestatic injury and repair: the persistent inflammatory response. J Pediatr Surg 2001;36(1):220-8.

201. Cassiman D, Libbrecht L, Desmet V, Denef C, Roskams T. Hepatic stellate cell/myofibroblast subpopulations in fibrotic human and rat livers. J Hepatol 2002;36(2):200-9.

202. Paranjpe S, Bowen W, Bell A, Nejak-Bowen K, Luo J, Michalopoulos G. Cell cycle effects resulting from inhibition of hepatocyte growth factor and its receptor c-Met in regenerating rat livers by RNA interference. Hepatology 2007 45(6):1471-7.

203. Ozeki M, Ishii T, Hirano Y, Tabata Y. Controlled release of hepatocyte growth factor from gelatin hydrogels based on hydrogel degradation. Journal of Drug Targeting 2001;9:461-71.

204. Ozeki M, Tabata Y. Affinity evaluation of gelatin for hepatocye growth factor of different types to design the release carrier. J Biomater Sci Polymer Edn 2006;17(1-2):139-50.

205. Pape L, Henne T, Offner G, et al. Computer-assisted quantification of fibrosis in chronic allograft nephropaty by picosirius red-staining: a new tool for predicting long-term graft function. Transplantation 2003 76(6):955-8.

206. Alison M, Chaudry Z, Baker J, Lauder I. Liver regeneration: a comparison of in situ hybridization for histone mRNA with bromodeoxyuridine labeling for the detection of S-phase cells. Histochem Cytochem 1994;42:1603-8.

207. Gratzner H. Monoclonal antibody to 5-bromo and 5-iododeoxyuridine: a new reagent for detection of DNA replication. Science 1982;218:474-5.

208. Alison M. Assessing cellular proliferation: what's worth measuring? Hum Exper Toxicol 1995;14:935-44.

Appendix 1 Machine Cutting

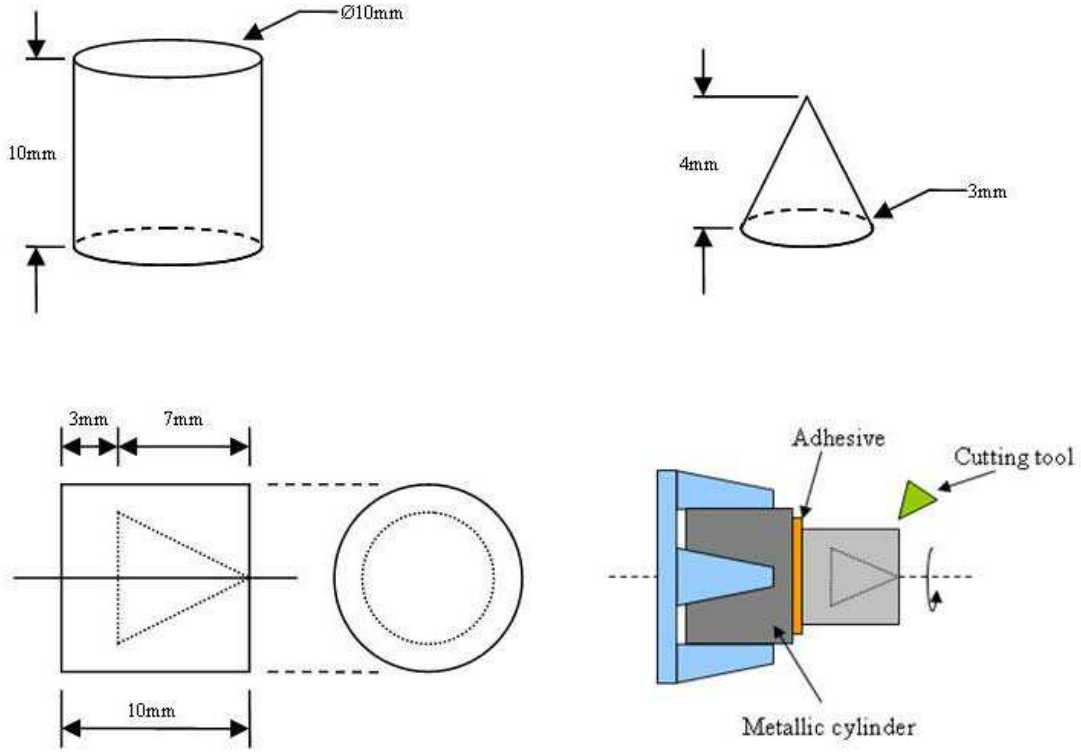

Figure A1 Schematic for design of machine cut $P_{DL}LA$ cones. Cylinders of foamed $P_{DL}LA$ were manufactured in a 10 mm x 10 mm mould (*top left*). The cylinders were then cut down into 3 mm x 4 mm cones (*top right & bottom left*) on a Boley lathe (*bottom right*).

Appendix 2 Scaffold Mould & Vacuum Pressing

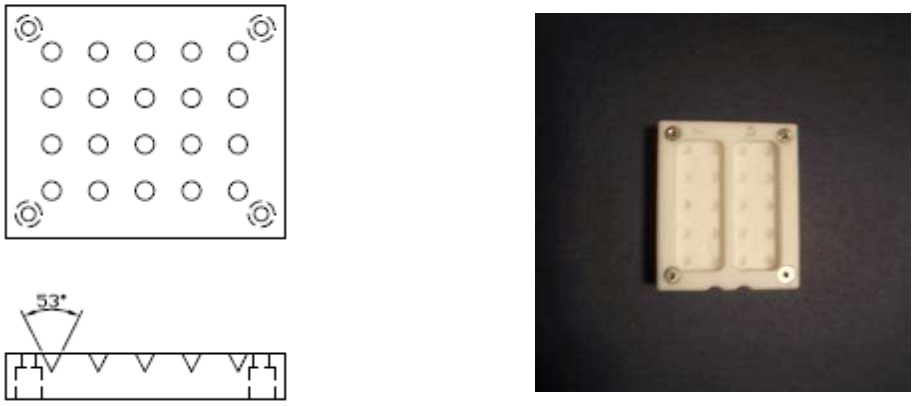

Figure A2 Schematic and photograph of a 20 well 4 mm x 4 mm conical teflon mould for heat sintering of PLGA + 5% PEG-based microparticles and vacuum pressing of L-ECM sheets.

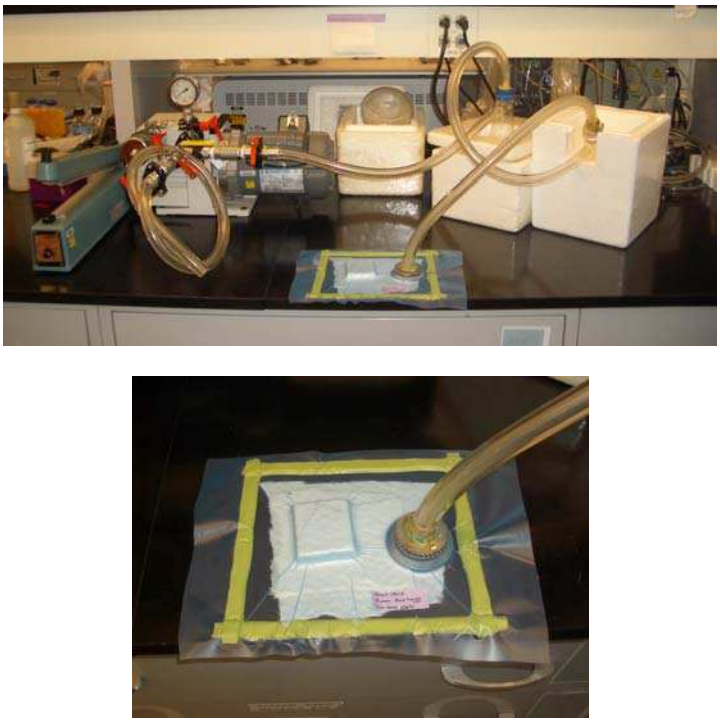

Figure A3 Photograph of the vacuum press for L-ECM only scaffold manufacture. 10 sheets of decellularised L-ECM were vacuum pressed in the Teflon mould and sterilised in EtO.

Appendix 3 Liver Tissue Processing Schedule

Table A1 Processing schedule for $P_{DL}LA$ and PLGA 5% PEG implanted rat livers.

Reagent	Time
10% Formalin	10 mins
Industrial Methylated Spirits	40 mins
Industrial Methylated Spirits	40 mins
Industrial Methylated Spirits	60 mins
Industrial Methylated Spirits	60 mins
Industrial Methylated Spirits	60 mins
Industrial Methylated Spirits	90 mins
Histoclear	60 mins
Histoclear	60 mins
Histoclear	60 mins
Paraffin wax	60 mins
Paraffin wax	90 mins
Paraffin wax	120 mins

Appendix 4 Protocol for Masson Trichrome Staining

Solutions:

Ponceau Acid Fuchsin Solution
1% Phosphomolybdic Acid
0.2% Light Green in 0.2% Acetic Acid
4% Iron Alum
Mayer's Haematoxylin

Method:

1. Dewax in histoclear
2. Take sections to water
3. Treat with 4% iron alum for 5 min
4. Rinse in dH_2O
5. Stain with Mayer's haematoxylin for 1 min
6. Wash in tap water until nuclei are blue
7. Stain with ponceau acid fuchsin for 5 min
8. Rinse in deionised water
9. Differentiate in 1% phosphomolybdic acid under microscopic control until collagen clear
10. Stain in 0.2% light green in 0.2% acetic acid for 30-60 sec
11. Dehydrate, clear and mount

Results:

Collagen	Green
Cytoplasm, muscle, erythrocytes	Red
Nuclei	Blue / Black

Appendix 5 Protocol for ED1 Immuohistochemistry

Solutions:

Histoclear
Hydrogen peroxide (3%)
Tris (0.05 M)
Trypsin (1 mg/ml)
Primary Antibody (MCA341R, Serotec)
PBST
Secondary Antibody (AP192B, Chemicon)
ABC Vector Elite kit (Vector Laboratories)
Chromagen
Aqueous Haematoxylin
Scotts Blue

Method:

1. Dewax in histoclear for 10 min
2. Quench in H_2O_2
3. Rinse in dH_2O
4. Incubate in Tris for 5 min
5. Rinse in dH_2O
6. Incubate in trypsin for 15 min
7. Rinse in dH_2O and dry
8. Incubate in primary antibody solution (1:200) for 1 hour
9. Rinse in PBST
10. Incubate in secondary antibody solution (1:500) for 30 min
11. Rinse in PBST
12. Label in ABC for 30 min
13. Rinse in PBST
14. Apply Chromagen for 10 min
15. Rinse in dH_2O
16. Counterstain in haematoxylin
17. Blue in Scotts and rinse in dH_2O
18. Air dry and mount in DPX

Results:

Nuclei	Blue / black
Sites of peroxidase activity	Brown

Appendix 6 Protocol for Desmin Immunohistochemistry

Solutions:

Histoclear
Hydrogen peroxide (3%)
Retrieval Buffer (Dako)
Blue block
Primary Antibody (SC-7559, Santacruz)
PBST
Secondary Antibody (AP180B, Chemicon)
ABC Vector Elite kit
Chromagen
Aqueous haematoxylin
Scott blue

Method:

1. Dewax in histoclear for 10 min
2. Quench in H_2O_2
3. Rinse in dH_2O
4. Steam for 30 min in retrieval buffer and cool
5. Rinse in dH_2O and dry
6. Block with blue block for 10 min and drain
7. Incubate with primary antibody (1:50) for 1 hour
8. Rinse with PBST
9. Incubate with secondary antibody (1:500) for 30 min
10. Rinse with PBST
11. Label in ABC for 20 min
12. Rinse with PBST
13. Apply Chromagen for 10 min
14. Counterstain for 1min with aqueous haematoxylin
15. Rinse in dH_2O
16. Blue in Scotts and rinse in dH_2O
17. Air dry and mount in DPX

Results

Nuclei	Blue / black
Sites of peroxidase activity	Brown

Appendix 7 Protocol for MIB-5 Immunohistochemistry

Solutions

Histoclear
10 mM Sodium Citrate pH 6.0
En Vision ™ Kit (Dako)
0.005mM Tris/HCl Buffered Saline (TBS) pH 7.6 Primary Antibody (M7248, Dako)
DAB Chromogen Solution
Gill's 3 Haematoxylin
1% Acid Alcohol
Scotts Blue

Method

1. Dewax in Histoclear for 10 min
2. Transfer to fresh alcohol x2
3. Wash in tap water followed by dH_2O
4. Place in Sodium Citrate and perform microwave antigen retrieval for 20 min at 560 W
5. Incubate peroxidase blocking solution for 5 min
6. Wash dH_2O
7. Rinse in 0.005 M TBS
8. Drain and incubate in unconjugated rat anti-Ki-67 antibody (1:100) for 30 min in moist incubating chamber
9. Wash and agitate in TBS for 5 min
10. Incubate in conjugated dextran antibody bound to peroxidase (Bottle 2 in EnVision kit) for 30 min
11. Wash and agitate in TBS for 5 min
12. Incubate in DAB chromogen solution in EnVision kit for 5 mins
13. Wash in tap water
14. Counterstain in Gill's 3 haematoxylin
15. Wash tap water
16. Differentiate in acid alcohol
17. Wash tap water
18. Blue in Scotts Tap Water Substitute
19. Wash tap water
20. Dehydrate in alcohol for 3 min x2
21. Histoclear for 3 min x2
22. Mount in DPX

Results

Nuclei	Blue
Sites of peroxidase activity	Brown

Appendix 8 Protocol for BrdU Immunohistochemistry

Solutions

Histoclear
10 mM Sodium Citrate pH 6.0
Dako REAL™ Detection Kit (Dako)
Primary Antibody (MO744, Dako)
0.005 M TRIS/HCl Buffered Saline (TBS) pH 7.6
Secondary Antibody (K5001, Dako)
HRP Solution (Dako)
DAB solution (Dako)
Gill's 3 Haematoxylin
1% Acid Alcohol
Scotts Tap Water Substitute

Method

1. Dewax in Histoclear for 10 min x2
2. Transfer to fresh alcohol for 3 min x2
3. Wash in tap water followed by dH_2O
4. Place in Sodium Citrate and perform microwave antigen retrieval for 23 min at 560 W
5. Wash in tap water followed by dH_2O
6. Incubate in Dako peroxidase blocking solution for 15 min
7. Wash well in dH_2O
8. Incubate in Buffer 1 for 20 mins
9. Drain, wipe off excess serum and incubate in unconjugated BrdU (1:200) for 1 hour
10. Jet wash in TBS x2
11. Incubate in Dako biotinylated secondary antibody for 30 min
12. Jet wash in TBS
13. Wash in TBS for 5 min
14. Incubate in Dako HRP for 30 min
15. Jet wash in TBS x2
16. Incubate in DAB solution for 10 min
17. Wash in tap water
18. Counterstain in Gill's 3 haematoxylin
19. Wash in running tap water
20. Differentiate in 1% acid alcohol
21. Wash in tap water
22. Blue in Scotts Tap Water Substitute
23. Wash in tap water
24. Dehydrate in alcohol for 3 min x2
25. Histoclear for 10 min x2
26. Air-dry
27. Mount in DPX

Results

Nuclei	Blue
Sites of peroxidase activity	Brown